PREVENTING NEOINTIMAL HYPERPLASIA BY PERIVASCULAR DRUG DELIVERY IN SYNTHETIC HEMODIALYSIS GRAFTS

by

William G. Sanders

A dissertation submitted to the faculty of
The University of Utah
in partial fulfillment of the requirements for the degree of

Doctor of Philosophy

Department of Pharmaceutics and Pharmaceutical Chemistry

The University of Utah

May 2012

The University of Utah Graduate School

STATEMENT OF DISSERTATION APPROVAL

The dissertation of **William G. Sanders**

has been approved by the following supervisory committee members:

Christi Terry	, Chair	**12/14/11** Date Approved
Alfred Cheung	, Member	**11/4/11** Date Approved
Steven Kern	, Member	**11/4/11** Date Approved
David Grainger	, Member	**11/4/11** Date Approved
Hamid Ghandehari	, Member	**11/4/11** Date Approved

and by **David Grainger**, Chair of the Department of **Pharmaceutics and Pharmaceutical Chemistry**

and by Charles A. Wight, Dean of The Graduate School.

ABSTRACT

Hyperplasia leading to stenosis of synthetic vascular accesses for chronic hemodialysis is a widespread problem with no established treatment for prevention. Inflammation around the anastomotic region in hemodialysis arteriovenous (AV) grafts is a constant reoccurring factor that likely contributes to hyperplasia development. Perivascular delivery of an anti-inflammatory drug around the anastomotic region could be an effective option in preventing AV graft failure due to stenosis. The objectives of this research were to investigate the involvement of inflammation in arteriovenous hemodialysis graft stenosis, ii) assess whether a novel drug, soluble epoxide hydrolase inhibitor (sEHI), would inhibit cytokine release from inflammatory cells; if so, sEHI may be useful to inhibit AV graft stenosis, and iii) to develop a perivascular drug delivery system that could deliver a wide range of potential therapeutics in a directional and controlled manner to prevent AV graft stenosis.

The first part of the dissertation investigates the involvement of inflammation in arteriovenous hemodialysis graft stenosis and if an experimental anti-inflammatory drug, sEHI, could be useful in inhibiting cytokine and chemokine release from primary macrophages. In our porcine AV graft model, macrophage and T-cell accumulation increased over the 7 week time course corresponding with an increase in the hyperplasia formation at the venous anastomosis. Elevated expression of prominent cytokine/chemokines TNF-α and MCP-1, was seen in vein-graft anastomotic tissue. The sEHI significantly inhibited LPS induced MCP-1 release and TNF-α from primary macrophages. The recruitment and activation of inflammatory cells around the graft anastomoses likely plays an influential role in causing hyperplasia in arteriovenous grafts and sEHI could be an effective therapeutic by preventing MCP-1 and TNF-α release.

The second part of the dissertation is development of a perivascular delivery system for controlled and directed release of sunitinib, which could be utilized for other

therapeutics. A bilayer wrap design using either polycaprolactone or poly(lactic-co-glycolide) (PLGA) was produced containing a monolithic backing to provide unidirectional release and to prevent loss of drug to the extravascular space, and either a drug loaded non-porous layer, or a porous layer that could be filled with drug loaded hydrogel. A biodegradable PLGA-based perivascular drug delivery system was created that provided early directed drug delivery and sustained release of sunitinib in vivo around the site of placement for at least four weeks.

These results demonstrated that the bilayer PLGA wrap presented is a promising perivascular drug delivery system for the local treatment of arteriovenous graft hyperplasia. sEHI could be useful to incorporate into this delivery system to target the recruitment of inflammatory cells to the anastomotic region by inhibiting MCP-1 release.

TABLE OF CONTENTS

LIST OF ABBREVIATIONS

AT.....adipose tissue

AA……arachidonic acid

AV.....arteriovenous

BMMΦ.....bone-marrow macrophage

DHETs.....dihydroxyeicosatrienoic acids

EETs.....epoxyeicosatrienoic acids

ePTFE.....expanded polytetrafluoroethylene

ESRD.....end-stage renal disease

FBGC.....foreign body giant cell

FGF.....fibroblast growth factor

HA.....hyaluronic acid

HAse.....hyaluronidase

JNK……jun-N-terminal kinase

LPS……lipopolysaccharide

MCP-1.....monocyte chemotactic protein-1

MIP-1α.....macrophage inflammatory protein-1α

MMP.....matrix metalloproteinase

NF-κB.....nuclear factor-κB

NH.....neointimal hyperplasia

NO.....nitric oxide

PCL.....polycaprolactone

PDGF……..platelet derived growth factor

PLGA.....poly(lactic-co-glycolic) acid

PTA.....percutaneous transluminal angioplasty

sEH.....soluble epoxide hydrolase

sEHI.....soluble epoxide hydrolase inhibitor

SMC.....smooth muscle cell

TGF-β1.....transforming growth factor-β1

TNF-α.....tumor necrosis factor-α

VEGF.....vascular endothelial growth factor

LIST OF FIGURES

LIST OF TABLES

ACKNOWLEDGEMENTS

I extend my appreciation and sincere gratefulness to those who have made this thesis possible. I would like to thank first and foremost my thesis advisor Dr. Christi Terry, who has helped improve me as a researcher and scientist, always supported me in my endeavors, and has been a model mentor to me. I would also like to thank Dr. Alfred Cheung in supporting my research and giving me guidance and advice whenever possible. I am thankful to my committee members, Drs. David Grainger, Steven Kern, and Hamid Ghandehari, for providing insightful suggestions that helped shape my research work.

I am also grateful to my colleagues in my research group both past and present, Dr. Donald Blumenthal, Dr. Shawn Owen, Ilya Zhuplatov, Dr. Huan Li, Dr. Yuxia He, Dr. Mary Carlson, Dr. Li Li, Dan Pike, and Sunny Kwon. I would like to extend my sincere thanks to Paul Hogrebe for his patience and contribution throughout this project. I owe thanks to Dr. Jim Muller for teaching me technical skills in mass spectrometry that was beneficial for my research.

This work was supported by the Merit Review Program of the Department of Veterans Affairs (AKC), RO1HL67646 from the National Heart, Lung and Blood Institute (AKC) and a grant from the Dialysis Research Foundation of Utah & Idaho (CMT).

My pursuit of the doctorate would not have been possible without the loving support and understanding of my wife, Carissa. I also want to thank our daughter, Metabel, for making everything seem better by just providing a smile.

CHAPTER 1

NEOINTIMAL HYPERPLASIA LEADING TO HEMODIALYSIS ARTERIOVENOUS GRAFT FAILURE

1.1 General Introduction

Chronic kidney disease (CKD) is the progressive loss of the kidney's ability to regulate electrolytes, remove waste from the blood, and concentrate urine. Diabetes, hypertension, and glomerulonephritis are the most common causes of CKD, and continued progression of CKD can result in end-stage renal disease (ESRD), where there is a nearly complete or complete loss of kidney functions. ESRD has commonly been treated with chronic hemodialysis, since it was made possible after the introduction of the external arteriovenous (AV) shunt in 1960 (1). High extracorporeal blood flow rates reaching around 500 mL/min are necessary for a hemodialysis treatment of reasonable duration. This requires vascular access to blood vessels that will permit high blood flow rates.

There are currently three main types of vascular access used in hemodialysis: expanded polytetrafluoroethylene (ePTFE) AV grafts, native AV fistulas, and dual-lumen venous catheters (Table 1.1). In ePTFE AV grafts, a length of synthetic graft is surgically connected between an artery and vein such that arterial flow is shunted into the vein. AV grafts are typically placed in the

Table 1.1 Main forms of hemodialysis vascular access

	Arteriovenous ePTFE Graft	Native Arteriovenous Fistula	Dual-lumen Venous Catheter
Concept			
Advantage	Less maturation time required	Low rates of thrombosis and infection	
Disadvantage	High rates of thrombosis and infection	Often fails to mature to a useable access	Very high rates of infection and thrombosis

arm, but access can also be created in the leg, across the anterior chest wall as well as other locations. AV fistulas are formed by connecting a vein directly to an artery, most frequently in the forearm, but also can be placed in the upper arm and upper leg around the groin (2). An end-to-side design, where the end of a vein is sutured to the side of the artery, or a side-to-side design where the side of the vein is anastomosed to the side of the artery, are the standard fistula formats. Both the AV graft and AV fistula have served primarily as the permanent accesses for hemodialysis. Dual-lumen venous catheters have an exceptionally high rate of thrombosis and infection and should be avoided if possible. However, due to delayed referrals to nephrology specialists, and due to frequent failures of permanent accesses, catheter use for hemodialysis is still common.

Native AV fistulas are the preferred form of vascular access in hemodialysis because of the much lower rates of stenosis development and infection compared to other forms of vascular access. This has led to the Centers of Medicare and Medicaid Services (CMS) and the ESRD Networks to implement the “Fistula First Initiative” pushing for increased AV fistula use in prevalent patients (patients already receiving dialysis) to 66% (3). The prevalent rate for fistula use has increased from 43% reported in July 2006 to 59% in July 2011 (4). The major limitation with the fistula is the failure of many new fistulas to mature into a useable access. The term maturation in general describes the development of an access that can be readily located by dialysis staff for cannulation and obtains blood flow rates that will consistently allow hemodialysis sessions to occur in a reasonable time frame (3-4 hours). The primary patency rate has been observed to be 85% after the first year and 75% after 2 years (5), but this data does not take into account the fistulas

that failed to mature into a viable access. In a recent randomized trial conducted by the National Institutes of Health-sponsored Dialysis Access Consortium, almost 60% of newly created fistulas in 877 patients failed to mature within six months (6). Several problems arise from the low maturation rates of native fistulas: Multiple attempts are required to create a sustainable fistula, which can deplete useable vascular sites. While waiting for the fistula to mature, the need for venous catheter use persists increasing the risk of infection from the catheter and damage to catheterized vessels.

Within the last couple of years the placement of ePTFE AV grafts for hemodialysis has decreased considerably due to the “Fistula First Initiative” in the United States. However, AV grafts have the advantage over AV fistulas that they can be used for dialysis shortly after placement as they require much shorter maturation times. These accesses can be used within one or two weeks of creation compared to fistulas that can take months to mature. The primary problem that plagues ePTFE grafts is the high rate of thrombosis that occurs due to underlying stenosis, which accounts for 85% of their failure (7). Stenosis is characterized by neointimal hyperplasia (NH) formation, typically at the graft anastomoses, resulting in decreased blood flow and often eventual thrombosis (2). The primary patency rate of AV grafts is quite low at around 50% at one year based on the data collected for the Dialysis Outcomes Quality Initiative (5). Effective preventative approaches are urgently needed to decrease NH formation in the AV grafts and increase their longevity.

1.2 Pathology of Hemodialysis Graft Stenosis

Stenosis due to the formation of NH in AV grafts occurs most commonly at the vein-graft anastomosis, the juxta-anastomotic venous segments, and with more limited occurrence at the arterial-graft anastomosis (2, 8-10). NH that forms in AV grafts is characterized by: 1) the presence of smooth muscle cells and myofibroblasts (fibroblasts that have converted from differentiated, quiescent fibroblasts to a synthetic, contractile fibroblast), 2) an abundance of extracellular matrix, 3) microvessel formation (angiogenesis) within the NH and adventitia, and 4) the presence of macrophages and T-cells lining the ePTFE graft material. Increased expression of growth factors like platelet-derived growth factor (PDGF), vascular endothelial growth factor (VEGF), basic fibroblast growth factor (bFGF), and transforming growth factor-β1 (TGF-β1) is seen within the venous NH (11-13). Pathology of NH from porcine and canine AV graft models is similar to what is seen in humans (10, 14-16).

The contribution of myofibroblasts to the NH lesion has only been realized recently in AV graft NH (15, 17). Myofibroblasts play a significant role in hyperplasia by proliferating and migrating from the adventitia to the neointima, at which point they secrete extracellular matrix contributing to the mass of the hyperplastic lesion. In our porcine AV graft model, presence of myofibroblasts was seen as early as one day after graft placement and marked proliferation and/or migration into the neointima occurred by two weeks. It was found that these proliferating cells from the adventitia stained positive for smooth muscle α-actin, a marker for both smooth muscle cell and fibroblasts, but negative for myosin heavy chain and smoothelin which are markers for smooth muscle cells (15). Roy Chaudhury et al. confirmed these results by observing that the majority of cells found

within tissue segments from stenotic portions of human AV grafts were myofibroblasts (18). The contribution of the adventitia, an outer layer of the vessel wall, to NH formation in the AV graft is of significance to these studies as it supports the logic of using perivascular delivery of drugs to inhibit NH.

Formation of NH is seen at both the arterial and venous graft anastomoses, but most of the stenosis occurs around the venous anastomosis with more limited occurrence at the arterial anastomosis (9). There are several factors that likely make the venous side prone to more hyperplasia formation and stenosis. The internal elastic lamina is much more defined in arteries, compared to veins. The elastic lamina acts as a barrier to cell migration, thus its scarcity in vein may allow more ready migration of smooth muscle cells and myofibroblasts to the intima. A decreased ability to produce prostacyclin and nitric oxide by veins may make them more susceptible to endothelial injury (2). There is also significant disordered blood flow patterns and both low and very high sheer stress observed at the graft-vein anastomosis. As the vein normally experiences a much lower and steady blood flow, this novel introduction of arterial flow conditions likely contributes to an increased hyperplasic reaction as described below (19).

1.3 Pathogenesis of Arteriovenous Graft Stenosis

Different initiating events and continuing aggravating factors contribute to the formation of NH in AV grafts. The factors that cause endothelial and smooth muscle cell injury are upstream events that trigger the complicated downstream interplay between cytokines, growth factors, and cells that lead to hyperplasia formation. Multiple upstream events (Figure 1.1) thought to promote

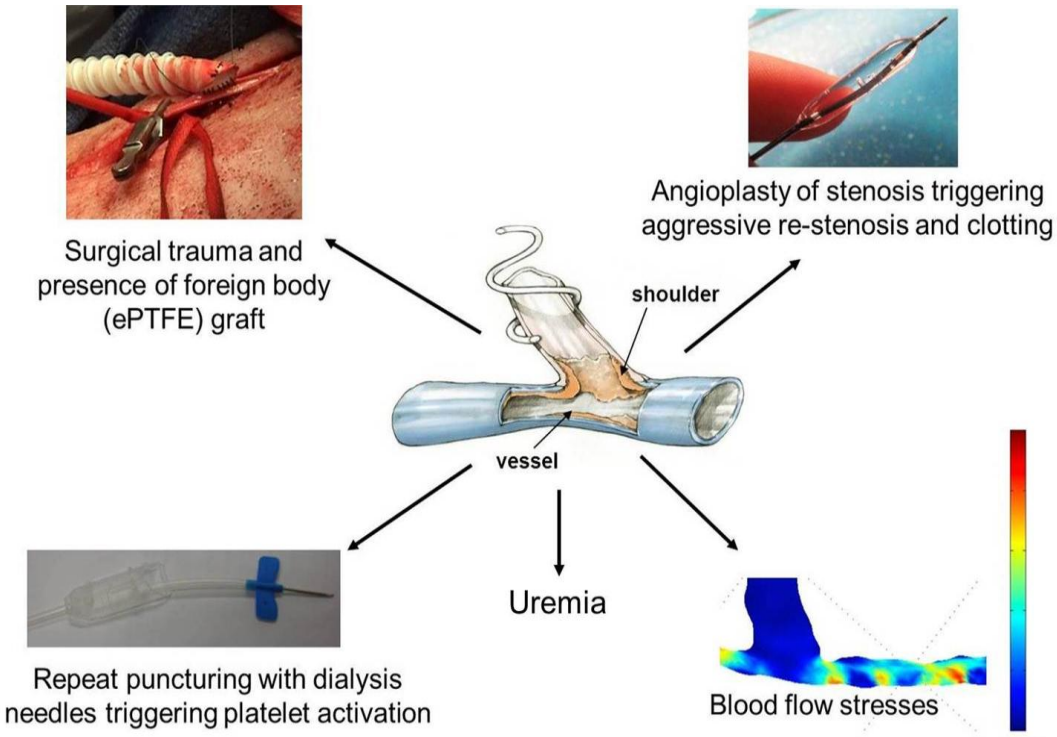

Figure 1.1 Pathogenic factors that contribute to NH formation in AV grafts

the formation of NH in AV grafts include (1) surgical trauma to the vessel during graft placement; (2) placement of foreign ePTFE graft material leading to a foreign body response and mechanical mismatch between vessel wall and graft material; (3) introduction of novel hemodynamic stress at the vein-graft anastomosis; (4) repeated needle punctures of the graft for dialysis treatment leading to chronic injury and platelet activation; and (5) the presence of uremia causing endothelial dysfunction (2).

1.3.1 Surgical Trauma

A functioning endothelial cell layer produces prostacyclin (PGI2) and nitric oxide (NO) which inhibits the activation, aggregation, and adhesion of platelets to the endothelium (20). Surgical placement of the graft causes damage to the protective endothelium (intima) exposing medial smooth muscle cells to blood flow and other proinflammatory and procoagulation blood components. Damage also occurs to the media and adventitia layers via surgical trauma as well as tissue hypoxia due to damage of the vaso vasorum. This injury to the connective tissue initiates the inflammatory response recruiting inflammatory cells to the area where they release a variety of proinflammatory cytokines, growth factors, reactive oxygen species, and matrix metalloproteinases (MMPs) that promote proliferation and migration of smooth muscle cells and myofibroblasts.

1.3.2 Biocompatibility Issues of ePTFE

The ePTFE graft materials were first introduced in 1973, and little advancement has been made in developing different biomaterials to use for AV grafts (21, 22). One problem that persists with using ePTFE is the biocompatibility problems of the material that may contribute to

hyperplasia development. Macrophages are commonly found in the NH at the vein-graft anastomosis particularly lining the ePTFE graft material (10, 13, 15). The ePTFE is recognized as a foreign body to macrophages, which leads to their activation upon adherence. Activated macrophages on ePTFE initially behave as classically activated macrophages where they release a variety of proinflammatory mediators, such as cytokines, growth factors, and MMPs that recruit other macrophages to the graft anastomosis and cause the proliferation and migration of SMCs and myofibroblasts. This likely contributes to the formation of NH. To support this idea, macrophages in the NH stained for PDGF, VEGF, and FGF in a porcine AV graft model (13).

The formation of foreign body giant cells (FBGCs), which are also found in the anastomotic region (13, 23), arises from the fusion of macrophages due to “frustrated phagocytosis” on ePTFE (24). FBGCs and macrophages adhered to biomaterials for extended periods of time (indication of chronic inflammation) switch phenotypes to an alternatively activated state (24, 25). They produce anti-inflammatory cytokines (such as IL-10), reduce the release of proinflammatory cytokines, and generate pro-fibrogenic factors (such as TGF-β1 and PDGF) that regulate fibrosis. The phenotypes of adherent macrophages do not completely switch over time to alternative phenotypes as there is continued secretion of chemokines like monocyte chemotactic protein-1 (MCP-1) and RANTES (26). FBGCs likely facilitate in hyperplasia formation by releasing TGF-β1 and PDGF that cause myofibroblasts to increase extracellular matrix deposition at the anastomosis and these growth factors also recruit cells involved in NH to the anastomosis. To support this notion, FBGCs also stained for PDGF, VEGF, and FGF in a porcine AV graft model and macrophages stained for TGF-β1 in vein segments from human stenosed AV fistulas (27). There is little published

information regarding macrophage response on ePTFE grafts in humans, and in vitro data has been relied upon to provide mechanistic insights into how the lack of biocompatibility of ePTFE factors into forming NH.

In vitro studies have shown ePTFE stimulation of macrophages might factor into several different biological processes that influence hyperplasia creation. Rat vascular SMC proliferation was significantly increased by conditioned media from human peripheral blood monocytes cultured on ePTFE graft material (28). Targeting tumor necrosis factor-α (TNF-α) using neutralizing antibodies inhibited this proliferative response indicating that TNF-α plays a mitogenic role in the effect of ePTFE graft stimulation. A human macrophage cell line (THP-1) cultured on ePTFE secreted TNF-α, MCP-1, IL-6, MIP-1α, and VEGF, all proinflammatory mediators that have been implicated in contributing to hyperplasia development (29). Primary human macrophages maintained on ePTFE with varying pore size stimulated the release of IL-1β and the upregulation of IL-6, TNF-α, MCP-1, and MIP-1β emphasizing again that ePTFE stimulates macrophages to produce proinflammatory mediators that can stimulate the proliferation and migration of SMCs and myofibroblasts (30). The biocompatibility problems of ePTFE also factors into angiogenesis and fibrogenesis, both processes that possibly assist in hyperplasia formation. Angiogenesis provides to the NH a blood supply, and fibrogenesis facilitates an increased ECM deposition around the vein-graft anastomosis. Human macrophages cultured on ePTFE released the pro-angiogenic factors VEGF and angiopoiten-1 and the conditioned media caused the sprouting of new blood capillaries from human placental blood vessel fragments (31). Also activated human macrophages co-cultured with a fibroblast cell line (WI-38) increased fibroblast proliferation and

collagen synthesis as TGF-β1 and PDGF production was elevated in the macrophages (32). Thus, recruitment and activation of macrophages by the ePTFE material may promote NH development in many different ways as described above.

1.3.3 Hemodynamic and Mechanical Stresses

Hemodynamic and mechanical stresses are likely important factors that lead to venous stenosis in AV grafts. Hemodynamic stresses arise from the mechanical forces of blood on the vessel wall. Blood flow produces a number of different stresses such as shear stress from the blood flow traveling over the stationary vessel wall, and strain from the blood pressure pushing against the vessel wall and expanding the lumen. Areas at the graft-vein anastomoses experience a variety of unique shear stresses. For example, the graft experiences pockets of low shear stress caused by disordered or stagnant flow resulting from the splitting of flow streams and other factors, which has been shown to stimulate smooth muscle cell proliferation. High shear stress can damage the protective endothelial layer resulting in direct exposure of the smooth muscle layer to higher blood flow forces than it would normally experience and to coagulation factors from which it is normally protected (19, 33, 34). Other non-flow induced stresses occur around the vein-graft anastomosis that arise from increased wall stress due to compliance mismatch between the stiff graft material and elastic native vein, and increased wall stress occurring at the suture line (35, 36).

There are three primary types of blood flow-induced stresses that cells in the vessel wall experience: 1) stress perpendicular to the vessel wall due to blood pressure as the blood travels in the vessel lumen, 2) circumferential wall stress leading to stretching of the compliant vessel wall

(37), and 3) “shear stress” as a result of the friction at the interface between luminal flowing blood and the endothelial cell surface. Typically, luminal flow is only experienced by endothelial cells, but upon vessel injury due to graft placement, SMC and possibly fibroblasts become exposed to flow. These types of hemodynamic stresses regulate the remodeling and function of the vascular wall, which also factor into other various pathological conditions (38-41). At the vein-graft anastomosis and other areas prone to hyperplasia, blood flow patterns are quite complex and are characterized by disordered flow, flow separation or flow split, low shear stress, and stagnation vortices or eddies (42-46). Most flow data available are derived from flow rates at only a few locations around the anastomosis and outside the anastomosis (34). More detailed studies are needed in order to thoroughly characterize the flow in the areas that are prone to hyperplasia in AV grafts.

Depending on the type of blood flow stress, the possible contributing affect on AV graft stenosis could be considered either negative or positive. In atheroma formation, low shear stress has been associated with SMC proliferation as first suggested in 1969 (47). Subsequent in vivo studies have confirmed this finding and suggest it may be due to the upregulation of PDGF expression (48, 49). However, higher shear stress inhibits SMC proliferation (50) possibly through TGF-β1 upregulation in an autocrine manner (51, 52). The question is how these findings translate to venous SMCs, since stenosis occurs more at the vein-graft anastomosis than arterial. Additionally, the effect of the very complex flow patterns that occur at the vessel-graft anastomosis or juxta-anastomosis segments on venous or arterial SMCs is not known.

The anastomosis region experiences increased tensile wall stress. After graft placement,

blood pressure and wall stress values can increase an order of magnitude on the venous side to levels similar to arterial blood flow and wall stress (37). Compliance mismatch between the elastic native tissue and stiff graft material and suture materials further elevates wall stress on both the venous and arterial sides of the AV ePTFE graft. A positive correlation is seen between tensile wall stress and cell proliferation (53-56). It has been debated whether it is increased strain or increased ensuing cellular stiffness that stimulates enhanced cell proliferation (57-59), but it is commonly accepted that wall tensile strain induces cell proliferation. Since the venous side in AV grafts undergoes a larger increase in circumferential wall strain, this likely makes it more prone to hyperplasia formation than the arterial.

1.3.4 Repeated Puncturing for Dialysis

Reccurring platelet activation due to repeated needle punctures of the ePTFE graft material for dialysis treatment contributes to chronic inflammation around the anastomosis. The resulting platelet thrombus that forms after dialysis needle removal causes the upregulation and secretion of PDGF and other cytokines. The downstream anastomosis then becomes exposed to these proinflammatory mediators that have the ability to elicit the recruitment and activation of macrophages and that promote proliferation and migration of SMCs and myofibroblasts. Chronic inflammation ensues due to repeated puncturing needed for dialysis three times a week, continuously initiating this response that likely contributes to hyperplasia at the venous anastomosis (60).

1.3.5 Downstream Events

The endothelial and SMC response to injury is what instigates the downstream events that form NH. This injury response triggers SMCs and myofibroblasts to migrate from the media and adventitia to the intima region. At the intima, they proliferate and deposit ECM that contributes significantly to NH formation. While this is occurring, inflammatory cells adhere to and extravasate through damaged endothelial cells at the injury site. Neutrophils accumulate first (61) followed by macrophages (62). Numerous inflammatory mediators orchestrate these various responses. Each one of these mediators is a potential therapeutic target that could help alleviate hyperplasia at the anastomotic regions.

Inflammation plays a key role in hyperplasia formation and proinflammatory cytokines such as TNF-α contribute to this process. TNF-α is synthesized by several key cell types relevant to NH, including macrophages, T-cells, endothelial cells, SMCs, and fibroblasts (63, 64). TNF can initiate processes linked to NH such as smooth muscle cell migration (65) and proliferation (63), matrix degradation (66) , and production of intercellular adhesion molecule-1 (ICAM-1) (67), MCP-1, and growth factors (PDGF, VEGF, and bFGF) (68). A number of studies suggest a primary role for TNF in NH formation. For example, after balloon injury of a rat aorta, increased levels of TNF-α were observed several days prior to the migration of smooth muscle cells into the intima (65). Additionally, basal TNF-α levels were significantly higher in Korean patients that had vascular access failure compared to the group with functioning vascular accesses (69). This supporting evidence indicates that TNF-α might play a pivotal role in NH development that leads to stenosis of AV grafts.

MCP-1 (CCL2), a CC chemokine, is a potent chemoattractant that recruits peripheral monocytes and memory T-cells into sites of inflammation (70). Besides monocytes/macrophages, many other cell types secrete MCP-1 including T-cells, endothelial cells, smooth muscle cells, and fibroblasts (71); all cell types that likely play a role in hyperplasia formation. Increased MCP-1 expression has been reported within the vascular wall of atherosclerotic lesions (72, 73) and in injured arterial walls upon balloon injury (74, 75), which corresponded with the increased accumulation of macrophages to the injured site. Inhibiting MCP-1 using either a neutralizing antibody for MCP-1 or a plasmid coding for an N-terminal deletion mutant MCP-1 has been effective in diminishing NH in different animal models of arterial injury (75-83). Recently, MCP-1 was shown to be upregulated in a mouse AV fistula model. MCP-1 knockout mice had increased fistula patency and a decrease in wall thickness at 6 weeks after fistula creation compared to wild-type mice, implicating a role for MCP-1 in vascular access dysfunction (84). Currently, substantial efforts are being made to develop a clinically useful treatment strategy to prevent the mechanism of action of MCP-1 (85-87); such a treatment could be beneficial in inhibiting AV graft stenosis.

PDGF plays a part in each stage of the wound healing response. Upon injury PDGF is released from activated platelets and this stimulates the chemotaxis and mitogenicity of neutrophils, macrophages, SMCs, and myofibroblasts to the injury site around the graft anastomosis (11, 88, 89). It also increases the formation of granulation tissue (ECM deposition) by causing the proliferation of fibroblasts and inducing the myofibroblast phenotype (90), which likely increases ECM in the anastomotic region. Typically, PDGF is not expressed in the normal

vasculature, but upon endothelial injury after angioplasty or graft placement, PDGF becomes upregulated along with its receptors (12, 13, 91). Ferns et al. showed that inhibition of PDGF using a PDGF-specific monoclonal antibody attenuated NH in a rat arterial injury model (92). Thus, using pharmacological inhibitors that target PDGF or the PDGF receptors would be a reasonable strategy in trying to prevent AV graft stenosis.

Breakdown of ECM proteins like collagen and elastin by MMPs (zinc dependent proteases), particularly MMP-2 and MMP-9, is a prerequisite for migration of SMCs. As the ECM is broken down by MMPs, it allows the SMCs to migrate from the media into the intima contributing to NH formation. Several cell types that have been associated with hyperplasia produce MMPs, such as endothelial cells, macrophages, SMCs and fibroblasts (93). MMPs are activated by increased flow and vascular injury (94, 95). Inhibition of MMP production should then in theory lead to a reduced amount of SMCs accumulating in NH. An experimental MMP inhibitor (BB2983) that was given orally significantly lessened NH formation when compared to untreated in a porcine AV graft model (96). However, one problem that has limited the use of MMP inhibitors clinically is the development of musculoskeletal toxicity observed in various clinical trials with these drugs (97, 98).

Arachidonic acid (AA), a polyunsaturated fatty acid, can be metabolized to form both proinflammatory and anti-inflammatory mediators. Cyclooxygenase (COX) and lipoxygenase (LOX) convert AA into prostaglandins and leukotrienes, of which many are potent lipid inflammatory mediators that can cause SMC proliferation and migration, platelet aggregation, and inflammatory cell adhesion (99-101). Elevated levels of both COX and LOX are observed in patients with atherosclerosis (102, 103). Targeting both enzymes using licofelone, a dual COX and LOX

antagonist, inhibited inflammation and neointimal formation in an atherosclerotic rabbit model (104). For these reasons, the COX and LOX pathways may be alternative therapeutic targets in the treatment of AV graft stenosis.

1.4 Treatment and Preventative Strategies for Neointimal Hyperplasia Formation

A better understanding of the pathogenesis leading to NH formation exists, which has helped in identifying potential therapeutic strategies that are useful in combating this problem. Several strategies to inhibit NH have been created and shown efficacious in various animal models, including some specifically focused on hyperplasia development in AV grafts. However, there currently is no effective treatment in preventing AV graft stenosis in hemodialysis patients.

The current first-line treatment of AV graft stenosis is percutaneous transluminal angioplasty (PTA). Initial studies revealed that PTA was an effective option that prolonged vascular access use in all types of venous stenoses (105, 106). Beathard reported a 94% initial success rate and primary patency rates of 90.6%, 61.3%, and 38.2% at 90, 180, and 360 days after angioplasty in hemodialysis patients with AV graft stenosis (105). Yet, balloon injury to the vascular wall promotes NH growth, which commonly leads to restenosis after coronary angioplasty (107, 108). Chang et al, demonstrated by immunohistochemistry increased cellular proliferation in restenotic lesions formed after PTA of AV fistula compared to primary stenotic lesions (109). In contrast to results reported by Beathard and others, a number of randomized clinical trials reported that treatment of AV grafts with prophylactic PTA failed to demonstrate any improvement in patency (110-112).

Mechanical device interventions such as bare metal or drug eluting stents are routinely employed after angioplasty to prevent coronary restenosis. Stent placement after PTA has been investigated as a potential treatment to target stenosis at the vein-graft anastomosis. Early randomized controlled trials failed to show any benefit of bare metal stents over PTA alone in AV grafts (113, 114). Recently a large multicenter, randomized, clinical trial by Haskal et al. detailed improved patency rates of stent grafts (nitinol stent covered in carbon-impregnated ePTFE) versus PTA alone in the treatment of stenosis at the venous anastomosis (115). At 6 months, patency in the stent graft group was 51% compared to 23% in the PTA group. However, thrombosis rates were comparable between stent (33% occlusion) and unstented (21% occlusion) groups at six months after stent graft placement with a trend that was actually worse in the stent treated group. Although stent grafts are currently used in hemodialysis access there is not any conclusive evidence that supports their benefit. There currently is not any clinical data using drug-eluting stents with PTA to prevent stenosis in AV graft vascular access. Promising results have been reported in a porcine AV graft model. Rapamycin-eluting stents but not bare metal stents significantly diminished hyperplasia and increased blood flow rate and graft diameter, compared to unstented grafts (116).

Delivery of biological and small molecule agents can be accomplished by systemic or local administration in order to treat AV graft stenosis. Two large multicenter trials that recently ended, evaluated the effect of systemically delivered anti-platelet agents (clopidogrel or dypridamole and aspirin) on preventing dialysis access stenosis. In the native AV fistula study, clopidogrel was able to significantly reduce the early occurrence of thrombosis in AV fistulas at 6 weeks, but did not

increase the proportion of AV fistulas that were suitable for dialysis (6). In the AV graft study, an oral combination of dipyridamole and aspirin reported a modest, but statistically significant improvement in unassisted patency rate in the treatment group (28%) compared to placebo (23%) at one year (117). These results raise the question if conventional systemic therapies can be successful in treating the complex and aggressive stenosis in AV grafts.

Local perivascular delivery circumvents many problems with systemic delivery. Local delivery to the site of stenosis can achieve greater local concentrations using a lower dose, minimizing undesired systemic toxicity. Drug placed directly around the “active adventitia” might be more effective in inhibiting activation and migration of fibroblasts (2). Various localized delivery approaches have been utilized: 1) placing a drug-eluting stent perivascularly at the anastomoses (116), 2) coating the ePTFE graft with drug and using it as a delivery conduit (118, 119), 3) placing an intravascular catheter at time of graft placement that can be used to inject drug into the anastomotic region (120), and 4) placing a drug depot such as a perivascular wrap (121, 122) or a polymer gel (14, 123, 124) around the anastomoses.

1.4.1 Biological Therapies

Cell-based therapy using allogeneic endothelial cell-loaded gelfoam perivascular wraps to prevent vascular access stenosis has been under investigation for the last decade. The reasoning behind using these endothelial cell implants is that endothelial cells can generate numerous beneficial mediators that in combination may inhibit cell proliferation and migration (125). In a porcine AV ePTFE graft model, endothelial cell-loaded wraps did not cause a significant decrease

in NH at 28 days, but there was increased venous lumen diameter and positive remodeling, and an 81% decrease in stenosis compared with controls (125). In a multicenter phase II trial, the safety of these wraps were demonstrated in hemodialysis patients with AV grafts, however, there was no statistically significant difference in primary and unassisted patency rates compared to placebo (126). Successful endothelialization of ePTFE by endothelial cell seeding could be beneficial in improving graft patency and has been shown to be effective in prosthetic bypass grafts in clinical trials (127). Rotmans et al. immobilized anti-CD34 on ePTFE grafts in order to capture endothelial progenitor cells in a porcine AV graft model (128). Successful endothelialization was accomplished using this method. However despite that, NH formation was significantly increased with these grafts at 4 weeks compared to untreated controls. These results raise doubt that endothelial cell-based therapies can be effective in NH prevention.

Anti-proliferative gene therapy strategies delivered locally could be an effective option in NH treatment. Antisense oligodeoxynucleotides (ODNs) targeting specific genes involved in cell proliferation can be generated, which can inhibit DNA transcription, formation of mature RNA, and protein synthesis. A number of studies using antisense ODNs have demonstrated inhibition of NH in arterial injury models by directly targeting PDGF-β receptor subunit, c-myc, proliferating cell nuclear antigen, cyclin-dependent kinase 2, nuclear factor-κB, and the transcription factors (E2F) (129-134). Large randomized trials using decoy ODNs targeting E2F following peripheral or coronary artery bypass grafting (PREVENT III and IV) (135, 136) failed to show efficacy in preventing vein graft failure even though success was seen in smaller randomized trials (137). A clinical phase I trial using the E2F decoy in hemodialysis patients with AV grafts was completed, but

further studies were halted due to the poor response in the PREVENT III and IV studies. Other gene therapy strategies to promote endothelialization by delivery of adenovirus encoding for VEGF-C, inhibited NH in angioplasty-induced restenosis in animal models (138). In contrast, other studies in various animal models that used either adenovirus coding for VEGF-A and VEGF-D, or delivery of VEGF-A protein from a fibrin coated graft, showed enhanced NH progression (139, 140). Enrollment of hemodialysis AV graft patients for a clinical phase III trial using adenovirus coding for VEGF-D to prevent stenosis was underway in 2009 since phase I/II studies exhibited technical feasibility and safety of the treatment (120).

1.4.2 Small Molecule Therapies

The use of small molecule drugs for treatment of NH has an advantage over biological therapies in that they are simpler agents and are unlikely to initiate a host immune response. Drugs that were used in first generation drug-eluting stents such as rapamycin and paclitaxel have garnered the most interest in perivascular delivery applications to deal with AV graft stenosis. Three other small molecules that will be discussed are nitric oxide, imatinib mesylate, and soluble epoxide hydrolase inhibitors.

Rapamycin, a potent immunosuppressant, inhibits cell cycle progression from the G_1 to S phase by complexing to FK506 binding protein (FKBP12), which causes inhibition of mammalian target of rapamycin (m-TOR) (141). It is used clinically to prevent allograft rejection by T-lymphocytes and employed in drug-eluting stents to thwart coronary restenosis after balloon angioplasty. Two large randomized trials (RAVEL and SIRIUS trials) proved that rapamycin-eluting

stents could decrease restenosis rates after angioplasty and major adverse cardiac events in patients (142) even five years post study (RAVEL) (143). One study as discussed earlier has provided insight into the ability of rapamycin-eluting stents to prevent NH in a porcine AV graft model (116). This study is promising, but there are some possible disadvantages with using a stent in treating NH in AV grafts. Drug-eluting stent placement is an invasive technique with only a limited duration of drug release available from the depot. The drug depot cannot be replenished in stents, which might limit the effectiveness against AV graft NH in which chronic pathogenic factors, and not a single insult such as angioplasty, contribute to the NH. In another study in a porcine AV graft model, rapamycin coated onto the ends of ePTFE using mixed methacrylates inhibited NH for four weeks (118). COLL-R®, a rapamycin-eluting collagen wrap, finished phase II trials in hemodialysis patients with AV grafts. Unassisted primary patency rates of 75% and 38% at one and two years were reported (120), which is better than the 50% patency rate stated for AV grafts at one year without any pharmacological interventions.

Paclitaxel is a mitotic inhibitor that stabilizes the mitotic spindle blocking cell division and migration. Just like the rapamycin drug-eluting stent, numerous clinical studies (TAXUS I – TAXUS VI, ASPECT, and ELUTES trials) have verified the effectiveness and safety of paclitaxel-coated stents to inhibit restenosis and in-stent stenosis after balloon angioplasty in coronary arteries (144-148). Our group has demonstrated the ability of a paclitaxel-loaded thermosensitive polymer, liquid at 4 ^{o}C then gels at 37 ^{o}C, placed perivascularly around the venous anastomosis could attenuate hyperplasia formation in a canine AV graft model (14). Recently, perivascular wraps laden with paclitaxel positioned around the anastomoses inhibited NH creation

in both porcine (121) and sheep (122) AV graft models. A large multicenter trial was underway testing the efficacy of a PLGA-based paclitaxel eluting wrap in preventing stenosis in AV grafts, but was halted due to an imbalance in the incidence of infections in one of the study arms (either the control or treatment group) (120). The sponsor was blinded to the treatment group thus it was not reported if it was the wrap-treated group that experienced the increased incidence of infection.

Nitric oxide (NO) is able to inhibit several key pathways involved in the progression of hyperplasia in AV grafts, including platelet activation, SMC proliferation and migration, and ECM synthesis (149). NO inhibited SMC proliferation in vitro (150) and in balloon injury models in both rat (151) and porcine (152) through cyclic guanosine monophosphate (cGMP)-dependent mechanisms. Stents eluting an NO donor or NO releasing compound (sodium nitroprusside) diminished restenosis in a rabbit (153) and porcine (154) balloon angioplasty injury models. NO generating polymeric hydrogels placed perivascularly suppressed hyperplasia development by 80% compared to controls in a rat carotid balloon injury model (149). Currently, no studies have been reported investigating the effect of NO delivery to prevent AV graft stenosis.

As discussed previously, PDGF is a potent chemoattractant and mitogen that plays an essential role in initiating SMC migration and proliferation (11, 88). Imatinib mesylate, a tyrosine kinase inhibitor that inhibits both PDGF receptor subtypes has been shown to inhibit restenosis after balloon angioplasty (155) and diet-induced atherosclerosis (156). Data obtained in our lab has demonstrated the ability of imatinib to deter both arterial and venous SMC proliferation, with increased potency (eight fold lower IC_{50}) in venous cells compared to arterial (157). Tyrosine kinase inhibitors with similar mechanisms of action as imatinib should also possibly be effective

against NH formation. Sunitinib is a multitarget receptor tyrosine kinase inhibitor of both PDGF receptor subtypes, all three VEGF receptor subtypes, KIT, FLT3, and CSR-1R (158). Sunitinib is currently FDA approved to treat gastrointestinal stromal tumors and metastatic renal cell carcinoma. Currently, the therapeutic efficacy of sunitinib in preventing hyperplasia formation has not been analyzed. Data from our laboratory have verified the ability of sunitinib to inhibit PDGF stimulated proliferation of human venous SMCs in vitro (IC_{50}~5 nM; manuscript in preparation). These findings suggest that both imatinib and sunitinib could be promising drugs to use in preventing AV graft stenosis.

AA can be metabolized to epoxyeicosatrienoic acids (EETs) by a third pathway involving the epoxygenase cytochrome P450 enzymes, particularly CYP2C and 2J. EETs have anti-inflammatory properties and are important modulators of vascular function. Experimental evidence indicates that EETs elicit their anti-inflammatory effects by inhibiting the activation of NF-κB (159), a key transcriptional factor that causes the upregulation of numerous proinflammatory genes. For example, EETs inhibit the expression of vascular cell adhesion molecule-1 (VCAM-1) in human endothelial cells in response to TNFα, interleukin-1-alpha (IL-1α) or lipopolysaccharide (LPS) (159). EETs also inhibit other important biological processes that contribute to NH such as SMC migration (160) and platelet aggregation (161). However, soluble epoxide hydrolase (sEH) quickly metabolizes EETs to the less active dihydroxyeicosatrienoic acids (DHETs). Potent and selective pharmacological inhibitors (soluble epoxide hydrolase inhibitors or sEHI) (162, 163) have been developed, which increase and extend the functional effects of EETs. Several studies have demonstrated the anti-inflammatory effects of these inhibitors after systemic administration (164,

165). We investigated the potential of these inhibitors as a possible therapeutic to prevent NH by examining their effects on inhibiting cytokine release from inflammatory cells (discussed in further detail in Chapter Two).

1.5 Statement of Objectives

The primary objectives of this work are to i) investigate the involvement of inflammation in arteriovenous hemodialysis graft stenosis, ii) assess whether a novel drug, a soluble epoxide hydrolase inhibitor (sEHI), would inhibit cytokine release from inflammatory cells; if so, sEHI may be useful to inhibit AV graft stenosis, and iii) to develop a perivascular drug delivery system that could deliver a wide range of potential therapeutics in a directional and controlled manner to treat AV graft stenosis. The fundamental hypothesis driving these objectives is that perivascular delivery of an anti-inflammatory drug around the anastomotic region could be an effective option in preventing AV graft stenosis.

1.6 References

1. Hakim R, Himmelfarb J. Hemodialysis access failure: a call to action. Kidney Int. 1998;54:1029-40.

2. Roy-Chaudhury P, Sukhatme VP, Cheung AK. Hemodialysis vascular access dysfunction: a cellular and molecular viewpoint. J Am Soc Nephrol. 2006;17:1112-27.

3. Lok CE. Fistula first initiative: advantages and pitfalls. Clin J Am Soc Nephrol. 2007;2:1043-53.

4. Yamauchi T, Nio Y, Maki T, Kobayashi M, Takazawa T, Iwabu M, et al. Targeted disruption of AdipoR1 and AdipoR2 causes abrogation of adiponectin binding and metabolic actions. Nat Med. 2007;13:332-9.

5. Schwab SJ, Harrington JT, Singh A, Roher R, Shohaib SA, Perrone RD, et al. Vascular access for hemodialysis. Kidney Int. 1999;55:2078-90.

6. Dember LM, Beck GJ, Allon M, Delmez JA, Dixon BS, Greenberg A, et al. Effect of clopidogrel on early failure of arteriovenous fistulas for hemodialysis: a randomized controlled trial. JAMA. 2008;299:2164-71.

7. Cabanelas A, Cordeiro A, Santos Almeida NA, Monteiro de Paula GS, Coelho VM, Ortiga-Carvalho TM, et al. Effect of triiodothyronine on adiponectin expression and leptin release by white adipose tissue of normal rats. Horm Metab Res. 2010;42:254-60.

8. Asif A, Gadalean FN, Merrill D, Cherla G, Cipleu CD, Epstein DL, et al. Inflow stenosis in arteriovenous fistulas and grafts: a multicenter, prospective study. Kidney Int. 2005;67:1986-92.

9. Kanterman RY, Vesely TM, Pilgram TK, Guy BW, Windus DW, Picus D. Dialysis access grafts: anatomic location of venous stenosis and results of angioplasty. Radiology. 1995;195:135-9.

10. Kelly BS, Heffelfinger SC, Whiting JF, Miller MA, Reaves A, Armstrong J, et al. Aggressive venous neointimal hyperplasia in a pig model of arteriovenous graft stenosis. Kidney Int. 2002;62:2272-80.

11. Swedberg SH, Brown BG, Sigley R, Wight TN, Gordon D, Nicholls SC. Intimal fibromuscular hyperplasia at the venous anastomosis of PTFE grafts in hemodialysis patients. Clinical, immunocytochemical, light and electron microscopic assessment. Circulation. 1989;80:1726-36.

12. Weiss MF, Scivittaro V, Anderson JM. Oxidative stress and increased expression of growth factors in lesions of failed hemodialysis access. Am J Kidney Dis. 2001;37:970-80.

13. Roy-Chaudhury P, Kelly BS, Miller MA, Reaves A, Armstrong J, Nanayakkara N, et al. Venous neointimal hyperplasia in polytetrafluoroethylene dialysis grafts. Kidney Int. 2001;59:2325-34.

14. Masaki T, Rathi R, Zentner G, Leypoldt JK, Mohammad SF, Burns GL, et al. Inhibition of neointimal hyperplasia in vascular grafts by sustained perivascular delivery of paclitaxel. Kidney Int. 2004;66:2061-9.

15. Li L, Terry CM, Blumenthal DK, Kuji T, Masaki T, Kwan BC, et al. Cellular and morphological changes during neointimal hyperplasia development in a porcine arteriovenous graft model. Nephrol Dial Transplant. 2007;22:3139-46.

16. Rotmans JI, Velema E, Verhagen HJ, Blankensteijn JD, Kastelein JJ, de Kleijn DP, et al. Rapid, arteriovenous graft failure due to intimal hyperplasia: a porcine, bilateral, carotid arteriovenous graft model. J Surg Res. 2003;113:161-71.

17. Misra S, Doherty MG, Woodrum D, Homburger J, Mandrekar JN, Elkouri S, et al. Adventitial remodeling with increased matrix metalloproteinase-2 activity in a porcine arteriovenous polytetrafluoroethylene grafts. Kidney Int. 2005;68:2890-900.

18. Roy-Chaudhury P, Wang Y, Krishnamoorthy M, Zhang J, Banerjee R, Munda R, et al. Cellular phenotypes in human stenotic lesions from haemodialysis vascular access. Nephrol Dial Transplant. 2009;24:2786-91.

19. Roy-Chaudhury P, Kelly BS, Zhang J, Narayana A, Desai P, Melham M, et al. Hemodialysis vascular access dysfunction: from pathophysiology to novel therapies. Blood Purif. 2003;21:99-110.

20. Radomski MW, Palmer RM, Moncada S. The anti-aggregating properties of vascular endothelium: interactions between prostacyclin and nitric oxide. Br J Pharmacol. 1987;92:639-46.

21. Baker LD, Jr., Johnson JM, Goldfarb D. Expanded polytetrafluoroethylene (PTFE) subcutaneous arteriovenous conduit: an improved vascular access for chronic hemodialysis. Trans Am Soc Artif Intern Organs. 1976;22:382-7.

22. Tellis VA, Kohlberg WI, Bhat DJ, Driscoll B, Veith FJ. Expanded polytetrafluoroethylene graft fistula for chronic hemodialysis. Ann Surg. 1979;189:101-5.

23. Mehta RI, Mukherjee AK, Patterson TD, Fishbein MC. Pathology of explanted polytetrafluoroethylene vascular grafts. Cardiovasc Pathol. 2011;20:213-21.

24. Anderson JM, Rodriguez A, Chang DT. Foreign body reaction to biomaterials. Semin Immunol. 2008;20:86-100.

25. Gordon S, Martinez FO. Alternative activation of macrophages: mechanism and functions. Immunity. 2010;32:593-604.

26. Jones JA, Chang DT, Meyerson H, Colton E, Kwon IK, Matsuda T, et al. Proteomic analysis and quantification of cytokines and chemokines from biomaterial surface-adherent macrophages and foreign body giant cells. J Biomed Mater Res A. 2007;83:585-96.

27. Stracke S, Konner K, Kostlin I, Friedl R, Jehle PM, Hombach V, et al. Increased expression of TGF-beta1 and IGF-I in inflammatory stenotic lesions of hemodialysis fistulas. Kidney Int. 2002;61:1011-9.

28. Mattana J, Effiong C, Kapasi A, Singhal PC. Leukocyte-polytetrafluoroethylene interaction enhances proliferation of vascular smooth muscle cells via tumor necrosis factor-alpha secretion. Kidney Int. 1997;52:1478-85.

29. Schutte RJ, Parisi-Amon A, Reichert WM. Cytokine profiling using monocytes/macrophages cultured on common biomaterials with a range of surface chemistries. J Biomed Mater Res A. 2009;88:128-39.

30. Bota PC, Collie AM, Puolakkainen P, Vernon RB, Sage EH, Ratner BD, et al. Biomaterial

topography alters healing in vivo and monocyte/macrophage activation in vitro. J Biomed Mater Res A. 2010;95:649-57.

31. Dagtekin G, Schiffer R, Klein B, Jahnen-Dechent W, Zwadlo-Klarwasser G. Modulation of angiogenic functions in human macrophages by biomaterials. Biomaterials. 2003;24:3395-401.

32. Song E, Ouyang N, Horbelt M, Antus B, Wang M, Exton MS. Influence of alternatively and classically activated macrophages on fibrogenic activities of human fibroblasts. Cell Immunol. 2000;204:19-28.

33. Sivanesan S, How TV, Black RA, Bakran A. Flow patterns in the radiocephalic arteriovenous fistula: an in vitro study. J Biomech. 1999;32:915-25.

34. Haruguchi H, Teraoka S. Intimal hyperplasia and hemodynamic factors in arterial bypass and arteriovenous grafts: a review. J Artif Organs. 2003;6:227-35.

35. Hofer M, Rappitsch G, Perktold K, Trubel W, Schima H. Numerical study of wall mechanics and fluid dynamics in end-to-side anastomoses and correlation to intimal hyperplasia. J Biomech. 1996;29:1297-308.

36. Ballyk PD, Walsh C, Butany J, Ojha M. Compliance mismatch may promote graft-artery intimal hyperplasia by altering suture-line stresses. J Biomech. 1998;31:229-37.

37. Fung Y. Mechanical Properties of Living Tissue. New York: Springer-Verlag; 1993.

38. Liu SQ. Biomechanical basis of vascular tissue engineering. Crit Rev Biomed Eng. 1999;27:75-148.

39. Davies PF, Polacek DC, Shi C, Helmke BP. The convergence of haemodynamics, genomics, and endothelial structure in studies of the focal origin of atherosclerosis. Biorheology. 2002;39:299-306.

40. Kakisis JD, Liapis CD, Sumpio BE. Effects of cyclic strain on vascular cells. Endothelium. 2004;11:17-28.

41. Davies MG, Hagen PO. Pathophysiology of vein graft failure: a review. Eur J Vasc Endovasc Surg. 1995;9:7-18.

42. Krueger U, Zanow J, Scholz H. Comparison of two different arteriovenous anastomotic forms by numerical 3D simulation of blood flow. Int J Angiol. 2000;9:226-31.

43. Krueger U, Zanow J, Scholz H. Computational fluid dynamics and vascular access. Artif Organs. 2002;26:571-5.

44. Ene-Iordache B, Mosconi L, Remuzzi G, Remuzzi A. Computational fluid dynamics of a vascular access case for hemodialysis. J Biomech Eng. 2001;123:284-92.

45. Van Tricht I, De Wachter D, Tordoir J, Verdonck P. Comparison of the hemodynamics in 6mm and 4-7 mm hemodialysis grafts by means of CFD. J Biomech. 2006;39:226-36.

46. Migliavacca F, Dubini G. Computational modeling of vascular anastomoses. Biomech Model Mechanobiol. 2005;3:235-50.

47. Caro CG, Fitz-Gerald JM, Schroter RC. Arterial wall shear and distribution of early atheroma in man. Nature. 1969;223:1159-60.

48. Mondy JS, Lindner V, Miyashiro JK, Berk BC, Dean RH, Geary RL. Platelet-derived growth factor ligand and receptor expression in response to altered blood flow in vivo. Circ Res. 1997;81:320-7.

49. Kraiss LW, Geary RL, Mattsson EJ, Vergel S, Au YP, Clowes AW. Acute reductions in blood flow and shear stress induce platelet-derived growth factor-A expression in baboon prosthetic grafts. Circ Res. 1996;79:45-53.

50. Sterpetti AV, Cucina A, Santoro L, Cardillo B, Cavallaro A. Modulation of arterial smooth muscle cell growth by haemodynamic forces. Eur J Vasc Surg. 1992;6:16-20.

51. Ueba H, Kawakami M, Yaginuma T. Shear stress as an inhibitor of vascular smooth muscle cell proliferation. Role of transforming growth factor-beta 1 and tissue-type plasminogen activator. Arterioscler Thromb Vasc Biol. 1997;17:1512-6.

52. Song RH, Kocharyan HK, Fortunato JE, Glagov S, Bassiouny HS. Increased flow and shear stress enhance in vivo transforming growth factor-beta1 after experimental arterial injury. Arterioscler Thromb Vasc Biol. 2000;20:923-30.

53. Li Q, Muragaki Y, Hatamura I, Ueno H, Ooshima A. Stretch-induced collagen synthesis in cultured smooth muscle cells from rabbit aortic media and a possible involvement of angiotensin II and transforming growth factor-beta. J Vasc Res. 1998;35:93-103.

54. Sumpio BE, Banes AJ. Response of porcine aortic smooth muscle cells to cyclic tensional deformation in culture. J Surg Res. 1988;44:696-701.

55. Mills I, Cohen CR, Kamal K, Li G, Shin T, Du W, et al. Strain activation of bovine aortic smooth muscle cell proliferation and alignment: study of strain dependency and the role of protein kinase A and C signaling pathways. J Cell Physiol. 1997;170:228-34.

56. Birukov KG, Shirinsky VP, Stepanova OV, Tkachuk VA, Hahn AW, Resink TJ, et al. Stretch affects phenotype and proliferation of vascular smooth muscle cells. Mol Cell Biochem.

1995;144:131-9.

57. Gladilin E, Micoulet A, Hosseini B, Rohr K, Spatz J, Eils R. 3D finite element analysis of uniaxial cell stretching: from image to insight. Phys Biol. 2007;4:104-13.

58. Maniotis AJ, Chen CS, Ingber DE. Demonstration of mechanical connections between integrins, cytoskeletal filaments, and nucleoplasm that stabilize nuclear structure. Proc Natl Acad Sci U S A. 1997;94:849-54.

59. Mizutani T, Haga H, Kawabata K. Cellular stiffness response to external deformation: tensional homeostasis in a single fibroblast. Cell Motil Cytoskeleton. 2004;59:242-8.

60. Albers FJ. Causes of hemodialysis access failure. Adv Ren Replace Ther. 1994;1:107-18.

61. Welt FG, Edelman ER, Simon DI, Rogers C. Neutrophil, not macrophage, infiltration precedes neointimal thickening in balloon-injured arteries. Arterioscler Thromb Vasc Biol. 2000;20:2553-8.

62. Danenberg HD, Fishbein I, Gao J, Monkkonen J, Reich R, Gati I, et al. Macrophage depletion by clodronate-containing liposomes reduces neointimal formation after balloon injury in rats and rabbits. Circulation. 2002;106:599-605.

63. Tanaka H, Sukhova G, Schwartz D, Libby P. Proliferating arterial smooth muscle cells after balloon injury express TNF-alpha but not interleukin-1 or basic fibroblast growth factor. Arterioscler Thromb Vasc Biol. 1996;16:12-8.

64. Ozaki CK. Cytokines and the early vein graft: strategies to enhance durability. J Vasc Surg. 2007;45 Suppl A:A92-8.

65. Jovinge S, Hultgardh-Nilsson A, Regnstrom J, Nilsson J. Tumor necrosis factor-alpha activates smooth muscle cell migration in culture and is expressed in the balloon-injured rat aorta. Arterioscler Thromb Vasc Biol. 1997;17:490-7.

66. Vaday GG, Hershkoviz R, Rahat MA, Lahat N, Cahalon L, Lider O. Fibronectin-bound TNF-alpha stimulates monocyte matrix metalloproteinase-9 expression and regulates chemotaxis. J Leukoc Biol. 2000;68:737-47.

67. Kumar A, Dhawan S, Hardegen NJ, Aggarwal BB. Curcumin (Diferuloylmethane) inhibition of tumor necrosis factor (TNF)-mediated adhesion of monocytes to endothelial cells by suppression of cell surface expression of adhesion molecules and of nuclear factor-kappaB activation. Biochem Pharmacol. 1998;55:775-83.

68. Gaur U, Aggarwal BB. Regulation of proliferation, survival and apoptosis by members of the TNF superfamily. Biochem Pharmacol. 2003;66:1403-8.

69. Sung SA, Ko GJ, Jo SK, Cho WY, Kim HK, Lee SY. Interleukin-10 and tumor necrosis factor-alpha polymorphisms in vascular access failure in patients on hemodialysis: preliminary data in Korea. J Korean Med Sci. 2008;23:89-93.

70. Niu J, Kolattukudy PE. Role of MCP-1 in cardiovascular disease: molecular mechanisms and clinical implications. Clin Sci (Lond). 2009;117:95-109.

71. Melgarejo E, Medina MA, Sanchez-Jimenez F, Urdiales JL. Monocyte chemoattractant protein-1: a key mediator in inflammatory processes. Int J Biochem Cell Biol. 2009;41:998-1001.

72. Takeya M, Yoshimura T, Leonard EJ, Takahashi K. Detection of monocyte chemoattractant protein-1 in human atherosclerotic lesions by an anti-monocyte chemoattractant protein-1 monoclonal antibody. Hum Pathol. 1993;24:534-9.

73. Yla-Herttuala S, Lipton BA, Rosenfeld ME, Sarkioja T, Yoshimura T, Leonard EJ, et al. Expression of monocyte chemoattractant protein 1 in macrophage-rich areas of human and rabbit atherosclerotic lesions. Proc Natl Acad Sci U S A. 1991;88:5252-6.

74. Furukawa Y, Matsumori A, Ohashi N, Shioi T, Ono K, Harada A, et al. Anti-monocyte chemoattractant protein-1/monocyte chemotactic and activating factor antibody inhibits neointimal hyperplasia in injured rat carotid arteries. Circ Res. 1999;84:306-14.

75. Mori E, Komori K, Yamaoka T, Tanii M, Kataoka C, Takeshita A, et al. Essential role of monocyte chemoattractant protein-1 in development of restenotic changes (neointimal hyperplasia and constrictive remodeling) after balloon angioplasty in hypercholesterolemic rabbits. Circulation. 2002;105:2905-10.

76. Horvath C, Welt FG, Nedelman M, Rao P, Rogers C. Targeting CCR2 or CD18 inhibits experimental in-stent restenosis in primates: inhibitory potential depends on type of injury and leukocytes targeted. Circ Res. 2002;90:488-94.

77. Egashira K, Zhao Q, Kataoka C, Ohtani K, Usui M, Charo IF, et al. Importance of monocyte chemoattractant protein-1 pathway in neointimal hyperplasia after periarterial injury in mice and monkeys. Circ Res. 2002;90:1167-72.

78. Ohtani K, Usui M, Nakano K, Kohjimoto Y, Kitajima S, Hirouchi Y, et al. Antimonocyte chemoattractant protein-1 gene therapy reduces experimental in-stent restenosis in hypercholesterolemic rabbits and monkeys. Gene Ther. 2004;11:1273-82.

79. Nakano K, Egashira K, Ohtani K, Zhao G, Funakoshi K, Ihara Y, et al. Catheter-based adenovirus-mediated anti-monocyte chemoattractant gene therapy attenuates in-stent neointima formation in cynomolgus monkeys. Atherosclerosis. 2007;194:309-16.

80. Schepers A, Eefting D, Bonta PI, Grimbergen JM, de Vries MR, van Weel V, et al. Anti-MCP-1

gene therapy inhibits vascular smooth muscle cells proliferation and attenuates vein graft thickening both in vitro and in vivo. Arterioscler Thromb Vasc Biol. 2006;26:2063-9.

81. Tatewaki H, Egashira K, Kimura S, Nishida T, Morita S, Tominaga R. Blockade of monocyte chemoattractant protein-1 by adenoviral gene transfer inhibits experimental vein graft neointimal formation. J Vasc Surg. 2007;45:1236-43.

82. Saiura A, Sata M, Hiasa K, Kitamoto S, Washida M, Egashira K, et al. Antimonocyte chemoattractant protein-1 gene therapy attenuates graft vasculopathy. Arterioscler Thromb Vasc Biol. 2004;24:1886-90.

83. Ikeda Y, Yonemitsu Y, Kataoka C, Kitamoto S, Yamaoka T, Nishida K, et al. Anti-monocyte chemoattractant protein-1 gene therapy attenuates pulmonary hypertension in rats. Am J Physiol Heart Circ Physiol. 2002;283:H2021-8.

84. Juncos JP, Grande JP, Kang L, Ackerman AW, Croatt AJ, Katusic ZS, et al. MCP-1 contributes to arteriovenous fistula failure. J Am Soc Nephrol. 2011;22:43-8.

85. Tesch GH. MCP-1/CCL2: a new diagnostic marker and therapeutic target for progressive renal injury in diabetic nephropathy. Am J Physiol Renal Physiol. 2008;294:F697-701.

86. Shin N, Baribaud F, Wang K, Yang G, Wynn R, Covington MB, et al. Pharmacological characterization of INCB3344, a small molecule antagonist of human CCR2. Biochem Biophys Res Commun. 2009;387:251-5.

87. Watson D, Zheng G, Wu H, Wang YM, Wang Y, Harris DC, et al. CCL2 DNA vaccine to treat renal disease. Int J Biochem Cell Biol. 2009;41:729-32.

88. Jawien A, Bowen-Pope DF, Lindner V, Schwartz SM, Clowes AW. Platelet-derived growth factor promotes smooth muscle migration and intimal thickening in a rat model of balloon angioplasty. J Clin Invest. 1992;89:507-11.

89. Lin H, Chen B, Sun W, Zhao W, Zhao Y, Dai J. The effect of collagen-targeting platelet-derived growth factor on cellularization and vascularization of collagen scaffolds. Biomaterials. 2006;27:5708-14.

90. Rhee S, Grinnell F. P21-activated kinase 1: convergence point in PDGF- and LPA-stimulated collagen matrix contraction by human fibroblasts. J Cell Biol. 2006;172:423-32.

91. Majesky MW, Reidy MA, Bowen-Pope DF, Hart CE, Wilcox JN, Schwartz SM. PDGF ligand and receptor gene expression during repair of arterial injury. J Cell Biol. 1990;111:2149-58.

92. Ferns GA, Raines EW, Sprugel KH, Motani AS, Reidy MA, Ross R. Inhibition of neointimal smooth muscle accumulation after angioplasty by an antibody to PDGF. Science.

1991;253:1129-32.

93. Abbruzzese TA, Guzman RJ, Martin RL, Yee C, Zarins CK, Dalman RL. Matrix metalloproteinase inhibition limits arterial enlargements in a rodent arteriovenous fistula model. Surgery. 1998;124:328-34; discussion 34-5.

94. de Kleijn DP, Sluijter JP, Smit J, Velema E, Richard W, Schoneveld AH, et al. Furin and membrane type-1 metalloproteinase mRNA levels and activation of metalloproteinase-2 are associated with arterial remodeling. FEBS Lett. 2001;501:37-41.

95. Southgate KM, Mehta D, Izzat MB, Newby AC, Angelini GD. Increased secretion of basement membrane-degrading metalloproteinases in pig saphenous vein into carotid artery interposition grafts. Arterioscler Thromb Vasc Biol. 1999;19:1640-9.

96. Rotmans JI, Velema E, Verhagen HJ, Blankensteijn JD, de Kleijn DP, Stroes ES, et al. Matrix metalloproteinase inhibition reduces intimal hyperplasia in a porcine arteriovenous-graft model. J Vasc Surg. 2004;39:432-9.

97. Coussens LM, Fingleton B, Matrisian LM. Matrix metalloproteinase inhibitors and cancer: trials and tribulations. Science. 2002;295:2387-92.

98. Bramhall SR, Rosemurgy A, Brown PD, Bowry C, Buckels JA. Marimastat as first-line therapy for patients with unresectable pancreatic cancer: a randomized trial. J Clin Oncol. 2001;19:3447-55.

99. Paul BZ, Jin J, Kunapuli SP. Molecular mechanism of thromboxane A(2)-induced platelet aggregation. Essential role for p2t(ac) and alpha(2a) receptors. J Biol Chem. 1999;274:29108-14.

100. Connolly E, Bouchier-Hayes DJ, Kaye E, Leahy A, Fitzgerald D, Belton O. Cyclooxygenase isozyme expression and intimal hyperplasia in a rat model of balloon angioplasty. J Pharmacol Exp Ther. 2002;300:393-8.

101. Pei H, Gu J, Thimmalapura PR, Mison A, Nadler JL. Activation of the 12-lipoxygenase and signal transducer and activator of transcription pathway during neointima formation in a model of the metabolic syndrome. Am J Physiol Endocrinol Metab. 2006;290:E92-E102.

102. Belton O, Byrne D, Kearney D, Leahy A, Fitzgerald DJ. Cyclooxygenase-1 and -2-dependent prostacyclin formation in patients with atherosclerosis. Circulation. 2000;102:840-5.

103. Riccioni G, Zanasi A, Vitulano N, Mancini B, D'Orazio N. Leukotrienes in atherosclerosis: new target insights and future therapy perspectives. Mediators Inflamm. 2009;2009:737282.

104. Vidal C, Gomez-Hernandez A, Sanchez-Galan E, Gonzalez A, Ortega L, Gomez-Gerique JA, et al. Licofelone, a balanced inhibitor of cyclooxygenase and 5-lipoxygenase, reduces

inflammation in a rabbit model of atherosclerosis. J Pharmacol Exp Ther. 2007;320:108-16.

105. Beathard GA. Percutaneous transvenous angioplasty in the treatment of vascular access stenosis. Kidney Int. 1992;42:1390-7.

106. Brooks JL, Sigley RD, May KJ, Jr., Mack RM. Transluminal angioplasty versus surgical repair for stenosis of hemodialysis grafts. A randomized study. Am J Surg. 1987;153:530-1.

107. Holmes DR, Jr., Vlietstra RE, Smith HC, Vetrovec GW, Kent KM, Cowley MJ, et al. Restenosis after percutaneous transluminal coronary angioplasty (PTCA): a report from the PTCA Registry of the National Heart, Lung, and Blood Institute. Am J Cardiol. 1984;53:77C-81C.

108. Liu MW, Roubin GS, King SB, 3rd. Restenosis after coronary angioplasty. Potential biologic determinants and role of intimal hyperplasia. Circulation. 1989;79:1374-87.

109. Chang CJ, Ko PJ, Hsu LA, Ko YS, Ko YL, Chen CF, et al. Highly increased cell proliferation activity in the restenotic hemodialysis vascular access after percutaneous transluminal angioplasty: implication in prevention of restenosis. Am J Kidney Dis. 2004;43:74-84.

110. Moist LM, Churchill DN, House AA, Millward SF, Elliott JE, Kribs SW, et al. Regular monitoring of access flow compared with monitoring of venous pressure fails to improve graft survival. J Am Soc Nephrol. 2003;14:2645-53.

111. Dember LM, Holmberg EF, Kaufman JS. Randomized controlled trial of prophylactic repair of hemodialysis arteriovenous graft stenosis. Kidney Int. 2004;66:390-8.

112. Lumsden AB, MacDonald MJ, Kikeri D, Cotsonis GA, Harker LA, Martin LG. Prophylactic balloon angioplasty fails to prolong the patency of expanded polytetrafluoroethylene arteriovenous grafts: results of a prospective randomized study. J Vasc Surg. 1997;26:382-90; discussion 90-2.

113. Quinn SF, Schuman ES, Demlow TA, Standage BA, Ragsdale JW, Green GS, et al. Percutaneous transluminal angioplasty versus endovascular stent placement in the treatment of venous stenoses in patients undergoing hemodialysis: intermediate results. J Vasc Interv Radiol. 1995;6:851-5.

114. Beathard GA. Gianturco self-expanding stent in the treatment of stenosis in dialysis access grafts. Kidney Int. 1993;43:872-7.

115. Haskal ZJ, Trerotola S, Dolmatch B, Schuman E, Altman S, Mietling S, et al. Stent graft versus balloon angioplasty for failing dialysis-access grafts. N Engl J Med. 2010;362:494-503.

116. Rotmans JI, Pattynama PM, Verhagen HJ, Hino I, Velema E, Pasterkamp G, et al. Sirolimus-eluting stents to abolish intimal hyperplasia and improve flow in porcine arteriovenous grafts: a 4-week follow-up study. Circulation. 2005;111:1537-42.

117. Dixon BS, Beck GJ, Vazquez MA, Greenberg A, Delmez JA, Allon M, et al. Effect of dipyridamole plus aspirin on hemodialysis graft patency. N Engl J Med. 2009;360:2191-201.

118. Cagiannos C, Abul-Khoudoud OR, DeRijk W, Shell DHt, Jennings LK, Tolley EA, et al. Rapamycin-coated expanded polytetrafluoroethylene bypass grafts exhibit decreased anastomotic neointimal hyperplasia in a porcine model. J Vasc Surg. 2005;42:980-8.

119. Lee BH, Nam HY, Kwon T, Kim SJ, Kwon GY, Jeon HJ, et al. Paclitaxel-coated expanded polytetrafluoroethylene haemodialysis grafts inhibit neointimal hyperplasia in porcine model of graft stenosis. Nephrol Dial Transplant. 2006;21:2432-8.

120. Lee T, Roy-Chaudhury P. Advances and new frontiers in the pathophysiology of venous neointimal hyperplasia and dialysis access stenosis. Adv Chronic Kidney Dis. 2009;16:329-38.

121. Kelly B, Melhem M, Zhang J, Kasting G, Li J, Krishnamoorthy M, et al. Perivascular paclitaxel wraps block arteriovenous graft stenosis in a pig model. Nephrol Dial Transplant. 2006;21:2425-31.

122. Kohler TR, Toleikis PM, Gravett DM, Avelar RL. Inhibition of neointimal hyperplasia in a sheep model of dialysis access failure with the bioabsorbable Vascular Wrap paclitaxel-eluting mesh. J Vasc Surg. 2007;45:1029-37; discussion 37-8.

123. Owen SC, Li H, Sanders WG, Cheung AK, Terry CM. Correlation of tissue drug concentrations with in vivo magnetic resonance images of polymer drug depot around arteriovenous graft. J Control Release. 2010;146:23-30.

124. Kuji T, Masaki T, Goteti K, Li L, Zhuplatov S, Terry CM, et al. Efficacy of local dipyridamole therapy in a porcine model of arteriovenous graft stenosis. Kidney Int. 2006;69:2179-85.

125. Nugent HM, Sjin RT, White D, Milton LG, Manson RJ, Lawson JH, et al. Adventitial endothelial implants reduce matrix metalloproteinase-2 expression and increase luminal diameter in porcine arteriovenous grafts. J Vasc Surg. 2007;46:548-56.

126. Conte MS, Nugent HM, Gaccione P, Guleria I, Roy-Chaudhury P, Lawson JH. Multicenter phase I/II trial of the safety of allogeneic endothelial cell implants after the creation of arteriovenous access for hemodialysis use: the V-HEALTH study. J Vasc Surg. 2009;50:1359-68 e1.

127. Deutsch M, Meinhart J, Fischlein T, Preiss P, Zilla P. Clinical autologous in vitro endothelialization of infrainguinal ePTFE grafts in 100 patients: a 9-year experience. Surgery. 1999;126:847-55.

128. Rotmans JI, Heyligers JM, Verhagen HJ, Velema E, Nagtegaal MM, de Kleijn DP, et al. In vivo cell seeding with anti-CD34 antibodies successfully accelerates endothelialization but stimulates

intimal hyperplasia in porcine arteriovenous expanded polytetrafluoroethylene grafts. Circulation. 2005;112:12-8.

129. Sirois MG, Simons M, Edelman ER. Antisense oligonucleotide inhibition of PDGFR-beta receptor subunit expression directs suppression of intimal thickening. Circulation. 1997;95:669-76.

130. Kipshidze N, Keane E, Stein D, Chawla P, Skrinska V, Shankar LR, et al. Local delivery of c-myc neutrally charged antisense oligonucleotides with transport catheter inhibits myointimal hyperplasia and positively affects vascular remodeling in the rabbit balloon injury model. Catheter Cardiovasc Interv. 2001;54:247-56.

131. Simons M, Edelman ER, Rosenberg RD. Antisense proliferating cell nuclear antigen oligonucleotides inhibit intimal hyperplasia in a rat carotid artery injury model. J Clin Invest. 1994;93:2351-6.

132. Morishita R, Gibbons GH, Ellison KE, Nakajima M, von der Leyen H, Zhang L, et al. Intimal hyperplasia after vascular injury is inhibited by antisense cdk 2 kinase oligonucleotides. J Clin Invest. 1994;93:1458-64.

133. Takeuchi K, Itoh H, Yonemitsu Y, Matsumoto T, Kume M, Komori K, et al. In vivo reduction of the nuclear factor-kappaB activity using synthetic cis-element decoy oligonucleotides suppresses intimal hyperplasia in the injured carotid arteries in rabbits. Surg Today. 2007;37:575-83.

134. Ahn JD, Morishita R, Kaneda Y, Kim HS, Chang YC, Lee KU, et al. Novel E2F decoy oligodeoxynucleotides inhibit in vitro vascular smooth muscle cell proliferation and in vivo neointimal hyperplasia. Gene Ther. 2002;9:1682-92.

135. Alexander JH, Hafley G, Harrington RA, Peterson ED, Ferguson TB, Jr., Lorenz TJ, et al. Efficacy and safety of edifoligide, an E2F transcription factor decoy, for prevention of vein graft failure following coronary artery bypass graft surgery: PREVENT IV: a randomized controlled trial. JAMA. 2005;294:2446-54.

136. Conte MS, Bandyk DF, Clowes AW, Moneta GL, Seely L, Lorenz TJ, et al. Results of PREVENT III: a multicenter, randomized trial of edifoligide for the prevention of vein graft failure in lower extremity bypass surgery. J Vasc Surg. 2006;43:742-51; discussion 51.

137. Mann MJ, Dzau VJ. Therapeutic applications of transcription factor decoy oligonucleotides. J Clin Invest. 2000;106:1071-5.

138. Hiltunen MO, Laitinen M, Turunen MP, Jeltsch M, Hartikainen J, Rissanen TT, et al. Intravascular adenovirus-mediated VEGF-C gene transfer reduces neointima formation in balloon-denuded rabbit aorta. Circulation. 2000;102:2262-8.

139. Bhardwaj S, Roy H, Heikura T, Yla-Herttuala S. VEGF-A, VEGF-D and

VEGF-D(DeltaNDeltaC) induced intimal hyperplasia in carotid arteries. Eur J Clin Invest. 2005;35:669-76.

140. Walpoth BH, Zammaretti P, Cikirikcioglu M, Khabiri E, Djebaili MK, Pache JC, et al. Enhanced intimal thickening of expanded polytetrafluoroethylene grafts coated with fibrin or fibrin-releasing vascular endothelial growth factor in the pig carotid artery interposition model. J Thorac Cardiovasc Surg. 2007;133:1163-70.

141. Kawatsu S, Oda K, Saiki Y, Tabata Y, Tabayashi K. External application of rapamycin-eluting film at anastomotic sites inhibits neointimal hyperplasia in a canine model. Ann Thorac Surg. 2007;84:560-7; discussion 7.

142. Holmes DR, Jr., Leon MB, Moses JW, Popma JJ, Cutlip D, Fitzgerald PJ, et al. Analysis of 1-year clinical outcomes in the SIRIUS trial: a randomized trial of a sirolimus-eluting stent versus a standard stent in patients at high risk for coronary restenosis. Circulation. 2004;109:634-40.

143. Morice MC, Serruys PW, Barragan P, Bode C, Van Es GA, Stoll HP, et al. Long-term clinical outcomes with sirolimus-eluting coronary stents: five-year results of the RAVEL trial. J Am Coll Cardiol. 2007;50:1299-304.

144. Grube E, Gerckens U, Muller R, Bullesfeld L. Drug eluting stents: initial experiences. Z Kardiol. 2002;91 Suppl 3:44-8.

145. Tanabe K, Serruys PW, Grube E, Smits PC, Selbach G, van der Giessen WJ, et al. TAXUS III Trial: in-stent restenosis treated with stent-based delivery of paclitaxel incorporated in a slow-release polymer formulation. Circulation. 2003;107:559-64.

146. Weissman NJ, Ellis SG, Grube E, Dawkins KD, Greenberg JD, Mann T, et al. Effect of the polymer-based, paclitaxel-eluting TAXUS Express stent on vascular tissue responses: a volumetric intravascular ultrasound integrated analysis from the TAXUS IV, V, and VI trials. Eur Heart J. 2007;28:1574-82.

147. Hong MK, Mintz GS, Lee CW, Song JM, Han KH, Kang DH, et al. Paclitaxel coating reduces in-stent intimal hyperplasia in human coronary arteries: a serial volumetric intravascular ultrasound analysis from the Asian Paclitaxel-Eluting Stent Clinical Trial (ASPECT). Circulation. 2003;107:517-20.

148. Gershlick A, De Scheerder I, Chevalier B, Stephens-Lloyd A, Camenzind E, Vrints C, et al. Inhibition of restenosis with a paclitaxel-eluting, polymer-free coronary stent: the European evaLUation of pacliTaxel Eluting Stent (ELUTES) trial. Circulation. 2004;109:487-93.

149. Lipke EA, West JL. Localized delivery of nitric oxide from hydrogels inhibits neointima formation in a rat carotid balloon injury model. Acta Biomater. 2005;1:597-606.

150. Cornwell TL, Arnold E, Boerth NJ, Lincoln TM. Inhibition of smooth muscle cell growth by nitric oxide and activation of cAMP-dependent protein kinase by cGMP. Am J Physiol. 1994;267:C1405-13.

151. Seki J, Nishio M, Kato Y, Motoyama Y, Yoshida K. FK409, a new nitric-oxide donor, suppresses smooth muscle proliferation in the rat model of balloon angioplasty. Atherosclerosis. 1995;117:97-106.

152. Groves PH, Banning AP, Penny WJ, Newby AC, Cheadle HA, Lewis MJ. The effects of exogenous nitric oxide on smooth muscle cell proliferation following porcine carotid angioplasty. Cardiovasc Res. 1995;30:87-96.

153. Do YS, Kao EY, Ganaha F, Minamiguchi H, Sugimoto K, Lee J, et al. In-stent restenosis limitation with stent-based controlled-release nitric oxide: initial results in rabbits. Radiology. 2004;230:377-82.

154. Hou D, Narciso H, Kamdar K, Zhang P, Barclay B, March KL. Stent-based nitric oxide delivery reducing neointimal proliferation in a porcine carotid overstretch injury model. Cardiovasc Intervent Radiol. 2005;28:60-5.

155. Myllarniemi M, Frosen J, Calderon Ramirez LG, Buchdunger E, Lemstrom K, Hayry P. Selective tyrosine kinase inhibitor for the platelet-derived growth factor receptor in vitro inhibits smooth muscle cell proliferation after reinjury of arterial intima in vivo. Cardiovasc Drugs Ther. 1999;13:159-68.

156. Boucher P, Gotthardt M, Li WP, Anderson RG, Herz J. LRP: role in vascular wall integrity and protection from atherosclerosis. Science. 2003;300:329-32.

157. Li L, Blumenthal DK, Masaki T, Terry CM, Cheung AK. Differential effects of imatinib on PDGF-induced proliferation and PDGF receptor signaling in human arterial and venous smooth muscle cells. J Cell Biochem. 2006;99:1553-63.

158. Faivre S, Demetri G, Sargent W, Raymond E. Molecular basis for sunitinib efficacy and future clinical development. Nat Rev Drug Discov. 2007;6:734-45.

159. Node K, Huo Y, Ruan X, Yang B, Spiecker M, Ley K, et al. Anti-inflammatory properties of cytochrome P450 epoxygenase-derived eicosanoids. Science. 1999;285:1276-9.

160. Sun J, Sui X, Bradbury JA, Zeldin DC, Conte MS, Liao JK. Inhibition of vascular smooth muscle cell migration by cytochrome p450 epoxygenase-derived eicosanoids. Circ Res. 2002;90:1020-7.

161. Krotz F, Riexinger T, Buerkle MA, Nithipatikom K, Gloe T, Sohn HY, et al. Membrane-potential-dependent inhibition of platelet adhesion to endothelial cells by

epoxyeicosatrienoic acids. Arterioscler Thromb Vasc Biol. 2004;24:595-600.

162. Kim IH, Heirtzler FR, Morisseau C, Nishi K, Tsai HJ, Hammock BD. Optimization of amide-based inhibitors of soluble epoxide hydrolase with improved water solubility. J Med Chem. 2005;48:3621-9.

163. Morisseau C, Goodrow MH, Dowdy D, Zheng J, Greene JF, Sanborn JR, et al. Potent urea and carbamate inhibitors of soluble epoxide hydrolases. Proc Natl Acad Sci U S A. 1999;96:8849-54.

164. Schmelzer KR, Kubala L, Newman JW, Kim IH, Eiserich JP, Hammock BD. Soluble epoxide hydrolase is a therapeutic target for acute inflammation. Proc Natl Acad Sci U S A. 2005;102:9772-7.

165. Olearczyk JJ, Quigley JE, Mitchell BC, Yamamoto T, Kim IH, Newman JW, et al. Administration of a substituted adamantyl urea inhibitor of soluble epoxide hydrolase protects the kidney from damage in hypertensive Goto-Kakizaki rats. Clin Sci (Lond). 2009;116:61-70.

CHAPTER 2

ANTI-INFLAMMATORY EFFECTS OF A PHARMACOLOGICAL INHIBITOR OF SOLUBLE EPOXIDE HYDROLASE

2.1 Introduction

The eicosanoid signaling molecules, epoxyeicosatrienoic acids (EETs), are products of the epoxidation of arachidonic acid by cytochrome P450 enzymes. EETs have anti-inflammatory properties and are important modulators of vascular function. For example, EETs are reported to inhibit the activation of nuclear factor kappa B (NF-κB) (1), a key transcription factor involved in the expression of numerous pro-inflammatory genes. EETs inhibit the expression of vascular cell adhesion molecule-1 (VCAM-1) in human endothelial cells in response to tumor necrosis factor-alpha (TNF-α), interleukin-1-alpha (IL-1α), or lipopolysaccharide (LPS) (1). EETs also induce vasodilation (2-4), inhibit the migration of rat aortic vascular smooth muscle cells in response to platelet-derived growth factor (5), inhibit platelet aggregation and activation (6), and induce endothelial cell proliferation (7). However, the intracellular enzyme soluble epoxide hydrolase (sEH) quickly metabolizes EETs to the less active dihydroxyeicosatrienoic acids (DHETs). Soluble epoxide hydrolase is broadly distributed in mammalian tissue although liver has the highest activity (8). Potent and selective pharmacological inhibitors (soluble epoxide hydrolase inhibitors or sEHI) have been developed (9, 10) and have been shown in some animal

models to have anti-hypertensive effects and to protect against end-organ damage due to hypertension and other cardiovascular disease (11). In addition, systemic exposure to sEHIs have been reported to (i) prevent mortality and reduce plasma levels of IL-6 and monocyte chemotactic protein-5 (MCP-5) in mice after intraperitoneal injection of a typically lethal dose of LPS (12), (ii) decrease macrophage recruitment to glomeruli in hypertensive rats (13), (iii) decrease the number of inflammatory cells present in bronchial lavage samples from rats exposed to tobacco smoke (14), (iv) and significantly inhibit urinary monocyte chemotactic protein-1 (MCP-1) levels in a rat model of hypertension (15). Together these data support the notion that sEHIs may be anti-inflammatory and could be particularly useful in the treatment of vascular inflammation.

Inflammation likely plays a role in the pathology of many vascular disorders such as atherosclerosis (16), restenosis after balloon angioplasty of stenotic lesions (17), failure of vein bypass grafts (18, 19), and the development of hyperplasia within vascular accesses for chronic hemodialysis (20, 21). Chronic hemodialysis requires access to high rates of blood flow, often achieved by the placement of synthetic tubing between an artery and a vein. Unfortunately approximately 50% of such synthetic vascular accesses fail due to stenosis at the juncture of the vein and graft, and treatment strategies are needed to inhibit graft failure. In the current work we characterized inflammation and sEH expression in an animal model of synthetic vascular access graft stenosis. We then tested the effects of sEHI on the release of various inflammatory chemokine/cytokines from primary human monocyte/macrophages with the goal of determining if sEHIs could be an effective treatment for hemodialysis vascular access graft stenosis. To our

knowledge this is the first report on the effects of sEHI on the production of inflammatory cytokines/chemokines from isolated monocyte/macrophages.

2.2 Materials and Methods

2.2.1 Materials

sEHI cis-4-{4-[3(4-trifluoromethoxyphenyl)ureido]cyclohexyloxy}-benzoic acid (c-TUCB) (Figure 2.1) was synthesized by the laboratory of Dr. Bruce Hammock (22). Epoxyeicosatrienoic acids (EETs) 8,9-EET, 11,12-EET and 14,15-EET were purchased from Caymen Chemical (Ann Arbor, MI). Flow cytometry antibodies were purchased from BD Biosciences (San Jose, CA). Serum free media (SFM) was from Invitrogen (Grand Island, NY). Lipopolysaccharide (LPS) (055:B5) was from Sigma-Aldrich (St. Louis, MO). Polyclonal rabbit anti-porcine-sEH antibody (23) for tissue immunostaining was generated in the laboratory of Dr. Bruce Hammock against recombinant porcine sEH. Polyclonal rabbit anti-human sEH antibody raised against an internal region of human sEH and blocking peptide (Santa Cruz, CA) were used for immunocytochemical staining and western immunoblotting. Polyclonal rabbit anti-human CD3, polyclonal rabbit anti-human myeloperoxidase, and polyclonal rabbit anti-human PAX5 were from Cell Marque (Rocklin MA). Polyclonal rabbit anti-pig MCP-1 (CCL2) was from Bethyl Laboratories (Montgomery, TX). Monoclonal mouse anti-pig phospho-inhibitory κB (IκB), monoclonal rabbit anti-human NF-κB p65, and polyclonal rabbit anti-human phospho-stress activated protein kinase (SAPK)/C-terminal and anti-human phospho-Jun N-terminal kinase (JNK) (Thr183/Tyr185) were

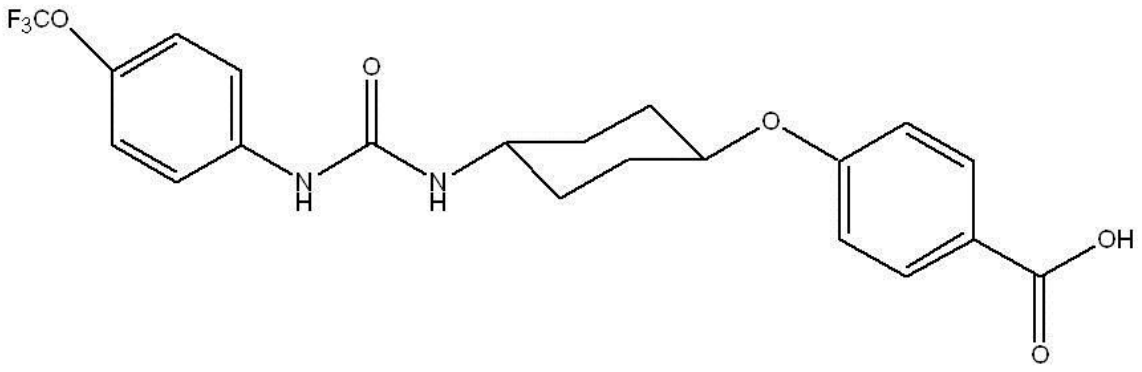

Figure 2.1 Chemical structure of c-TUCB

purchased from Cell Signaling Technology (Danvers MA).

2.2.2 Animal Model

A porcine arteriovenous (AV) expanded polytetrafluoroethylene (ePTFE) graft model was utilized as described in previous studies (24). Briefly, three month old Yorkshire cross-domestic swine (~30kg) were anesthetized using a mixture of ketamine (4mg/kg; Hospira Inc., Lake Forest, IL), xylazine (4 mg/kg; Lloyd Laboratories, Shenandoah, IA), and tiletamine/zolazepam (4mg/kg; Fort Dodge Animal Health, Fort Dodge, IA). To maintain anesthesia, 1-3% isoflurane was administered via tracheal intubation. Sodium heparin (100 U/kg) was given by a bolus intravenous injection intra-operatively. Sterile spiral reinforced ePTFE graft (7-cm in length, 6-mm internal diameter) was sutured in place between the ipsilateral external jugular vein and the common carotid artery. After verification of patency and hemostasis, the wound was closed and the animals were maintained until euthanasia as indicated below. All animal work was performed using protocols approved by the Institutional Animal Care and Use Committee of the University of Utah and Veterans Affairs Salt Lake City Healthcare System and followed guidelines specified by the Guidelines for the Care and Use of Laboratory Animals.

The animals were euthanized at designated time points: 1 day, and 1, 2, 3, 4, 6, and 7 weeks after graft placement. The graft with connected artery and vein were explanted en bloc, fixed, and embedded in paraffin as previously described (24, 25). Briefly, after surgical exposure of the grafts in anesthetized animals, heparin was administered (200 U/kg), the artery was cannulated and the lumen of the grafts and adjoining artery and vein were rinsed with saline. The animals

were euthanized by intravenous injection of pentobarbital sodium (80-100 mg/kg) and the grafts and attached vessels were perfused in situ with 10% zinc formalin. The artery and veins were ligated under physiologic pressure to maintain lumen circumference then explanted en bloc and further fixed in formalin overnight. The tissue was paraffin-embedded and 5-μm sections were cut perpendicular to the vein lumen (as illustrated in Figure 2.2) and processed for immunostaining using standard techniques.

2.2.3 Neointimal hyperplasia (NH) Index

The surface area of hyperplastic tissue within 5-μm cross-sections of the AV graft was manually quantified in tissue stained with Elastin von Gieson as previously described (25). The NH index was defined as: the sum of the intimal hyperplasia within the lumen of the ePTFE graft (region delineated by dashed lines in Figure 2.2A) and the hyperplasia within the native vein wall, and divided by the sum of the medial area in the native vein wall and the PTFE graft area in the same tissue cross-section. The hyperplastic tissue area was divided by the medial and PTFE graft area to normalize for the angle at which the tissue section was obtained.

2.2.4 Tissue Immunostaining

Formalin-fixed paraffin-embedded tissue sections from the vein-graft anastomosis region were dewaxed and rehydrated following standard protocols. Tissue sections were immunostained with anti-CD3 (1:1000), anti-PAX-5 (undiluted), and anti-myeloperoxidase (1:1000) antibodies to detect T lymphocytes, B lymphocytes, and neutrophils respectively. Immunostaining with anti-MCP-1 (1:100), anti-sEH (1:400) and anti-phospho-IκB (1:200) was performed on control

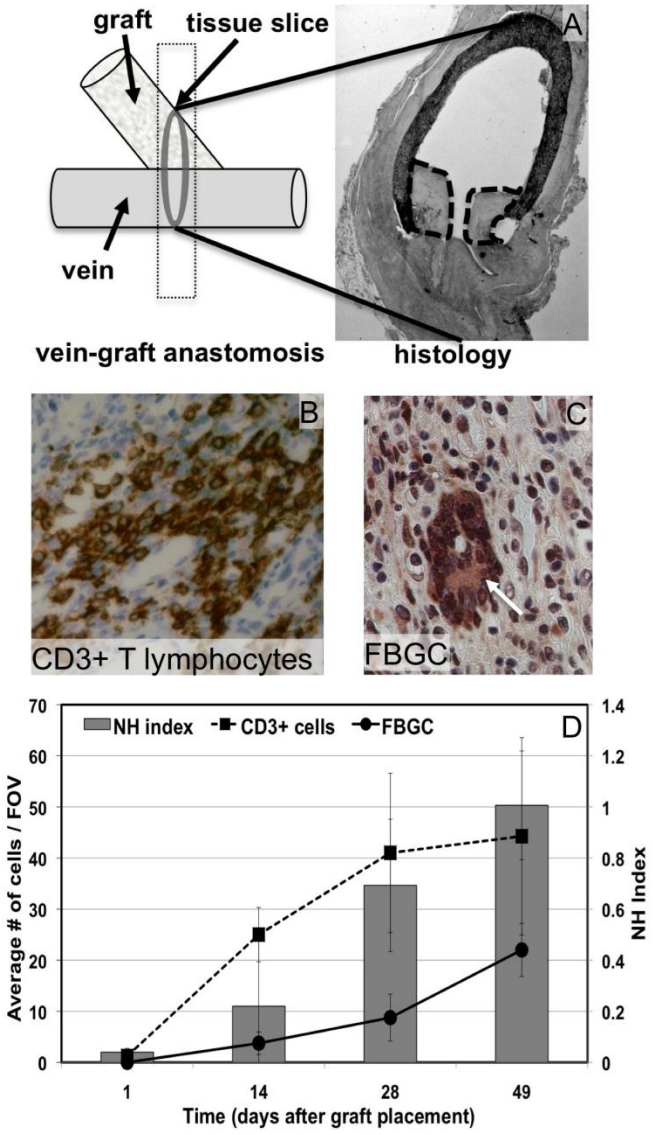

Fig 2.2 Foreign body giant cell (FBGC) and T-lymphocyte accumulation in AV graft hyperplasia. Hyperplastic tissue (outlined by the dashed line in "A") in histological cross-sections obtained from pigs euthanized at various time points after graft placement (one to 49 days) was assessed for T-lymphocytes by immunostaining with anti-CD3 antibody ('B' rust color), and FBGC, by immunostaining with anti-phospho-IκB followed by visual assessment of multinucleated cells ('C' white arrow). CD3+ cells and FBGC accumulation in the vein-graft anastomoses was plotted over time (left y-axis) (D). Neointimal hyperplasia (NH) was assessed in tissue sections as described in Methods and plotted over time (right y-axis) and correlated with inflammatory cell accumulation (D). FOV=field of view.

ungrafted porcine external jugular vein, and vein-graft anastomotic tissue collected at 1 day and 1, 2, 3, 4, 6 and 7 weeks after graft placement. For T and B lymphocyte, neutrophil detection and phospho-IκB detection, antigen retrieval was performed in Trilogy solution (CellMarque) by heating at 100 ^{o}C for 15 min (EZ retriever system, BioGenex Laboratories Inc., San Ramon, CA). Tissue sections were blocked with 2% goat serum for one hr at room temperature (RT) and incubated with antibodies at 4 ^{o}C overnight. Antibody binding was detected with HRP-conjugated anti-rabbit and DAB chromogen following the manufacturer's protocol (Envision Systems, DAKO, Carpenteria, CA) and sections were counterstained with hemotoxylin. For MCP-1 expression, a previously published protocol with minor modifications was followed (26). Briefly, heat-induced antigen retrieval was performed on tissue sections by heating to 95 ^{o}C for 15 min in Tris-EDTA buffer (pH 9.0) (EZ-Retriever System). Tissue sections were blocked with 2% goat serum for 1 hr at RT and then incubated with antibody overnight at 4 ^{o}C. Sections were then washed three times with 0.05%Tween/PBS and incubated with biotinylated anti-rabbit IgG (1:200) for 1 hr at RT followed by incubation with streptavidin Alexa-fluor 546 (1:200) (Invitrogen, Carlsbad, CA) for 1 hr at RT in the dark. Nuclei were stained using DAPI Fluoromount (Southern Biotech, Birmingham, AL).

2.2.5 Monocyte Isolation and Cell Culture

Peripheral blood mononuclear cells (PBMC) were obtained from the heparin anticoagulated blood of healthy adult volunteers using Ficoll-Hypaque (GE Healthcare, Piscataway, NJ) density gradient centrifugation following the manufacturer's protocol. Monocytes were isolated by adherence to tissue culture plastic during a 2-hr incubation in SFM culture media plus 20% autologous serum. The non-adherent cells were then removed by repeat washing with 1x

phosphate-buffered saline (PBS). The remaining adherent cell population was enriched in monocytes as determined by flow cytometry assessment of immunostained cells using standard techniques; typically ≥70% monocytes, ≤10% CD3+ T-lymphocytes, ≤1% B-lymphocytes, ≤8% natural killer cells, and <1% neutrophils were observed in each isolation. Isolation of PBMCs from blood from adult volunteers was performed using protocols approved by the Institutional Review Board of the University of Utah and Veterans Affairs Salt Lake City Healthcare System.

The adherent cells were dislodged from the plastic after incubation for 15 min with calcium- and magnesium-free PBS then counted and seeded into 96-well culture plates (5×10^4 cells/0.3 cm^2) in SFM with 20% autologous serum. c-TUCB was dissolved in dimethylsulfoxide (DMSO). Monocytes were pretreated with either DMSO or ethanol solvent alone, c-TUCB (5 μM) dissolved in DMSO, EETs (100 nM) dissolved in ethanol, or both c-TUCB and EETs for 1 hr before LPS stimulation. The concentration of solvent was always kept below 0.1%. After pretreatment, monocytes were stimulated with LPS (10 ng/mL) for 24 hr at 37 ^oC. Media was then collected and stored at -80 ^oC for later chemokine/cytokine quantification by ELISA. Media alone and monocytes without LPS treatment were used as controls.

2.2.6 Chemokine/cytokine Quantification by ELISA.

Media from the tissue culture experiments was assayed for IL-6, MCP-1, macrophage inflammatory protein-1α (MIP-1α), and TNF-α using commercially available ELISA kits (PeproTech, Rocky Hill, NJ) in accordance with the manufacturer protocols. The ELISA detection range for IL-6 was 32-2000 pg/mL, MCP-1 was 8-1000 pg/mL, MIP-1α was 16-3000 pg/mL, and TNF-α was

16-2000 pg/mL. The measured chemokine/cytokine concentrations produced with each drug treatment in the presence of LPS was expressed as a percentage of that seen with treatment of LPS alone.

2.2.7 Cell Immunostaining

sEH expression was detected in the mononuclear cell population after plating cells at 1.2 x 10^6 /1.8 cm^2 in 4-well chamber slides (Lab-Tek, Nunc, Rochester, NY) in SFM with 20% autologous serum. After 2 hr, the nonadherent cells were removed by sequential washing with PBS. The adherent cells (majority monocytes) were then fixed in 2% paraformaldehyde (15 min at RT), washed with PBS, permeabilized using PBS + 0.1% Triton-x100 + 0.5% BSA (PBST) for 30 min at RT, and incubated with anti-human-sEH antibody (1:200) alone or in the presence of blocking peptide overnight at 4 ^oC. Primary sEH antibody binding was detected as described above for MCP-1 detection except streptavidin Alexa-fluor 546 was carried out at a 1:500 dilution.

Expression and cellular location of NF-κB and phospho-JNK was detected as follows: A monocyte-enriched cell population was cultured in SFM with 20% autologous serum for 3 days to convert to a macrophage phenotype before removing serum and starving for 48 hr. The cells were then pretreated with vehicle or c-TUCB (5 μM) alone for 1 hr. Cells were then exposed to LPS (10 ng/mL) for 5, 15 or 45 min then fixed with 2% paraformaldehyde. Fixed cells were immunostained with anti-NF-κB (1:100) or phospho-JNK (1:100) using the same antibody binding detection procedure described above for sEH. The same experiments were repeated on monocyte/macrophages that did not undergo the three day culturing to convert to a complete

macrophage phenotype, but were adhered for 2 hr, washed then pretreated with sEHI for 1 hr, and exposed to LPS and fixed as described above.

2.2.8 Foreign Body Giant Cell Detection

A number of antibodies reported to be specific for macrophages were tested for cross-reactivity against porcine macrophages. No antibody tested was found to be sufficiently specific for reliable quantification of macrophages in the paraffin-embedded porcine tissue sections. Foreign body giant cells, which occur in response to frustrated phagocytosis and are formed by the fusion of multiple macrophages, were thus used as a measure of macrophage recruitment to the vein-graft anastomosis region. Phosphorylation of inhibitory kappa B (IκB) releases NF-κB for translocation to the nucleus and subsequent transcription of genes involved in inflammation. To determine the activation state of the FBGCs, tissue sections were stained with anti-phospho-IκB. FBGC accumulation in the AV graft anastomotic regions was assessed by visual microscopic inspection of the stained tissue sections and a cell was counted as a FBGC if it contained two or more nuclei regardless if it stained positive for phospho-IκB. Four field of views (FOV) at 40x magnification were counted in each tissue section and the number of FBGC in the four fields of view were averaged.

2.2.9 Western Immunoblot Analysis for sEH Protein

The monocyte-enriched cell population was isolated by Ficoll-Hypaque as described above. Adherent cells were lysed with RIPA buffer containing a protease inhibitor cocktail (Complete mini, Roche Diagnostic, Mannheim, Germany). The cells were sonicated, soluble lysate collected by

centrifugation, and protein concentrations were determined using the bicinchoninic acid (BCA) assay (Pierce, Rockford, IL). Twenty μg of lysate were resolved on 4-12% NuPAGE® Bis-Tris polyacrylamide gels (Invitrogen). The resolved protein was then electroblotted onto nitrocellulose membranes (Invitrogen, Carlsbad, CA). Membranes were blocked in 5% nonfat dry milk for 1 hr at RT and then incubated with anti-human-sEH antibody (1:2000) alone or in the presence of blocking peptide overnight at 4 ^{o}C. The antibody binding was detected by incubation with anti-rabbit IgG-horseradish peroxidase (HRP) (Santa Cruz Biotechnology) and chemiluminescence substrate following manufacturer protocols (Supersignal® West Dura Extended Duration Substrate kit, Thermo Scientific, Rockford, IL). Western blot was quantified using densitometry analysis (ImageJ, NIH, Bethesda, MD).

2.2.10 Cell Harvest and Culture from Wild-type and sEH Knockout Mice

Procedures and animal care were approved by the Institutional Animal Care and Use Committee of the University of Utah. Wild-type (WT) C57BL/6 mice (Jackson Labs, Sacramento, CA) and Ephx2 gene deleted mice (Ephx2-/-) (sEH knockout) were utilized for bone marrow cell harvest. Bone marrow cells (BMCs) were harvested from femurs and tibias of both WT and Ephx2-/- mice and differentiated into bone marrow macrophages (BMMΦ) as described previously (27, 28). Briefly, isolated BMCs were plated in BMMΦ media (Dulbecco's modified Eagle's medium (DMEM, Invitrogen) containing 10% L929 conditioned media, 10% fetal calf serum (FCS), 1% non-essential amino acids, 1% sodium pyruvate, 1% HEPES, and antibiotic/antimycotics) for ten days, allowing the cells to mature to a macrophage phenotype. Cells were seeded at 5 x 10^4

cells/0.3 cm^2 in 96 well plates in SFM with 20% FCS. BMMΦs were pretreated with c-TUCB, EETs, or both, or solvent alone and stimulated with LPS (10 ng/mL) following the same protocol mentioned above for human monocytes. After 24 hr, media was then collected from each well and stored at -80 ^oC for later MCP-1 quantification by ELISA. To serve as controls, media alone and BMMΦs without LPS treatment were used.

2.2.11 Statistical Analysis

Data presented for inflammatory cell accumulation was expressed as mean ± SD. For cytokine release studies, cytokine release from cells treated with LPS alone was set as 100% and results from other treatments (LPS plus c-TUCB or LPS plus c-TUCB plus EETs) were calculated as percent of LPS alone ± SD. All statistical analyses were performed on the log scale and results were exponentiated to express results as ratio of geometric means. For the human and mouse data, LPS plus c-TUCB vs. LPS alone and LPS plus c-TUCB plus EETs vs. LPS alone were the two primary comparisons analyzed for each cytokine/chemokine. Mixed effects analysis of variance were used, treating the individual or mouse as a random effect and treatment as a fixed effect, nesting the individual mouse within the mouse type (WT vs. KO) for the mice data, significance was determined using the Holm-Bonferroni procedure for each cytokine/chemokine tested in humans and MCP-1 in mice. For the mice data, cytokine release from LPS alone in WT vs. LPS alone in the KO mice and basal cytokine release from untreated WT vs. untreated KO were also compared by 2-sample unpaired t-tests.

2.3 Results

2.3.1 Inflammatory Cells Infiltrate the Vein-graft Anastomosis in the Porcine AV Graft Model

Both CD3+ cells (T lymphocytes) (Figure 2.2B) and foreign body giant cells (FBGC) (macrophages) (Figure 2.2C), accumulated at the vein-graft anastomotic region near the graft material preceding or in parallel with the accumulation of hyperplasia as indicated in Figure 2.2D. The majority of FBGC stained positive for phospho-IκB expression (data not shown) as determined by visual assessment of multiple tissue sections suggesting activation of NF-κB.Neutrophil infiltration was observed around the graft sutures within the first week after graft placement, but their presence declined rapidly thereafter (data not shown). Sporadic clusters of B-lymphocytes were occasionally observed in the hyperplastic tissue at various time points (data not shown).

2.3.2 sEH Expression is Upregulated in the Vein-graft Anastomosis Tissue

Figure 2.3 shows sEH expression was low in ungrafted porcine external jugular vein, but markedly increased over time in tissue collected from the vein-graft anastomosis region in the porcine model. sEH expression was first upregulated in the media of the native vessel of the vein-graft anastomosis but by one week sEH expression was observed in both adventitia and media.

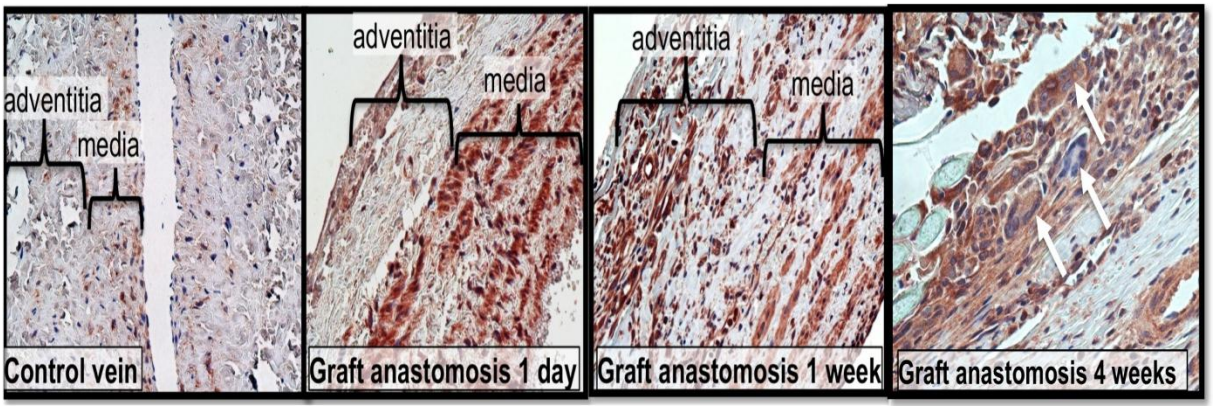

Figure 2.3 sEH expression as assessed by immunohistochemical staining in the porcine model of AV graft stenosis. The expression of sEH protein increased in the vein-graft anastomotic tissue over time after graft placement (rust color indicates antibody binding; tissue was collected 1 day, 1 week and 4 weeks after graft placement). The majority of FBGC (white arrows last frame) stained positive for sEH expression but some FBGC showed low sEH expression (middle arrow).

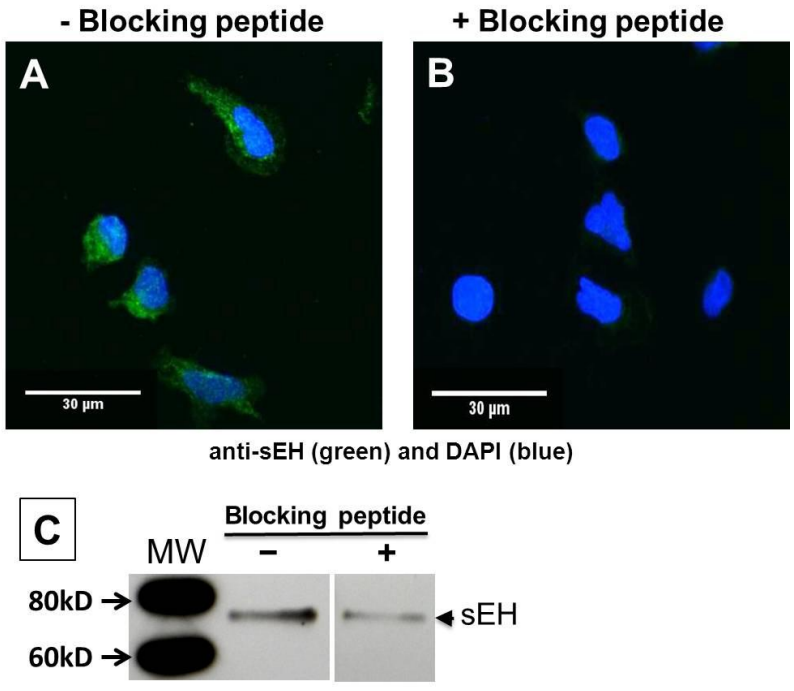

Figure 2.4. sEH expression in human monocytes. Confocal images (60x) of immunocytofluorescence of human adherent monocytes immunostained with anti-sEH (green) (A) alone or (B) in the presence of sEH blocking peptide merged with the fluorescence of the nuclear marker, DAPI (blue). C) Western immunoblot analysis of lysate from human monocytes. Blocking peptide decreased sEH staining in both confocal images and western blotting indicating staining was specific for sEH.

2.3.3 Human Adherent Monocytes Express sEH

Adherent human monocytes stained strongly for sEH protein in the cytoplasm but also somewhat in the nuclei (Figure 2.4A-B) similar to what others have recently reported in rat neutrophils, macrophages, and brain cortical astrocytes (29, 30). Western immunoblotting confirmed sEH expression in human monocytes (Figure 2.4C). Incubating with blocking peptide decreased sEH staining as seen by both confocal and western blotting (decreased by ~60% determined by densitometry), signifying that staining was specific for sEH.

2.3.4 Chemokine/cytokine Expression is Upregulated in Porcine Tissue

TNF-α expression, as evaluated by visual assessment of immunohistochemical staining, increased after graft placement from a low level at day 1, similar to that seen in control vein, to increasing, widespread expression in the hyperplastic tissue out to seven weeks after placement (data not shown). Expression of TNF-α was often more intense in FBGC than surrounding tissue (Figure 2.5). Immunofluorescent staining for MCP-1 protein was performed on paraffin-embedded tissue from the anastomosis at 1 week, 2 weeks, 3 weeks, and 6 weeks after graft placement. MCP-1 staining in control vein was minimal whereas the vein-graft anastomosis tissue had elevated expression of MCP-1 by one week (Figure 2.6) that remained elevated at six weeks which was the latest time point tested (data not shown).

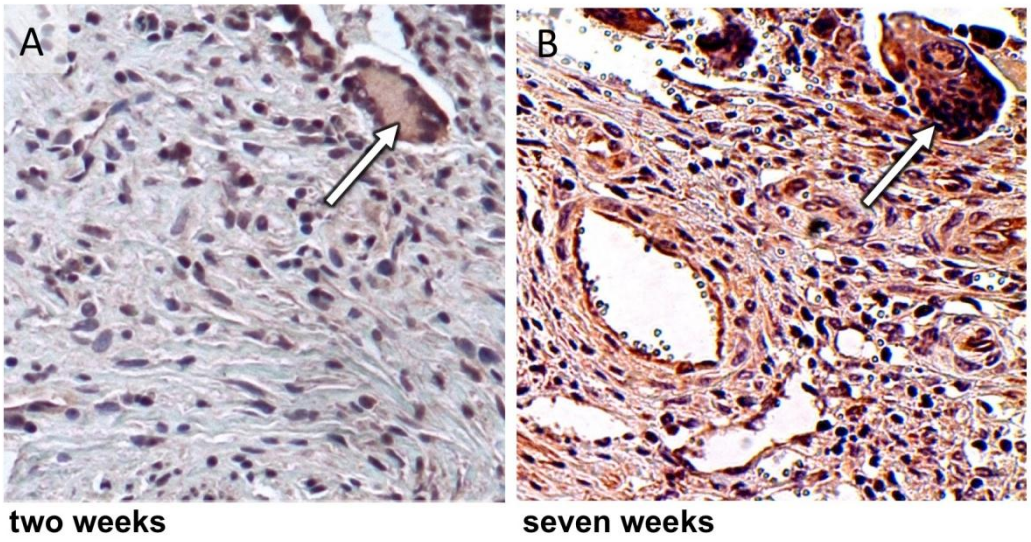

Figure 2.5 TNF-α expression in hyperplastic tissue of the porcine vein-graft anastomosis. (A) Tissue obtained at 2 weeks after graft placement had moderate expression of TNF-α (rust color) but expression in FBGC (white arrow) was typically enhanced above surrounding tissue. (B) Tissue obtained at 7 weeks after graft placement had high expression of TNF-α but expression in FBGC (white arrow) was still often elevated above that seen in surrounding tissue.

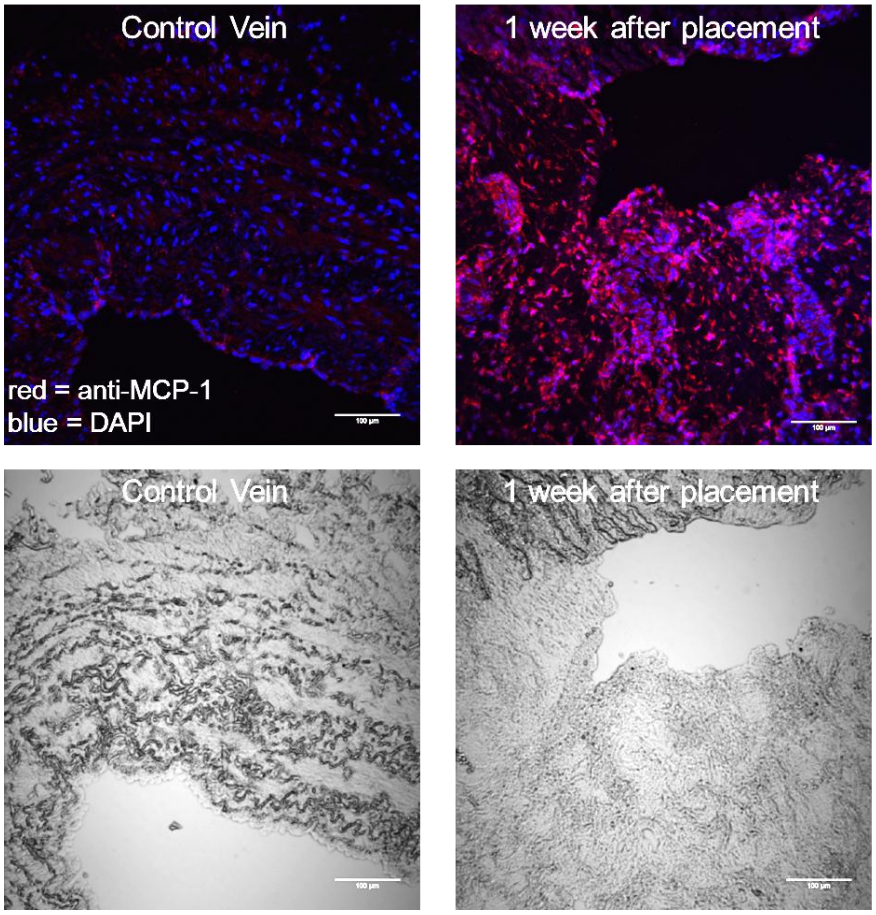

Figure 2.6 Immunohistofluorescent staining of MCP-1 in porcine AV graft tissue. MCP-1 expression (red) increased at 1 week after graft placement above that seen in control vein, and remained elevated at 6 weeks after placement (not shown). The light microscopy images of the tissue sections are shown below the fluorescent images. Images were obtained at 20x magnification and the scale bar is 100 μm.

2.3.5 sEH Inhibitor (c-TUCB) Attenuates Chemokine/cytokine

Release from Human Monocytes

C-TUCB is a potent and selective inhibitor of sEH (IC_{50} against recombinant sEH ~0.6 nM) (22). LPS-stimulated MCP-1 and TNF-α release from adherent human monocytes was significantly inhibited by pretreatment with c-TUCB or c-TUCB plus 14,15-EETs, compared to LPS alone ($p<0.05$) (Figure 2.7A-B). There was no observable effect on LPS-induced MCP-1 and TNF- α release with the addition of 14,15 EETs to the c-TUCB treated cells, or from the addition of 14,15 EETs alone (data not shown). The addition of 8,9 EETs and 11,12 EETs was also tested but neither inhibited MCP-1 or TNF-α release when added alone or with c-TUCB (data not shown). The secretion of IL-6 (Figure 2.7C) or MIP-1α (Figure 2.7D) after LPS exposure was not inhibited by pretreatment with c-TUCB alone or c-TUCB with EETs. EETs alone had no discernible effect (compared to LPS alone) on release of any of the chemokine/cytokines tested (data not shown).

2.3.6 Response of BMMΦ from Wild-type and sEH Knock-out

Mice to LPS and c-TUCB

LPS-stimulated release of MCP-1 from WT mouse BMMΦ was significantly inhibited by pre-incubation with c-TUCB ($p<0.01$) (Figure 2.8), similar to that seen in the human monocyte experiments (Figure 2.7). However, no inhibition was observed when BMMΦ from sEH □KO animals were exposed to LPS after preincubation with c-TUCB (Figure 2.8**)**. There was no discernible effect on LPS-stimulated MCP-1 release with the addition of EETs to c-TUCB-treated cells from either WT or KO animals (data not shown). However, untreated as well as LPS-treated

BMMΦ from sEH KO animals had elevated levels of MCP-1 release compared with BMMΦ from WT animals (untreated: 2162.5 pg/mL ± 599.4 vs. 1415.6 pg/mL ± 1010.8; LPS-treated: 6531.2 ± 5537.4 vs. 2255.7 ± 1424.3; $p < 0.009$).

2.3.7 c-TUCB Effects on NF-κB Translocation in Human Adherent Monocytes

EETs have previously been reported to inhibit IκB kinase (1, 31), which phosphorylates IκB. Phosphorylation of IκB results in its disassociation from the transcription factor NF-κB, allowing NF-κB to translocate to the nucleus and participate in transcription of genes involved in inflammation. Using a different sEHI than c-TUCB, others have reported inhibition of NF-κB translocation in cardiomyocytes (31). We tested the effects of c-TUCB on NF-κB translocation in human adherent monocytes. NF-κB was present in the cytoplasm and nucleus of control monocytes as determined by immunofluorescent staining (Figure 2.9). Exposure of cells to LPS (10 ng/mL) was associated with NF-κB translocation to the nucleus, but preincubation with c-TUCB had no marked inhibitory effect on that translocation. No inhibition of NF-κB translocation was observed at any time point examined or when cells were adhered for either two hrs or three days prior to experimentation (data not shown).

2.3.8 Effect of c-TUCB on JNK in Human Adherent Monocytes

The activation of JNK, a member of the mitogen activated protein kinase (MAPK) pathway, has been reported to be involved in LPS-induced expression of MCP-1 in microglia (32) and TNF-induced expression of MCP-1 in astrocytes (33). EETs have also been reported to inhibit the phosphorylation (activation) of JNK in endothelial cells (34) and hepatocytes (35). When

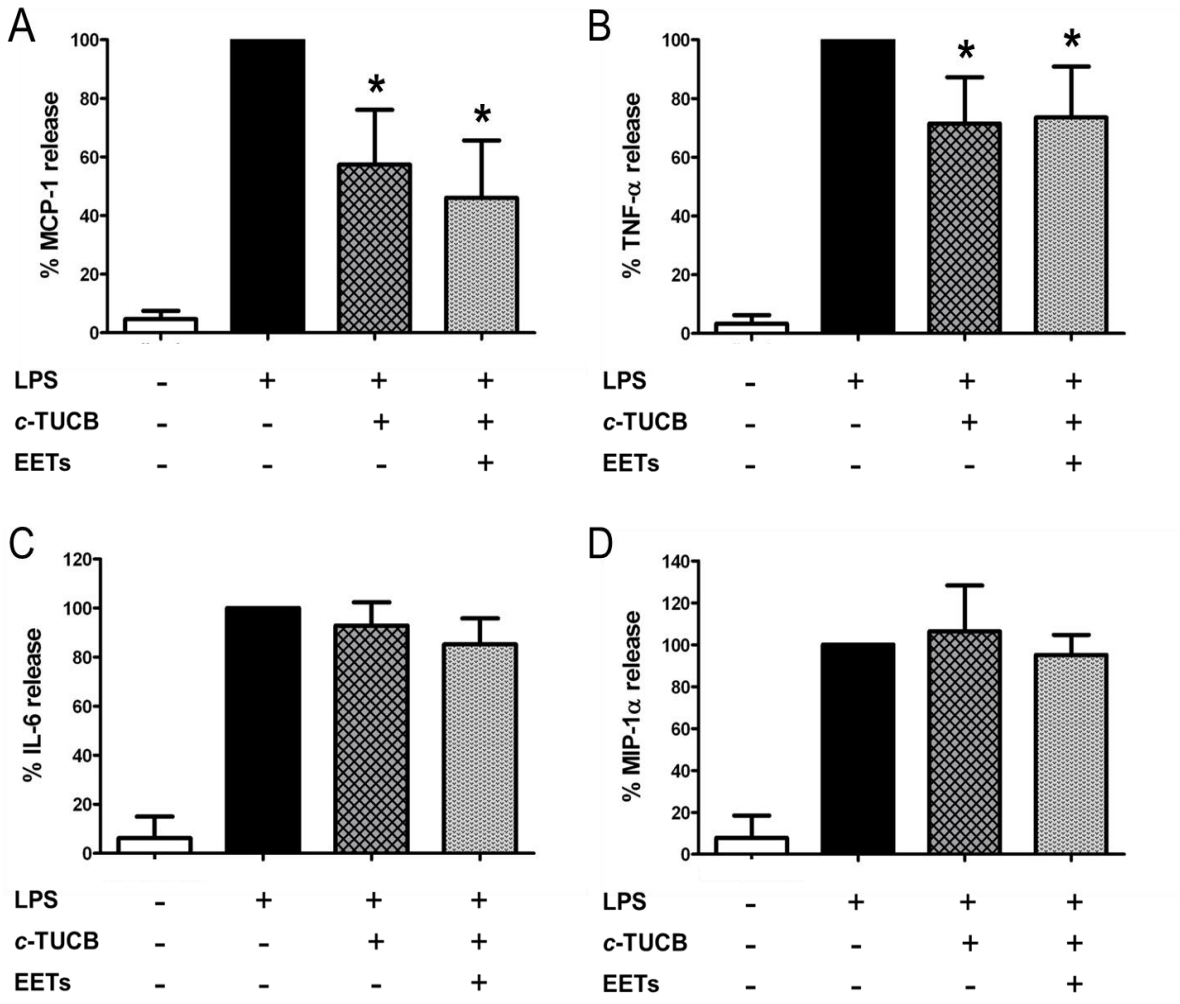

Figure 2.7 Effect of c-TUCB on LPS-stimulated release of (A) MCP-1, (B) TNF-α, (C) IL-6, or (D) MIP-1α from adherent human monocytes. White bars indicate cytokine levels in media alone. Cytokine/chemokine release from cells exposed to LPS alone was set as 100% then release that occurred with other treatments (c-TUCB plus or minus 14,15 EETs) was expressed as percent of that seen with LPS alone. The asterisks denote a statistically significant difference between cells treated with LPS alone vs. c-TUCB alone, or vs. c-TUCB and EETs: $*$, $p<0.05$. Cells were from three subjects.

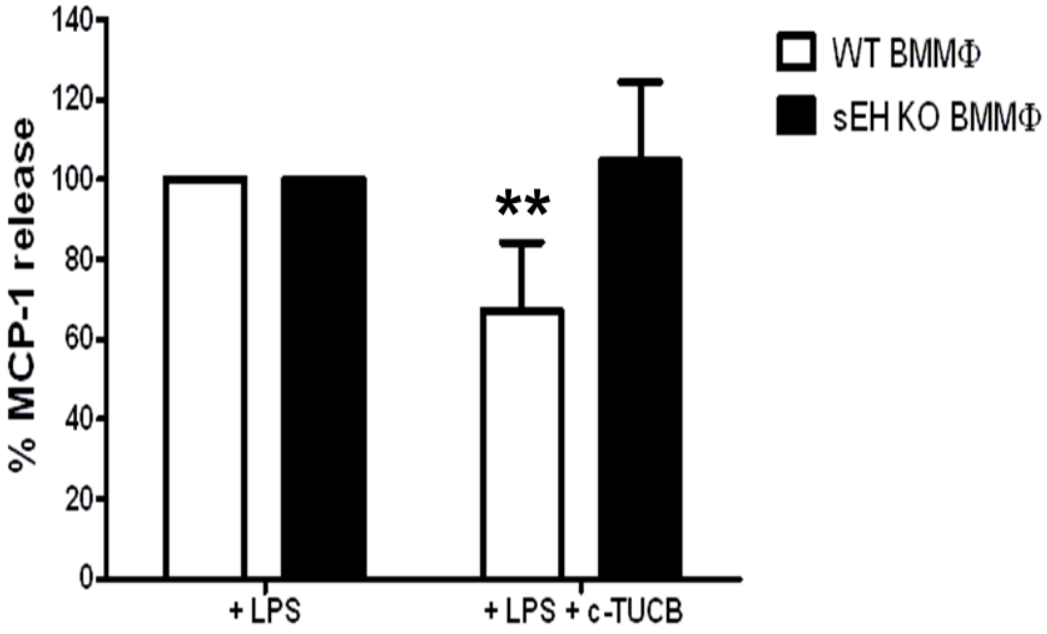

Figure 2.8 Release of MCP-1 from LPS-stimulated BMMΦ from wild-type (WT) (white bars) or sEH knock-out (KO) (Ephx2-/-) mice (black bars) in the absence or presence of c-TUCB. MCP-1 release from cells exposed to LPS alone was set as 100% and release that occurred with c-TUCB was expressed as percent of that seen with LPS alone. The data shown are from cells collected from five mice for both WT and KO mice. Asterisks denote a statistically significant difference ($p<0.01$) between LPS alone and LPS + c-TUCB.

monocytes were exposed to LPS, phosphorylation of JNK was enhanced (Figure 2.10). However when cells were exposed to LPS after pretreatment with c-TUCB, phospho-JNK levels were markedly decreased, as assessed by immunofluorescent staining (Figure 2.10).

2.4 Discussion

We used a validated porcine model to examine the time course for inflammatory cell recruitment and sEH expression, within the vascular tissue of synthetic AV grafts. Others have investigated cell phenotypes in human AV graft and fistula vein samples collected during vascular revision of stenosed accesses and reported the presence of numerous macrophages (21, 36). However, the percentage of grafts that had undergone percutaneous transluminal angioplasty prior to revision was unknown, which complicates interpretations since angioplasty itself initiates inflammation. The pool of available human AV graft tissue that has not previously undergone angioplasty for treatment of stenosis is small because angioplasty is a first-line treatment for AV graft stenosis (37). The porcine model recapitulates the hyperplasia development that occurs in human AV grafts but in a shorter time frame and is a well-accepted large animal model of AV graft stenosis (21, 36). One caveat to this model is the animals are not uremic and uremia may impact inflammation. A porcine chronic renal insufficiency AV graft model has been reported but requires 28 days to establish uremia prior to graft placement surgery (38). Up to 6 weeks would further be required for advanced stenosis development to occur and the animals would become quite large in that time frame and the costs of upkeep would be prohibitive.

T lymphocytes and macrophages were observed to accumulate in large numbers in our

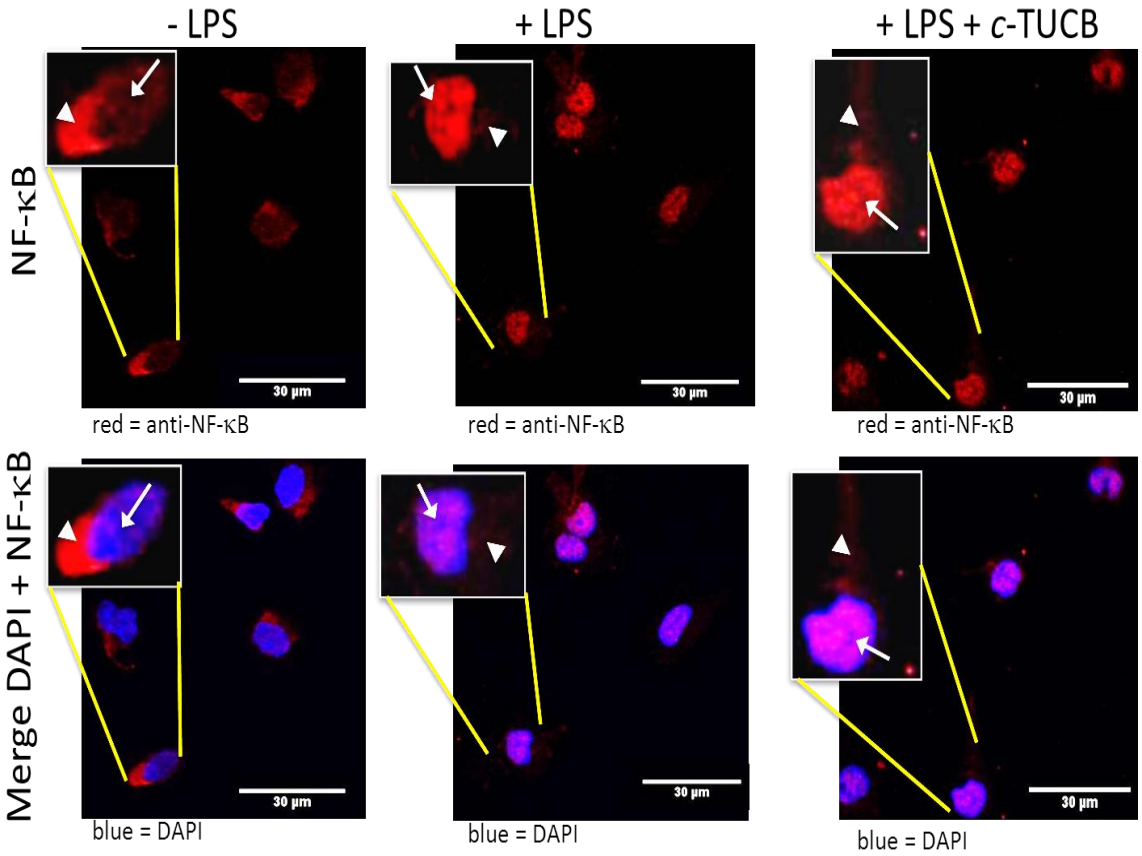

Figure 2.9 Effect of c-TUCB on LPS-stimulated NF-κB nuclear translocation in adherent human monocytes. Confocal images of cells immunostained with anti-NF-κB (red) (top row) and then merged with images of DAPI nuclear stain (blue) (bottom row). NF-κB is located primarily in the cytoplasm (arrowhead) of cells before exposure to LPS (first column) with little observed in the nuclear compartment (arrow). After a 45 min LPS exposure, an increased immunostaining of NF-κB in the nuclei (arrow) and decreased immunostaining in the cytoplasm (arrowhead) was observed (second column). Pre-exposure to c-TUCB did not inhibit LPS-induced nuclear translocation (arrow) (third column). All images were obtained at 60x magnification. Scale bar is 30 μm.

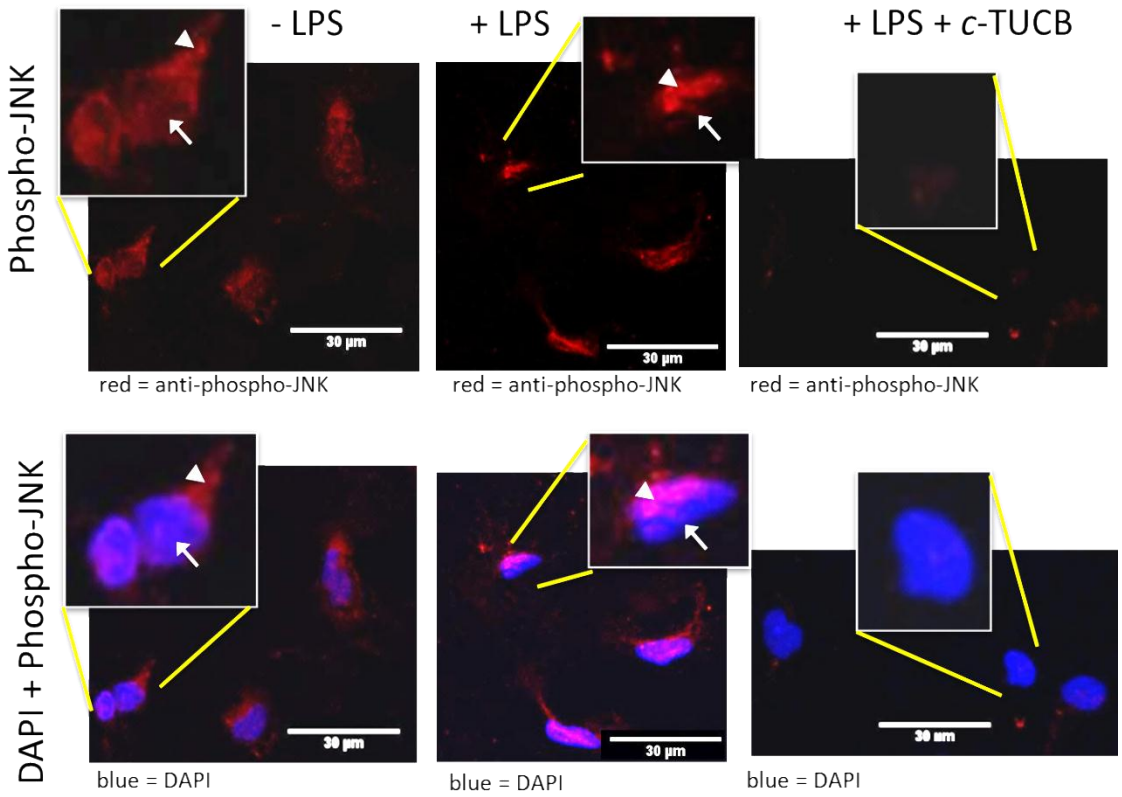

Figure 2.10 Effect of c-TUCB on LPS-stimulated phosphorylation of JNK in adherent human monocytes. Confocal images of cells immunostained with anti-phospho-JNK (Phospho-JNK) (red) (top row) and then merged with images of DAPI nuclear stain (blue) (bottom row). Low levels of cytoplasmic phospho-JNK immunostaining (arrowhead) were observed in untreated cells (first column) whereas increased cytoplasmic phospho-JNK immunostaining (arrowhead) was observed after 15 min LPS treatment (middle column). Pre-exposure to c-TUCB markedly reduced immunostaining of phospho-JNK (red) (last column). All images were obtained at 60x magnification. Scale bar is 30 μm.

porcine model after AV graft placement. T lymphocyte accumulation was notable for its early appearance and this is the first report to our knowledge on the presence of T cells in AV graft tissue. A previous study reported accumulation of T lymphocytes in thrombosed arteriovenous fistulas but in the fistula setting the presence of T cells was likely due to thrombosis and unrelated to a foreign body response (39). T lymphocytes may be influencing the macrophage response to the ePTFE graft material. In support, T cells have been shown in vitro to enhance the adherence of macrophages, and the formation of FBGC, on certain synthetic biomaterials (40). In another study, rat aortic smooth muscle cells exposed to conditioned media from human PBMC exposed to PTFE had increased proliferation rates compared to smooth muscle cells exposed to conditioned media from unexposed PBMC (20). In vivo studies reported that T-cell-deficient mice had lower granulocyte numbers near a variety of subcutaneous biomaterials compared to WT mice (41). Also, the mice had lower numbers of adherent macrophages on polyether urethane biomaterial implants compared to WT mice. However, the number of macrophages adhered to other biomaterial implants was similar between the two groups. These data indicate, at least in mice, T lymphocyte involvement in macrophage activation is likely material-dependent. However, the precise role that T lymphocytes play in the stenosis of AV grafts is not yet completely known and requires further study.

A number of factors doubtless contribute to the recruitment of inflammatory cells to the AV graft including i) the surgical trauma that occurs during graft placement, ii) the bioincompatability of the ePTFE graft material and sutures, and iii) the presence of aberrant blood flow that may traumatize the vessel wall and also more readily allow inflammatory cell attachment and infiltration.

We, and others, have reported the elevated expression of growth factors, cytokines and chemokines within the anastomotic tissue of the AV grafts (42-46). Inflammatory cells are likely sources of these factors. Since macrophages and T lymphocytes are early and prevalent inhabitants of the AV graft tissue and release cytokines and chemokines that induce migration and proliferation, they are attractive targets for pharmacotherapy against AV graft stenosis.

The hypothesis that sEH may play a role in the marked inflammation observed in AV grafts has not previously been investigated. However it is reasonable to posit that sEH may be involved since i) the sEH enzyme catabolizes anti-inflammatory EETs and other epoxy fatty acids to the less biologically active diols such as DHET, and ii) sEH has been shown to be important in other inflammatory conditions. For example, after middle cerebral artery occlusion, the levels of TNF-α, IL-6, interferon-gamma and IL-1β mRNA in the brains of sEH KO mice were significantly less compared to levels in the brains of WT mice (47). Also, in animals made hypertensive by DOCA-salt treatment, NF-κB activity in kidney lysates and MCP-1 levels in urine were significantly decreased in sEH knockout mice compared to WT mice (48). Also MCP-1 protein and NF-κB activity were decreased in lung homogenates from sEH KO mice compared to WT mice after in vivo LPS exposure (49). Additionally, intraperitoneal injection for two weeks of a dual EET agonist/sEHI significantly inhibited plasma levels of TNF-α and MCP-1 in heme oxygenase-2 KO mice (50). We showed the expression of sEH was markedly upregulated after AV graft creation in the vessel wall, first in the medial layer, then in the adventitia and finally the stenotic tissue at the anastomosis. Due to a lack of a sufficiently specific antibody against porcine monocyte/macrophages, we were unable to confidently colocalize macrophage identity and sEH

immunostaining in our animal model. However, expression of sEH was detected in ficoll-hypaque isolated human peripheral blood monocytes by both immunoblotting and immunocytochemistry. Also, FBGCs that are produced by the fusion of multiple macrophages and are readily identified by histological analysis, specifically immunostained with anti-sEH antibody suggesting that porcine macrophages indeed express sEH. Subsequently, elevated sEH expression in both the vascular tissue and infiltrating inflammatory cells may contribute to inflammation in the AV graft by decreasing anti-inflammatory EET levels.

In this study, we examined the hypothesis that a pharmacological inhibitor of sEH would attenuate release of various pro-inflammatory chemokine/cytokines from LPS-stimulated monocyte/macrophages. The hypothesis was proven correct for both MCP-1 and TNF-α To confirm that sEHI was attenuating MCP-1 release through a direct effect on sEH, BMMΦs from both WT and sEH KO mice were stimulated with LPS after being pretreated with either sEHI alone, EETs alone or both together. Exposure with c-TUCB was associated with decreased MCP-1 release from LPS-induced WT BMMΦ but not from LPS-induced KO BMMΦ. If EETs are involved in the inhibition of MCP-1 expression, one might expect a decreased basal expression of MCP-1 in the sEH KO mice BMMΦ since sEH is not expressed in these animals and their EET levels have been reported to be elevated (51). However MCP-1 release was actually elevated from untreated- as well as LPS-stimulated BMMΦ from sEH knockout mice, compared to WT BMMΦ. Similarly unexpected findings were reported by Luria et al. who showed that although sEH KO mice had elevated plasma levels of 14,15-EET and other cytochrome P450 expoxygenase metabolites, they did not have decreased basal blood pressure compared to WT mice (51). This

was surprising since EETs are potent vasodilators (2-4). However, there were also concomitant 4-fold increases in production of the potent vasoconstrictor 20-hydroxyeicosatetraenoic acid (20-HETE) in the sEH KO mouse kidneys and urine (51). Of note, sEH KO mice experienced markedly less hypotension after an LPS infusion compared to WT mice and their blood pressure recovered much more quickly after the LPS insult (51). It was postulated that the elevated 20-HETE levels in the sEH KO animals counteracted the hypotensive actions of the elevated levels of EETs. Thus it is possible that other pathways are upregulated in response to sEH inhibition in monocyte/macrophage cells similar to what was observed in the whole animal studies. Other lipoxygenase metabolites (12- and 15-HETE) are known to induce MCP-1 in murine peritoneal macrophages (52). Levels of 20-HETE or other lipid mediators may be altered in the monocyte/macrophages in response to deletion of the sEH pathway resulting in elevated levels of MCP-1 but further studies are needed to investigate such possibilities. Regardless, the pharmacological inhibitor of sEH, c-TUCB, inhibited monocyte release of MCP-1 and TNF-α.

The expression of sEH in monocyte/macrophages detected by immunocytochemical and immunohistochemical staining is in contrast to a study that reported that human monocytes isolated from peripheral blood by column elution had no detectable sEH activity against trans-stilbene oxide (53). That our current study observed i) significant inhibition of MCP-1 and TNF-α release from monocytes by a selective pharmacological inhibitor of sEH, ii) the sEHI did not significantly inhibit MCP-1 release from BMMΦ from sEH KO mice but did in BMMΦ from WT mice, and iii) that a blocking peptide specific for sEH markedly decreased anti-sEH antibody binding in western immunoblots supports our results that monocyte/macrophages do express sEH.

EETs are anti-inflammatory in a number of settings (1, 49). However, the administration of exogenous EETs along with sEHI did not significantly augment the inhibitory effects of sEHI, and the addition of EETs alone did not significantly alter cytokine release compared to LPS alone. A possible explanation for the lack of effect of EETs alone is that EETs are metabolized to DHETs rapidly within the cell before being able to elicit a response (54). In support of this, the formation of the metabolite 14,15 DHET could be detected in the media of cultured porcine aortic smooth muscle cells within 3 min after adding 14,15 EETs (54). However, others have reported effects of exogenously applied EETs on cell functions such as cell adhesion molecule expression indicating exogenously applied EETs are capable of intracellular effects (1). Another possibility is that albumin, supplemented in the cell culture media in the form of fetal calf serum, reduces uptake of EETs enabling rapid hydrolysis to DHETs in the media. Albumin was shown to decrease the uptake of 14,15 EETs by over 50% in mastocytoma cells and increasing the albumin concentration reduced uptake even further (55). Also, the exogenously applied EETs could be depleted via β-oxidation and esterification pathways.

MCP-1 (CCL2), a CC chemokine, is a potent chemoattractant that recruits peripheral monocytes and memory T-cells into sites of inflammation (56). Besides monocytes/macrophages, many other cell types secrete MCP-1 including T-cells, endothelial cells, smooth muscle cells, and fibroblasts (57); all cell types that likely play a role in hyperplasia formation in our porcine AV graft model. Tissue at the vein-graft anastomosis stained positively for MCP-1 at 1, 2, 3, and 6 weeks after graft placement showing that MCP-1 production is enhanced and sustained and subsequently may be contributing to inflammatory cell recruitment. Control vein did not express

MCP-1. Increase in MCP-1 expression occurs in other experimental models of neointimal hyperplasia. For instance, upregulation of MCP-1 appeared as early as one day after balloon injury in hypercholesterolemic rabbits and was significantly higher than in noninjured control vessels, even at 28 days after injury (58). Also, MCP-1 mRNA levels increased 117-fold in tissue one week after epicardial vein-to-femoral artery bypass grafting in rats and remained seven times greater than baseline at 8 weeks after grafting (59). In both cases an increase in inflammatory cell infiltration was simultaneously observed. Treatment targeting MCP-1 using either a neutralizing antibody for MCP-1 or a plasmid coding for N-terminal deletion mutant MCP-1 was effective in inhibiting hyperplasia and macrophage infiltration in a rat carotid injury (60) and a mouse or monkey periarterial injury model (61). Recently, in-stent restenosis in porcine coronary arteries was significantly inhibited by oral treatment with bindarit, a selective small molecule inhibitor of MCP chemokines (62). Thus, the ability of sEHI to inhibit MCP-1 and TNF-α release makes it a potential therapeutic for the treatment of neointimal hyperplasia.

Previous studies have shown that EETs elicit anti-inflammatory effects by inhibiting the phosphorylation of IκB thereby preventing the activation and subsequent nuclear translocation of NF-κB. Schmelzer et al. reported that AUDA (another sEHI) decreased IL-6, TNF-α, and MCP-5 plasma levels in LPS-challenged mice and alluded that this effect was derived from the blocking of NF-κB nuclear translocation (12). Olearczyk et al. demonstrated that sEHI given in drinking water diminished urinary MCP-1 secretion, inhibited NF-κB activity and attenuated macrophage infiltration into the kidney in hypertensive rats (15). Others reported that sEH KO mice made hypertensive with DOCA-salt, had decreased NF-κB activity, decreased urinary MCP-1 and fewer

CD68 positive cells in the kidney (48). In the current study, LPS induced the nuclear translocation of NF-κB in adherent human monocytes yet pretreatment with sEHI did not inhibit the NF-κB translocation. This inability of c-TUCB to inhibit NF-κB translocation is consistent with our data showing sEHI did not significantly alter IL-6 or MIP-1α release, as NF-κB is a key inflammatory transcription factor involved in the production of these chemokine/cytokines (63-67). Our data indicate that the role of sEH in inflammation is more complex than originally proposed and is likely cell specific.

The enzymes in the MAPK pathway (ERK1/2, p38 and JNK) (68) are also activated by LPS exposure (69-72). Each of these kinases has been reported to participate in MCP-1 and TNF-α secretion induced by different stimuli in various cell types, and decreased phosphorylation of these kinases has been reported to attenuate MCP-1 and TNF-α release (73-79). Elevated EET levels were shown to correlate with increased activation of ERK1/2 in endothelial cells (80), and ERK1/2 and p38 in endothelial cells (81) and macrophages (82). Potente et al. demonstrated that overexpressing CYP2C9 in endothelial cells resulted in increased EET levels and a concomitant dephosphorylation of JNK, suggesting that JNK may participate in EET signaling (34). EETs were shown to inhibit JNK activity, and JNK inhibition by dexamethasone suppressed MCP-1 release in microglia (32), and TNF-α release in murine macrophages (83). We showed that levels of phosphorylated JNK were increased after LPS-stimulation in human monocytes, but pre-exposure to sEHI almost completely blocked the phosphorylation. Thus, in human monocytes, sEH inhibition likely attenuates MCP-1 and TNF-α release via an effect on the JNK pathway and not the NF-κB pathway. The proposed pathway of how c-TUCB affects MCP-1 and

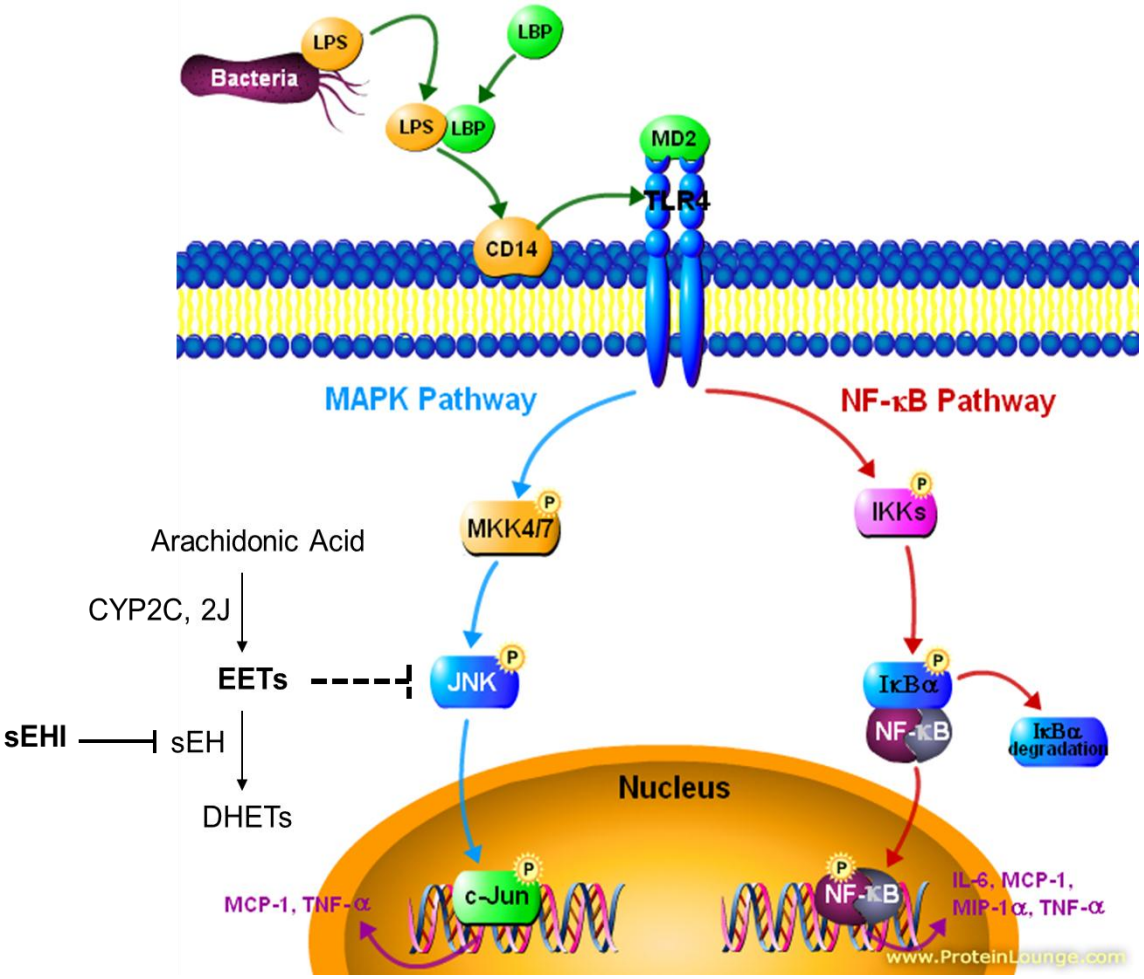

Figure 2.11 Proposed signaling pathway of how sEHI affects MCP-1 and TNF-α release in LPS stimulated monocytes. sEHI binds to sEH which increases the accumulation of EETs that then block phosphorylation of JNK, but does not effect the translocation of NF-κB. The effect of EETs on JNK has not been shown to be a direct effect which is indicated by the hatched line from EETs to JNK.

TNF-α release from LPS stimulated macrophages is presented in Figure 2.11. As multiple pathways, such as the NF-κB pathway, have been shown by others to be involved in MCP-1 and TNF-α expression, and such pathways may not be affected by sEH inhibition in monocytes, this may explain the lack of complete knockdown of both MCP-1 and TNF-α release by c-TUCB.

2.5 Conclusion

As discussed above, MCP-1 is a potent chemoattractant and migration stimulus for monocytes/macrophages and vascular smooth muscle cells and its high expression level in the AV graft anastomotic tissue suggests it may play a role in hyperplasia formation. This study is the first to report that sEHI can inhibit MCP-1 and TNF-α release from monocyte/macrophages and not through the NF-κB pathway, but instead via the JNK pathway (Figure 2.11). However, as expression of other cytokines was not affected, whole animal studies are required to determine whether sEHIs will be useful in preventing AV grafts stenosis.

2.6 References

1. Node K, Huo Y, Ruan X, Yang B, Spiecker M, Ley K, et al. Anti-inflammatory properties of cytochrome P450 epoxygenase-derived eicosanoids. Science. 1999;285:1276-9.

2. Gebremedhin D, Ma YH, Falck JR, Roman RJ, VanRollins M, Harder DR. Mechanism of action of cerebral epoxyeicosatrienoic acids on cerebral arterial smooth muscle. Am J Physiol. 1992;263:H519-25.

3. Imig JD, Navar LG, Roman RJ, Reddy KK, Falck JR. Actions of epoxygenase metabolites on the preglomerular vasculature. J Am Soc Nephrol. 1996;7:2364-70.

4. Sudhahar V, Shaw S, Imig JD. Epoxyeicosatrienoic acid analogs and vascular function. Curr Med Chem. 2010;17:1181-90.

5. Sun J, Sui X, Bradbury JA, Zeldin DC, Conte MS, Liao JK. Inhibition of vascular smooth muscle cell migration by cytochrome p450 epoxygenase-derived eicosanoids. Circ Res.

2002;90:1020-7.

6. Krotz F, Riexinger T, Buerkle MA, Nithipatikom K, Gloe T, Sohn HY, et al. Membrane-potential-dependent inhibition of platelet adhesion to endothelial cells by epoxyeicosatrienoic acids. Arterioscler Thromb Vasc Biol. 2004;24:595-600.

7. Yan G, Chen S, You B, Sun J. Activation of sphingosine kinase-1 mediates induction of endothelial cell proliferation and angiogenesis by epoxyeicosatrienoic acids. Cardiovasc Res. 2008;78:308-14.

8. Newman JW, Morisseau C, Hammock BD. Epoxide hydrolases: their roles and interactions with lipid metabolism. Prog Lipid Res. 2005;44:1-51.

9. Kim IH, Heirtzler FR, Morisseau C, Nishi K, Tsai HJ, Hammock BD. Optimization of amide-based inhibitors of soluble epoxide hydrolase with improved water solubility. J Med Chem. 2005;48:3621-9.

10. Morisseau C, Goodrow MH, Dowdy D, Zheng J, Greene JF, Sanborn JR, et al. Potent urea and carbamate inhibitors of soluble epoxide hydrolases. Proc Natl Acad Sci U S A. 1999;96:8849-54.

11. Imig JD, Hammock BD. Soluble epoxide hydrolase as a therapeutic target for cardiovascular diseases. Nat Rev Drug Discov. 2009;8:794-805.

12. Schmelzer KR, Kubala L, Newman JW, Kim IH, Eiserich JP, Hammock BD. Soluble epoxide hydrolase is a therapeutic target for acute inflammation. Proc Natl Acad Sci U S A. 2005;102:9772-7.

13. Imig JD, Zhao X, Zaharis CZ, Olearczyk JJ, Pollock DM, Newman JW, et al. An orally active epoxide hydrolase inhibitor lowers blood pressure and provides renal protection in salt-sensitive hypertension. Hypertension. 2005;46:975-81.

14. Smith KR, Pinkerton KE, Watanabe T, Pedersen TL, Ma SJ, Hammock BD. Attenuation of tobacco smoke-induced lung inflammation by treatment with a soluble epoxide hydrolase inhibitor. Proc Natl Acad Sci U S A. 2005;102:2186-91.

15. Olearczyk JJ, Quigley JE, Mitchell BC, Yamamoto T, Kim IH, Newman JW, et al. Administration of a substituted adamantyl urea inhibitor of soluble epoxide hydrolase protects the kidney from damage in hypertensive Goto-Kakizaki rats. Clin Sci (Lond). 2009;116:61-70.

16. Libby P, Okamoto Y, Rocha VZ, Folco E. Inflammation in atherosclerosis: transition from theory to practice. Circ J. 2010;74:213-20.

17. Tanaka H, Sukhova GK, Swanson SJ, Clinton SK, Ganz P, Cybulsky MI, et al. Sustained

activation of vascular cells and leukocytes in the rabbit aorta after balloon injury. Circulation. 1993;88:1788-803.

18. Owens CD, Kim JM, Hevelone ND, Hamdan A, Raffetto JD, Creager MA, et al. Novel adipokines, high molecular weight adiponectin and resistin, are associated with outcomes following lower extremity revascularization with autogenous vein. J Vasc Surg. 2010;51:1152-9.

19. Ozaki CK. Cytokines and the early vein graft: strategies to enhance durability. J Vasc Surg. 2007;45 Suppl A:A92-8.

20. Mattana J, Effiong C, Kapasi A, Singhal PC. Leukocyte-polytetrafluoroethylene interaction enhances proliferation of vascular smooth muscle cells via tumor necrosis factor-alpha secretion. Kidney Int. 1997;52:1478-85.

21. Roy-Chaudhury P, Wang Y, Krishnamoorthy M, Zhang J, Banerjee R, Munda R, et al. Cellular phenotypes in human stenotic lesions from haemodialysis vascular access. Nephrol Dial Transplant. 2009;24:2786-91.

22. Hwang SH, Tsai HJ, Liu JY, Morisseau C, Hammock BD. Orally bioavailable potent soluble epoxide hydrolase inhibitors. J Med Chem. 2007;50:3825-40.

23. Newman JW, Stok JE, Vidal JD, Corbin CJ, Huang Q, Hammock BD, et al. Cytochrome p450-dependent lipid metabolism in preovulatory follicles. Endocrinology. 2004;145:5097-105.

24. Terry CM, Kim SE, Li L, Goodrich KC, Hadley JR, Blumenthal DK, et al. Longitudinal assessment of hyperplasia using magnetic resonance imaging without contrast in a porcine arteriovenous graft model. Acad Radiol. 2009;16:96-107.

25. Li L, Terry CM, Blumenthal DK, Kuji T, Masaki T, Kwan BC, et al. Cellular and morphological changes during neointimal hyperplasia development in a porcine arteriovenous graft model. Nephrol Dial Transplant. 2007;22:3139-46.

26. Ehrnfelt C, Kumagai-Braesch M, Uzunel M, Holgersson J. Adult porcine islets produce MCP-1 and recruit human monocytes in vitro. Xenotransplantation. 2004;11:184-94.

27. Chamberlain LM, Godek ML, Gonzalez-Juarrero M, Grainger DW. Phenotypic non-equivalence of murine (monocyte-) macrophage cells in biomaterial and inflammatory models. J Biomed Mater Res A. 2009;88:858-71.

28. Godek ML, Sampson JA, Duchsherer NL, McElwee Q, Grainger DW. Rho GTPase protein expression and activation in murine monocytes/macrophages is not modulated by model biomaterial surfaces in serum-containing in vitro cultures. J Biomater Sci Polym Ed. 2006;17:1141-58.

29. Draper AJ, Hammock BD. Soluble epoxide hydrolase in rat inflammatory cells is indistinguishable from soluble epoxide hydrolase in rat liver. Toxicol Sci. 1999;50:30-5.

30. Rawal S, Morisseau C, Hammock BD, Shivachar AC. Differential subcellular distribution and colocalization of the microsomal and soluble epoxide hydrolases in cultured neonatal rat brain cortical astrocytes. J Neurosci Res. 2009;87:218-27.

31. Xu D, Li N, He Y, Timofeyev V, Lu L, Tsai HJ, et al. Prevention and reversal of cardiac hypertrophy by soluble epoxide hydrolase inhibitors. Proc Natl Acad Sci U S A. 2006;103:18733-8.

32. Zhou Y, Ling EA, Dheen ST. Dexamethasone suppresses monocyte chemoattractant protein-1 production via mitogen activated protein kinase phosphatase-1 dependent inhibition of Jun N-terminal kinase and p38 mitogen-activated protein kinase in activated rat microglia. J Neurochem. 2007;102:667-78.

33. Gao YJ, Zhang L, Samad OA, Suter MR, Yasuhiko K, Xu ZZ, et al. JNK-induced MCP-1 production in spinal cord astrocytes contributes to central sensitization and neuropathic pain. J Neurosci. 2009;29:4096-108.

34. Potente M, Michaelis UR, Fisslthaler B, Busse R, Fleming I. Cytochrome P450 2C9-induced endothelial cell proliferation involves induction of mitogen-activated protein (MAP) kinase phosphatase-1, inhibition of the c-Jun N-terminal kinase, and up-regulation of cyclin D1. J Biol Chem. 2002;277:15671-6.

35. Skepner JE, Shelly LD, Ji C, Reidich B, Luo Y. Chronic treatment with epoxyeicosatrienoic acids modulates insulin signaling and prevents insulin resistance in hepatocytes. Prostaglandins Other Lipid Mediat. 2011;94:3-8.

36. Kelly BS, Heffelfinger SC, Whiting JF, Miller MA, Reaves A, Armstrong J, et al. Aggressive venous neointimal hyperplasia in a pig model of arteriovenous graft stenosis. Kidney Int. 2002;62:2272-80.

37. Foundation NK. KDOQI Clinical Practice Guidelines and Clinical Practice Recommendations for 2006 Updates: Hemodialysis Adequacy, Peritoneal Dialysis Adequacy and Vascular Access; 2006 (suppl 1).

38. Misra S, Fu AA, Puggioni A, Glockner JF, Rajan DK, McKusick MA, et al. Increased expression of hypoxia-inducible factor-1 alpha in venous stenosis of arteriovenous polytetrafluoroethylene grafts in a chronic renal insufficiency porcine model. J Vasc Interv Radiol. 2008;19:260-5.

39. Chang CJ, Ko YS, Ko PJ, Hsu LA, Chen CF, Yang CW, et al. Thrombosed arteriovenous fistula for hemodialysis access is characterized by a marked inflammatory activity. Kidney Int.

2005;68:1312-9.

40. Brodbeck WG, Macewan M, Colton E, Meyerson H, Anderson JM. Lymphocytes and the foreign body response: lymphocyte enhancement of macrophage adhesion and fusion. J Biomed Mater Res A. 2005;74:222-9.

41. Rodriguez A, Meyerson H, Anderson JM. Quantitative in vivo cytokine analysis at synthetic biomaterial implant sites. J Biomed Mater Res A. 2009;89:152-9.

42. Kuji T, Masaki T, Li L, Cheung AK. Expression of C-reactive protein in myointimal hyperplasia in a porcine arteriovenous graft model. Nephrol Dial Transplant. 2007;22:2469-75.

43. Li L, Terry CM, Shiu YT, Cheung AK. Neointimal hyperplasia associated with synthetic hemodialysis grafts. Kidney Int. 2008;74:1247-61.

44. Misra S, Fu AA, Puggioni A, Karimi KM, Mandrekar JN, Glockner JF, et al. Increased shear stress with upregulation of VEGF-A and its receptors and MMP-2, MMP-9, and TIMP-1 in venous stenosis of hemodialysis grafts. Am J Physiol Heart Circ Physiol. 2008;294:H2219-30.

45. Roy-Chaudhury P, Kelly BS, Miller MA, Reaves A, Armstrong J, Nanayakkara N, et al. Venous neointimal hyperplasia in polytetrafluoroethylene dialysis grafts. Kidney Int. 2001;59:2325-34.

46. Weiss MF, Scivittaro V, Anderson JM. Oxidative stress and increased expression of growth factors in lesions of failed hemodialysis access. Am J Kidney Dis. 2001;37:970-80.

47. Koerner IP, Zhang W, Cheng J, Parker S, Hurn PD, Alkayed NJ. Soluble epoxide hydrolase: regulation by estrogen and role in the inflammatory response to cerebral ischemia. Front Biosci. 2008;13:2833-41.

48. Manhiani M, Quigley JE, Knight SF, Tasoobshirazi S, Moore T, Brands MW, et al. Soluble epoxide hydrolase gene deletion attenuates renal injury and inflammation with DOCA-salt hypertension. Am J Physiol Renal Physiol. 2009;297:F740-8.

49. Deng Y, Edin ML, Theken KN, Schuck RN, Flake GP, Kannon MA, et al. Endothelial CYP epoxygenase overexpression and soluble epoxide hydrolase disruption attenuate acute vascular inflammatory responses in mice. FASEB J. 2011;25:703-13.

50. Sodhi K, Inoue K, Gotlinger KH, Canestraro M, Vanella L, Kim DH, et al. Epoxyeicosatrienoic acid agonist rescues the metabolic syndrome phenotype of HO-2-null mice. J Pharmacol Exp Ther. 2009;331:906-16.

51. Luria A, Weldon SM, Kabcenell AK, Ingraham RH, Matera D, Jiang H, et al. Compensatory mechanism for homeostatic blood pressure regulation in Ephx2 gene-disrupted mice. J Biol Chem. 2007;282:2891-8.

52. Wen Y, Gu J, Vandenhoff GE, Liu X, Nadler JL. Role of 12/15-lipoxygenase in the expression of MCP-1 in mouse macrophages. Am J Physiol Heart Circ Physiol. 2008;294:H1933-8.

53. Seidegard J, DePierre JW, Pero RW. Measurement and characterization of membrane-bound and soluble epoxide hydrolase activities in resting mononuclear leukocytes from human blood. Cancer Res. 1984;44:3654-60.

54. Fang X, Kaduce TL, Weintraub NL, Spector AA. Cytochrome P450 metabolites of arachidonic acid: rapid incorporation and hydration of 14,15-epoxyeicosatrienoic acid in arterial smooth muscle cells. Prostaglandins Leukot Essent Fatty Acids. 1997;57:367-71.

55. Bernstrom K, Kayganich K, Murphy RC, Fitzpatrick FA. Incorporation and distribution of epoxyeicosatrienoic acids into cellular phospholipids. J Biol Chem. 1992;267:3686-90.

56. Niu J, Kolattukudy PE. Role of MCP-1 in cardiovascular disease: molecular mechanisms and clinical implications. Clin Sci (Lond). 2009;117:95-109.

57. Melgarejo E, Medina MA, Sanchez-Jimenez F, Urdiales JL. Monocyte chemoattractant protein-1: a key mediator in inflammatory processes. Int J Biochem Cell Biol. 2009;41:998-1001.

58. Mori E, Komori K, Yamaoka T, Tanii M, Kataoka C, Takeshita A, et al. Essential role of monocyte chemoattractant protein-1 in development of restenotic changes (neointimal hyperplasia and constrictive remodeling) after balloon angioplasty in hypercholesterolemic rabbits. Circulation. 2002;105:2905-10.

59. Stark VK, Hoch JR, Warner TF, Hullett DA. Monocyte chemotactic protein-1 expression is associated with the development of vein graft intimal hyperplasia. Arterioscler Thromb Vasc Biol. 1997;17:1614-21.

60. Furukawa Y, Matsumori A, Ohashi N, Shioi T, Ono K, Harada A, et al. Anti-monocyte chemoattractant protein-1/monocyte chemotactic and activating factor antibody inhibits neointimal hyperplasia in injured rat carotid arteries. Circ Res. 1999;84:306-14.

61. Ni W, Egashira K, Kitamoto S, Kataoka C, Koyanagi M, Inoue S, et al. New anti-monocyte chemoattractant protein-1 gene therapy attenuates atherosclerosis in apolipoprotein E-knockout mice. Circulation. 2001;103:2096-101.

62. Ialenti A, Grassia G, Gordon P, Maddaluno M, Di Lauro MV, Baker AH, et al. Inhibition of In-Stent Stenosis by Oral Administration of Bindarit in Porcine Coronary Arteries. Arteriosclerosis, thrombosis, and vascular biology. 2011.

63. Deng YY, Lu J, Ling EA, Kaur C. Monocyte chemoattractant protein-1 (MCP-1) produced via NF-kappaB signaling pathway mediates migration of amoeboid microglia in the periventricular white matter in hypoxic neonatal rats. Glia. 2009;57:604-21.

64. Doyle SL, O'Neill LA. Toll-like receptors: from the discovery of NFkappaB to new insights into transcriptional regulations in innate immunity. Biochem Pharmacol. 2006;72:1102-13.

65. Hirschfeld M, Weis JJ, Toshchakov V, Salkowski CA, Cody MJ, Ward DC, et al. Signaling by toll-like receptor 2 and 4 agonists results in differential gene expression in murine macrophages. Infect Immun. 2001;69:1477-82.

66. Ivanenkov YA, Balakin KV, Tkachenko SE. New approaches to the treatment of inflammatory disease : focus on small-molecule inhibitors of signal transduction pathways. Drugs R D. 2008;9:397-434.

67. Yang L, Cohn L, Zhang DH, Homer R, Ray A, Ray P. Essential role of nuclear factor kappaB in the induction of eosinophilia in allergic airway inflammation. J Exp Med. 1998;188:1739-50.

68. Hambleton J, Weinstein SL, Lem L, DeFranco AL. Activation of c-Jun N-terminal kinase in bacterial lipopolysaccharide-stimulated macrophages. Proc Natl Acad Sci U S A. 1996;93:2774-8.

69. Chen CC, Wang JK. p38 but not p44/42 mitogen-activated protein kinase is required for nitric oxide synthase induction mediated by lipopolysaccharide in RAW 264.7 macrophages. Mol Pharmacol. 1999;55:481-8.

70. Cario E, Rosenberg IM, Brandwein SL, Beck PL, Reinecker HC, Podolsky DK. Lipopolysaccharide activates distinct signaling pathways in intestinal epithelial cell lines expressing Toll-like receptors. J Immunol. 2000;164:966-72.

71. Thorley AJ, Ford PA, Giembycz MA, Goldstraw P, Young A, Tetley TD. Differential regulation of cytokine release and leukocyte migration by lipopolysaccharide-stimulated primary human lung alveolar type II epithelial cells and macrophages. J Immunol. 2007;178:463-73.

72. Guha M, Mackman N. LPS induction of gene expression in human monocytes. Cell Signal. 2001;13:85-94.

73. Hall DJ, Bates ME, Guar L, Cronan M, Korpi N, Bertics PJ. The role of p38 MAPK in rhinovirus-induced monocyte chemoattractant protein-1 production by monocytic-lineage cells. J Immunol. 2005;174:8056-63.

74. Nakayama K, Furusu A, Xu Q, Konta T, Kitamura M. Unexpected transcriptional induction of monocyte chemoattractant protein 1 by proteasome inhibition: involvement of the c-Jun N-terminal kinase-activator protein 1 pathway. J Immunol. 2001;167:1145-50.

75. Waetzig V, Czeloth K, Hidding U, Mielke K, Kanzow M, Brecht S, et al. c-Jun N-terminal kinases (JNKs) mediate pro-inflammatory actions of microglia. Glia. 2005;50:235-46.

76. Yamana J, Santos L, Morand E. Enhanced induction of LPS-induced fibroblast MCP-1 by

interferon-gamma: involvement of JNK and MAPK phosphatase-1. Cell Immunol. 2009;255:26-32.

77. Ciallella JR, Saporito M, Lund S, Leist M, Hasseldam H, McGann N, et al. CEP-11004, an inhibitor of the SAPK/JNK pathway, reduces TNF-alpha release from lipopolysaccharide-treated cells and mice. Eur J Pharmacol. 2005;515:179-87.

78. Hommes D, van den Blink B, Plasse T, Bartelsman J, Xu C, Macpherson B, et al. Inhibition of stress-activated MAP kinases induces clinical improvement in moderate to severe Crohn's disease. Gastroenterology. 2002;122:7-14.

79. Srivastava S, Weitzmann MN, Cenci S, Ross FP, Adler S, Pacifici R. Estrogen decreases TNF gene expression by blocking JNK activity and the resulting production of c-Jun and JunD. J Clin Invest. 1999;104:503-13.

80. Yang S, Lin L, Chen JX, Lee CR, Seubert JM, Wang Y, et al. Cytochrome P-450 epoxygenases protect endothelial cells from apoptosis induced by tumor necrosis factor-alpha via MAPK and PI3K/Akt signaling pathways. Am J Physiol Heart Circ Physiol. 2007;293:H142-51.

81. Fleming I, Fisslthaler B, Michaelis UR, Kiss L, Popp R, Busse R. The coronary endothelium-derived hyperpolarizing factor (EDHF) stimulates multiple signalling pathways and proliferation in vascular cells. Pflugers Arch. 2001;442:511-8.

82. Chen Y, Falck JR, Tuniki VR, Campbell WB. 20-125Iodo-14,15-epoxyeicosa-5(Z)-enoic acid: a high-affinity radioligand used to characterize the epoxyeicosatrienoic acid antagonist binding site. J Pharmacol Exp Ther. 2009;331:1137-45.

83. Swantek JL, Cobb MH, Geppert TD. Jun N-terminal kinase/stress-activated protein kinase (JNK/SAPK) is required for lipopolysaccharide stimulation of tumor necrosis factor alpha (TNF-alpha) translation: glucocorticoids inhibit TNF-alpha translation by blocking JNK/SAPK. Mol Cell Biol. 1997;17:6274-82.

CHAPTER 3

A DEGRADABLE PERIVASCULAR WRAP FOR CONTROLLED AND DIRECTED DRUG DELIVERY

3.1 Introduction

The pathological overgrowth of cells into the intimal layer of blood vessels is termed neointimal hyperplasia (NH). It is a common problem affecting interpositional vein grafts, arteries treated with balloon angioplasty, and catheterized veins, often resulting in stenosis and subsequent occlusion. It is a particularly widespread problem in synthetic arteriovenous (AV) grafts used for chronic hemodialysis resulting in the thrombotic occlusion of up to 50% of grafts within the first year of placement (1, 2). Currently there is no effective prevention strategies of neointimal hyperplasia associated with AV grafts that are used in routine clinical practice. Stenosis typically occurs at the graft-venous anastomosis and is due to the proliferation and migration of adventitial myofibroblasts and medial smooth muscle cells (SMCs) to the intimal layer (3, 4). A number of factors likely contribute to NH development, including (i) the presence of the synthetic graft material that initiates a foreign body response and (ii) the introduction of arterial blood directly into the vein causing flow disturbance and altered wall shear stress.

The current first-line treatment of AV graft stenosis is percutaneous angioplasty, which has not been shown to improve graft survival (5, 6). Controversy exists as to whether endovascular stent

placement after angioplasty provides benefit over angioplasty alone (7). Haskell et al. reported improved restenosis rates with stent placement after angioplasty compared to angioplasty alone, but similar thrombotic occlusion rates between the two groups (8). Systemic pharmacological strategies to prevent AV graft stenosis have produced largely disappointing results (9). A large prospective clinical trial testing the efficacy of an oral combination of dipyridamole (an anti-platelet agent) and aspirin reported a modest, albeit statistically significant, improvement in one year patency rates of the treatment group compared to placebo control (10, 11). Systemic drug administration, especially using anti-thrombotics or anti-neoplastic agents, can result in serious systemic toxicities that could be circumvented by localized drug delivery treatment. Local delivery to the stenosis-prone graft-vein anastomosis region would likely achieve much greater local drug concentrations with minimal systemic exposure. As the outer adventitial and medial layers are considered to be primary contributors of cells that participate in NH development in AV grafts (12, 13), a perivascular approach to drug delivery to inhibit NH is logical. In a proof-of-concept study, we previously reported the inhibition of NH using the perivascular delivery of paclitaxel with a polymer gel to the graft-vein anastomosis in a canine model of AV graft stenosis (14). Although the technique inhibited NH, the polymer gel was observed to migrate from the site of application. A wrap would provide a more stationary means of perivascular drug delivery.

Edelman et al. were the first to report the use of ethylene-vinyl acetate (EVA) polymer wraps to deliver heparin perivascularly to rat carotid arteries that sustained luminal injury (15). Subsequently, others have used perivascularly applied EVA films to deliver a variety of agents to the vasculature, including paclitaxel delivery to injured rat artery (16, 17), growth factor delivery to

ischemic rat myocardium (18), and verapamil delivery to a rabbit vein graft (19). An EVA wrap was also used to deliver paclitaxel to the graft-vein anastomosis in a porcine AV graft model and was associated with significantly decreased luminal stenosis (20). As the hemodialysis AV graft is subjected to chronic insults such as the thrice weekly puncturing of the graft for dialysis and continued presence of uremia, repeat exposure to perivascularly applied drug may be necessary to maintain patency over the lifetime of the access. However, the EVA films are non-degradable, thus prohibiting the replenishment of the drug depot, which is likely to be necessary for the suppression of NH in a vessel that is under chronic stimulation. In addition, chronic presence of a polymer wrap could initiate a foreign body response. Film preparations utilizing degradable polymers, such as polycaprolactone (PCL) and poly(lactic-co-glycolic acid) (PLGA), may be better suited for this application. In addition to be degradable, both PCL and PLGA are FDA-approved for use as suture materials, biocompatible, and can be made into thin flexible sheets suitable for an implantable perivascular wrap. Inhibition of NH was reported with perivascular delivery of paclitaxel (21) to a rat carotid artery after balloon injury using a PCL wrap (17), or to a sheep AV graft model using a PLGA wrap (22). However, the PCL wrap was inflexible, making it difficult to manipulate and position around the vessel. A large multicenter clinical trial was initiated to test the efficacy of the PLGA-based paclitaxel-eluting wrap for preventing stenosis in AV grafts, but was prematurely terminated due to an increased incidence of infection. Paclitaxel has been reported to have inhibitory effects on T lymphocytes in vivo that could diminish the immune system's ability to fight infection (23). Also, suppression of local immune activity by paclitaxel- or sirolimus-eluting stents was suggested to play a role in occurrence of stent infections (24). Thus,

the increased infection incidence was likely a result of paclitaxel not the PLGA wrap. There is need for better degradable platforms for drug delivery to the vasculature.

The choice of drug to target NH warrants consideration. Platelet-derived growth factor (PDGF) is a potent chemoattractant and mitogen that plays an essential role in initiating SMC migration and proliferation (25, 26). PDGF is not usually expressed in the normal vasculature, but upon injury, such as after angioplasty or graft placement, the tissue levels of PDGF and its receptors are markedly up-regulated (27-29). The importance of PDGF in the pathogenesis of NH can be illustrated by the attenuation of NH using a polyclonal antibody specific for PDGF in a rat arterial injury model (30). Thus, using pharmacological inhibitors that target PDGF or the PDGF receptor family could be a reasonable strategy to inhibit NH development in AV grafts. Imatinib, is a tyrosine kinase inhibitor that inhibits both PDGF receptor subtypes and has been shown to inhibit restenosis after balloon angioplasty (31). Sunitinib (Figure 3.1) is a multi-target receptor tyrosine kinase inhibitor of both PDGF receptor subtypes, all three VEGF receptor subtypes, KIT, FLT3, and CSR-1R; (32) and is currently approved by the FDA to treat gastrointestinal stromal tumors and metastatic renal cell carcinoma. VEGF has also shown to contribute to NH by increasing smooth muscle cell activation and neovessel formation at the anastomotic region (33). The ability of sunitinib to inhibit VEGF binding could be beneficial. The therapeutic efficacy of sunitinib in preventing NH formation, however, has not yet been evaluated. Data from our laboratory have confirmed the high potency of sunitinib to inhibit PDGF-stimulated proliferation of human venous SMCs in vitro (manuscript in preparation). Sunitinib was recently

Figure 3.1 Chemical structures of (A) sunitinib malate salt and (B) sunitinib free base

shown to restore immunocompetence and enhance immune-dependent chemotherapy against leishmaniasis infection in mice (34). Thus, sunitinib appears to a promising drug for inhibiting NH in AV grafts and was utilized in the present proof-of-concept studies.

We here report the development and characterization of novel degradable, tunable, bilayer, wraps using either PCL or PLGA for directed perivascular delivery of sunitinib. To provide unidirectional delivery, a monolithic backing was composed to prevent drug release away from the vascular wall and into the extravascular space. To provide tunability, the drug-laden layer of the constructs can be made porous or nonporous and drug can be loaded directly into the PCL or PLGA constructs during casting, or drug can be loaded into a hydrogel that is then infused into the porous layer. Since the wrap polymer is degradable, drug can be replenished by injection of drug loaded hydrogel to the anastomotic region. The in vitro release profiles for sunitinib were assessed for each wrap formulation. Additionally, we report the mechanical properties and in vivo tissue distribution of sunitinib from a PLGA nonporous bilayer wrap formulation over a one-month time course in a porcine model.

3.2 Materials and Methods

3.2.1 Materials

Sunitinib malate (>99% purity) and free-base sunitinib (>99% purity) were purchased from LC Laboratories (Woburn, MA). The internal standard sunitinib-d10 were purchased from Toronto Research Chemicals (North York, ON, Canada). Glycosil™ (thiolated hyaluronic acid (HA)) and

Extralink™ (polyethylene glycol diacrylate (PEGDA)) were purchased from Glycosan Biosystems (Salt Lake City, UT). Acetonitrile (ACN), methyl-tert-butyl ether (MTBE), ethanol, and acetone were of HPLC grade and polycaprolactone (PCL) of various molecular weights (14 kDa - polydispersity (PDI) 1.39, 45 kDa - PDI 1.4, and 80 kDa - PDI ~1.6-1.7), were purchased from Sigma-Aldrich (St. Louis, MO). Bovine testicular hyaluronidase (HAse) and other chemicals of reagent grade were also obtained from Sigma-Aldrich. Poly(lactic-co-glycolic acid) (PLGA) (106 kDa, inherent viscosity 0.65 dL/g) of copolymer ratio 50:50 was acquired from Surmodics Pharmaceuticals (Birmingham, AL). Di-ionized water was prepared with a Millipore Synergy UV system (Billerica, MA).

3.2.2 Preparation of PCL and PLGA Drug-laden and Drug-free Formulations

Four distinct types of degradable vascular wraps were prepared: (i) nonporous sunitinib-loaded PCL monolith, ii) laminated PLGA bilayer of a nonporous sunitinib-loaded film and a nonporous unloaded film, (iii) PCL bilayer of a nonporous monolith and a porous monolith, and (iv) laminated PLGA bilayer of nonporous film and porous film. Nonporous formulations (i and ii) were loaded with sunitinib during formulation, while porous composites (iii and iv) were loaded with sunitinib after fabrication using the HA hydrogel carrier. Solvent casting and phase inversion techniques were used to create all variations of the matrices. For preparation (i), PCL was dissolved at 20% w/v in acetone with stirring at 45^{o}C. Three PCL species were investigated: 45 kDa, 80 kDa, and a blend of 14 kDa and 80 kDa (at a 2:1 ratio). Upon complete dissolution of the polymer after 60 min, 8% v/v water nonsolvent was added with continued stirring. After the

solution reached homogeneity, sunitinib was added at 0.2% w/w and dispersed with vigorous stirring. The polymer/drug solution was cast into a Pyrex crystallizing dish and permitted to degas to the ambient through bubble dissipation with a foil cover. The dish was placed in a -20^{o}C freezer overnight to instigate and complete phase inversion of the polymer. The solvent was evaporated from the resulting monolith for 48 hr at room temperature in a chemical fume hood to produce the final slab that is suitable for sample punching.

Preparation (ii) was processed similar to (i) with the following exceptions: a PLGA solution concentration of 50% w/v with ethanol was employed as the non-solvent species at 30% v/v. Additionally, upon solvent evaporation from the phase inverted system, PLGA collapses to a film, instead of maintaining the monolith structure as occurs with PCL. The film is flexible and can be peeled from the evaporative template. The final bilayer composite was fabricated by lamination of the blank films to the drug-loaded films with a small amount of acetone applied with a spray bottle. The bilayer was placed in vacuum at ambient temperature for overnight to eliminate residual solvent.

For preparation (iii), first a layer of nonporous PCL monolith was cast as described in a Pyrex crystallization dish, but without loaded drug and solvent evaporation. Identical polymer solution mixed with NaCl porogen (>425 μm) to form a slurry was added to the top of the cast monolith and allowed to settle. This construct was phase-inverted at -20^{o}C and placed in a series of deionized water baths for 24 hr to completely extract the porogen and solvent, air dried, and cut to size.

Preparation (iv) employed the polymer solution described in (ii), but without drug loading and slightly different processing than described in (iii) to fabricate the porous bilayer. PLGA solution

was mixed with NaCl porogen (>425 μm) to form a slurry in a 50 mL Falcon tube, for a total volume of approximately 35 mL. This mixture was centrifuged at 500 rcf for 5 min, after which 15 mL of DI water was added to the tube and recentrifuged at the same settings for 30 min to complete system phase inversion. The bottom tip of the tube was shaved off and the porogen network was extracted in multiple excess DI water baths over 24 hr, ensuring that the tube is upright throughout. The resultant porous network was air dried, trimmed to 2 mm and welded to a placard of preparation (ii) using a small amount of acetone applied with a spray bottle. Samples were solvent evacuated in a chemical fume hood and punched to sample size.

3.2.3 Scanning Electron Microscopy (SEM) Imaging

SEM was performed on representative sample cross-sections and surfaces of each polymer matrix. After gold deposition, samples were imaged on a Hitachi S3000-N model instrument, PCL matrices at 3 kV and PLGA at 10 kV.

3.2.4 In Vitro Drug Release Experiments

In vitro drug release studies were performed using polymer constructs with the sunitinib incorporated into either the bulk polymer material or the impregnated hydrogel. For drug release experiments from monolithic drug-laden PCL samples, 250 μL of each MW PCL or the PCL blend was cast into 1.5 mL Eppendorf tubes then processed as described. Drug release was also tested from (i) a drug-loaded porous PCL layer welded to a drug-free nonporous PCL layer, (ii) a drug-loaded nonporous PLGA layer welded to a drug-free nonporous PLGA layer, or (iii) a drug-loaded porous PLGA layer welded to a drug-free nonporous PLGA layer. Uniform samples

of monolithic PCL and bilayer PLGA polymer constructs were created using a 10-mm biopsy punch. For the bilayer PCL constructs, strips (2 x 0.5 x 0.6 cm) were used.

Drug-release studies were also performed using porous/nonporous bilayer polymer constructs infused with Glycosil hydrogel. Briefly, 1% w/v hydrogel solution was dissolved in deionized H_2O, then crosslinked with 2% (w/v) Extralink in deionized H_2O at a volume ratio of 4:1 following manufacturer instructions. Sunitinib or sunitinib free-base powder was added prior to crosslinking of the hydrogel (5 mg drug/mL hydrogel in the PCL constructs; 3 mg drug/mL hydrogel in the PLGA constructs). Directly after addition of the crosslinking agent and prior to gelling, the hydrogel was infused into the porous layer of the polymer constructs by applying the hydrogel to the surface of the porous layer, then placing the constructs under vacuum. The hydrogel was then allowed to gel overnight. To examine the effect of porous PCL without hydrogel on drug release, dry sunitinib free base was vacuum pulled into the porous PCL without hydrogel.

For drug release kinetics, the polymer constructs were placed in 20-mL borosilicate scintillation vials covered with 5 mL of release medium, which was comprised of 1x PBS with 2% bovine serum albumin (BSA), then incubated in a water bath at $37^{o}C$ with gentle shaking. Release medium was removed daily for testing and replaced with an equal volume of fresh medium.

The release profile of free base sunitinib from hydrogel alone (no polymer construct) in the presence or absence of hyaluronidase (5 mU/mL), a concentration similar to that found at wound sites (35), was also examined. All in vitro release experiments were completed in triplicate and the cumulative release was expressed as the mean (± SD) percentage of the original loaded mass.

The final concentration of all samples was 5 mg of sunitinib per mL of hydrogel. Directly after addition of the crosslinker, the drug-loaded hydrogel samples (0.4 mL) were placed in the bottom of 20-mL borosilicate scintillation vials and allowed to fully crosslink overnight. In the experiment incorporating HAse into the release medium, HAse-containing medium was made fresh daily.

One milliliter of release media samples were spiked with internal standard (sunitinib-d10). Drug was extracted from the release media by vortexing with MTBE (4 mL) for 2 min in 16 x 100 mm screw-capped borosilicate test tubes. The tubes were centrifuged at 25 ^{o}C at 2000xg for 15 min. The organic layer was collected and solvent evaporated at 42 ^{o}C overnight. Dried samples were reconstituted in 200 μL of 65:35 ACN:H_2O containing 0.1% formic acid and injected into the HPLC MS/MS system and sunitinib concentrations were determined using the HPLC MS/MS protocol described below.

3.2.5 Unidirectional Transport Studies with PCL and PLGA Monolithic Backing

PCL and PLGA monoliths (1 mm thickness) were cast without porogen as described above. Uniform discs were cut from the polymer monoliths with an 8-mm biopsy punch. Costar Transwell® cell culture inserts (Corning, Corning, NY) were modified as follows. The polycarbonate insert membranes were replaced with either the PCL or PLGA discs. Discs were affixed into the insert position using ethyl cyanoacrylate adhesive. For the PCL study, solid sunitinib free base was mixed with hydrogel (8 mg/mL) prior to crosslinking and 50 μL of the hydrogel/drug mixture was applied on top of the PCL disc. Then 100 μL of release media was added above the hydrogel. For the PLGA study, sunitinib malate was dissolved in the release

media (200 μg/mL) and 125 μL was added above the PLGA discs. For visual tracking of solute traffic, Oil Red O (a hydrophobic dye) was dissolved in release media instead of drug, and 125 μL of the mixture was added above the polymer discs. The inserts were placed into 24-well plates with 1.2 mL release media in the bottom of the well. The plates were incubated at 37^{o}C for 72 hr to allow for possible drug/dye diffusion through the polymer membrane. After 72 hr, a sample of the media above the polymer discs and a sample below the discs were collected. Oil Red O content in the media was quantitated by absorbance at 521 nm using the NanoDrop 2000 spectrophotometer (Thermo Scientific, Waltham, MA) and sunitinib concentrations were quantified using the HPLC MS/MS protocol described below.

3.2.5 Mechanical Testing

PLGA constructs with and without sunitinib were cut into dog-bone shapes (2 cm x 3.5 mm in the middle at the breakpoint; 0.5 mm thickness). The effect of hydration on the elasticity of the PLGA samples with and without drug was analyzed after immersing the samples in PBS at 37^{o}C at various durations (0 days, 1 day, and 7 days). The samples were then subjected to tensile testing using an Instron 4465 (Instron Corp., Norwood, MA) at a speed of 1 cm-min^{-1} for all samples except for the 7-days -non-drug-loaded PLGA constructs that were assessed at 1 mm-min^{-1}. Force was measured as a function of the elongation until breakage of the sample. Young's modulus of elasticity, a measure of elasticity, was calculated by the Instron from the slope of the initial linear section of the stress strain curve. Five repetitions for each sample treatment were performed.

3.2.6 Polymer Constructs for Animal Experiments

PLGA bilayer constructs were created following the method described above. In short, a PLGA monolith backing (3 cm x 3 cm) was solvent-welded to (i) a drug-loaded (sunitinib malate (0.1% w/w, 143±5.5 μg drug)) monolithic PLGA layer (3 cm x 2.5 cm), or (ii) drug-free PLGA monolithic layer (control wrap). The wraps were sterilized using a STERRAD® system (ASP, Irvine, CA) that uses low-temperature hydrogen peroxide gas plasma.

3.2.7 Surgical Procedures

All animal work was performed using protocols approved by the Institutional Animal Care and Use Committee of the University of Utah and Veterans Affairs Salt Lake City Healthcare System and followed guidelines specified by the Guidelines for the Care and Use of Laboratory Animals.

A porcine model was utilized for perivascular wrap testing. Briefly, three-month old Yorkshire cross-domestic swine (~30 kg) were anesthetized using a mixture of ketamine (4 mg/kg; Hospira Inc., Lake Forest, IL), xylazine (4 mg/kg; Lloyd Laboratories, Shenandoah, IA), and tiletamine/zolazepam (4 mg/kg; Fort Dodge Animal Health, Fort Dodge, IA). To maintain anesthesia, 1-3% isoflurane was administered via tracheal intubation. Under sterile conditions, bilateral external jugular veins were dissected. The adventitial layer was removed from the external jugular veins to elicit an injury response. A sunitinib-loaded perivascular wrap was placed around the external jugular vein on one side and a control wrap was placed on the contralateral external jugular vein in each pig. To seal the wrap edge, Loctite (Westlake, OH) medical grade adhesive was applied along the length of the wrap edge. Two sutures were placed

at either end of the wrap. The surgical wounds were closed. Post-operatively, the surgical wounds were assessed daily for adverse effects such as bleeding, swelling and infection. In the first animal, in order to increase the amount of tissue pharmacokinetic data obtained, a drug-loaded wrap and a contralateral drug-free wrap were also placed around the femoral veins in the upper hind limbs in addition to the wraps placed in the neck. However, swelling occurred in the operated hind limbs that required draining, although the swelling did not affect the animal's mobility. Nonetheless, because of the swelling, polymer wraps were placed in the neck region and not in the femoral areas. Blood was drawn weekly to detect sunitinib in the peripheral circulation.

3.2.8 In Vivo Drug Distribution in Tissues

The external jugular veins and surrounding tissues from the porcine model were collected at one, two, and four weeks after wrap placement and processed immediately after explantation. The tissue from one animal was used for each time point. A 0.5-cm segment of the wrapped veins was formalin-fixed and paraffin-embedded for histological assessment. The remaining length of the wrapped vein was processed for drug detection. Briefly, fibrous tissue and wrap that surounded the vein was removed separately and retained for drug extraction. The vein tissue was isolated and retained for drug extraction in a similar manner. Sections of the vein that were proximal and distal to the wrapped vein segment were also isolated separately for drug extraction. The ipsilateral stenocleidomastoid muscle adjacent to the vein was removed from the drug-treated side and separated into six segments. Lateral tissue adjacent to the veins was also

isolated. The position and weight of each tissue section were recorded.

Tissue segments were homogenized in 1X PBS (PowerGen 700, Fisher Scientific, Pittsburgh, PA) for 1 min. To monitor the drug recovery during tissue extraction, 200 μL of sunitinib-d10 (internal standard solution at 500 ng/mL) in running buffer was added to 0.5 mL of tissue homogenate. The extraction procedure was the same as previously described for extracting sunitinib from the release media, but was repeated once more by adding 100 μL of 0.05 N NH_4OH and 4 mL TBME to the aqueous layer. The two collected organic fractions were then combined and evaporated to dryness at 42°C overnight. Samples were reconstituted in 200 μL of 65:35 ACN:H_2O running buffer containing 0.1% formic acid and 10 μL was injected into the HPLC MS/MS system. The concentrations of sunitinib were determined using the HPLC MS/MS protocol described below.

3.2.9 Sample Analysis by HPLC Tandem Mass Spectrometry

The sample analysis protocol was modified and adapted from previously published protocols (36-38). The analytical separation of sunitinib and sunitinib-d10 internal standard were performed using an Atlantis dC_{18} column (2.1 x 30 mm, 3.0 μm) (Waters Corp., Milford, MA), protected by a 4 mm x 2 mm C_{18} packed guard column (Phenomenex) at 25°C on an Acquity 2695 HPLC system (Waters Corp.) or on an Acquity UPLC H-Class system (Waters Corp.), both equipped with a refrigerated autosampler. The mobile phase consisted of acetonitrile-deionized H_2O (65:35, v/v) containing 0.1% formic acid and was run isocratically at a flow rate of 0.3 mL/min. Sample run times were 6 min on the Acquity 2695 HPLC and 4 min on the Acquity UPLC H-Class

and were followed by a 2-min needle wash to prevent possible carryover. The internal standard and the sunitinib extracted from the samples eluted at 1.2 min on the Acquity 2695 HPLC. For the Acquity UPLC H-Class the internal standard an sunitinibeluted at 0.42 min.

Two independent triple quadropole tandem mass spectrometers (Micromass® Quattro II or Acquity TQD, Waters Corp.) equipped with an electrospray ionization (ESI) interface were used for analytical detection. The Micromass® Quattro II was coupled with the Acquity 2695 HPLC system, while the Acquity TQD was coupled with the Acquity UPLC H-Class system. For the Micromass® Quattro II, quantification was performed in positive-ion mode using multiple reaction monitoring (MRM) of the transition masses of sunitinib (m/z 399.4 → 283) and the sunitinib-D10 internal standard (m/z 409.3 → 283). Instrument parameters were optimized for simultaneous detection of both sunitinib and the internal standard. The capillary energy was set at 3.50 kV, cone voltage at 35 V, extractor at 3 V, source block temperature at 125^{o}C, desolvation temperature at 325^{o}C, and the optimal collision energy was determined to be 18 V. Calibration curves for both sunitinib and internal standard were established using standard samples at 11 concentrations ranging from 4 ng/mL to 500 ng/mL. The coefficient of determination (r^2) from a least squares linear regression was 0.999 for sunitinib and 0.998 for the internal standard. The lower limit of quantification (LLOQ) was 4 ng/mL for both sunitinib and sunitinib-D10.

For the Acquity TQD, quantification was performed in positive-ion mode using multiple reaction monitoring (MRM) of the transition masses of sunitinib (m/z 399.4 → 283.1) and sunitinib-D10 (m/z 409.4 → 283.1). Instrument parameters were optimized for simultaneous detection of both. The capillary energy was set at 1 kV, cone voltage at 35 V, extractor at 4 V,

source block temp at 100 ^{o}C, desolvation temperature at 250 ^{o}C, and the optimal collision energy was 35 V. Calibration curves for sunitinib and sunitinib-D10 were established using standard samples at seven concentrations ranging from 6 ng/mL to 500 ng/mL. The coefficient of determination (r^2) from a least squares linear regression was 0.999 for sunitinib and 0.999 for sunitinib-D10. The LLOQ was 3 ng/mL for sunitinib and sunitinib-D10.

Validation of the HPLC MS/MS method was performed using spiked samples of release media, plasma, and tissue for accuracy and precision. Sample recovery >90% was attained for sunitinib, as determined by percent recovery of the internal standard.

3.2.10 Data Analysis

Linear regression for calibration curves, graphing, and statistical calculations for comparing sunitinib in vitro release from various MW monolithic PCL were performed using Graphpad Prism® software (La Jolla, CA).

Cumulative release data from each formulation tested were fitted by nonlinear curve fitting using Graphpad Prism® software. For all formulations tested except for sunitinib free base out of the hydrogel and nonporous bilayer PLGA construct, cumulative release was fitted using one-phase exponential association. A linear fit (indicating zero order release) was used to fit release of sunitinib free base from the hydrogel. Drug release from the nonporous PLGA construct demonstrated a two-phase release mechanism, consisting initially of diffusion out of the matrix followed by a rapid release of drug due to bulk degradation of the PLGA matrix (which dominates release in this phase) and diffusion. A two-phase model that was modified by Duvvuri

et al. (39) to describe the release of ganciclovir from PLGA microspheres was used to fit the release data. The following equation was applied (1):

$$F = A[1 - \exp(-K_1 * T)] + \frac{B}{\{1 + \exp[-K_2 * (T - T_{50})]\}} \qquad (1)$$

where F is the fraction of total drug released over the entire observation period; A is the percentage of total drug released during phase I; K_1 is the rate constant of drug release in phase I; B is the percentage of drug released during phase II; K_2 is the drug release rate constant during phase II; and T_{50} is the time taken to release 50% of the loaded drug. Release parameters obtained from the curve fit of this equation: A was 30%, K_1 was 0.081 day^{-1}, B was 76.4%, K_2 was 0.65 day^{-1}, and T_{50} was 33.1 days. Rate constants for each formulation were derived from the curve fitting and were used to calculate the $t_{1/2}$ of drug release for each phase if more than one.

3.3 Results

3.3.1 Physical Characteristics of PCL and PLGA Perivascular Wrap Formulations

As shown in Figure 3.2, small pores were visible in the PCL monolith surface even in the absence of a porogen during casting (Figure 3.2A). In contrast, in the PLGA film, a solid layer (Figure 3.2B) was observed with no notable porosity. Large-pore PLGA and PCL constructs were prepared by incorporating NaCl as a porogen during the casting process. The porous PCL construct contains both large pores formed by the NaCl porogen and smaller pores within the

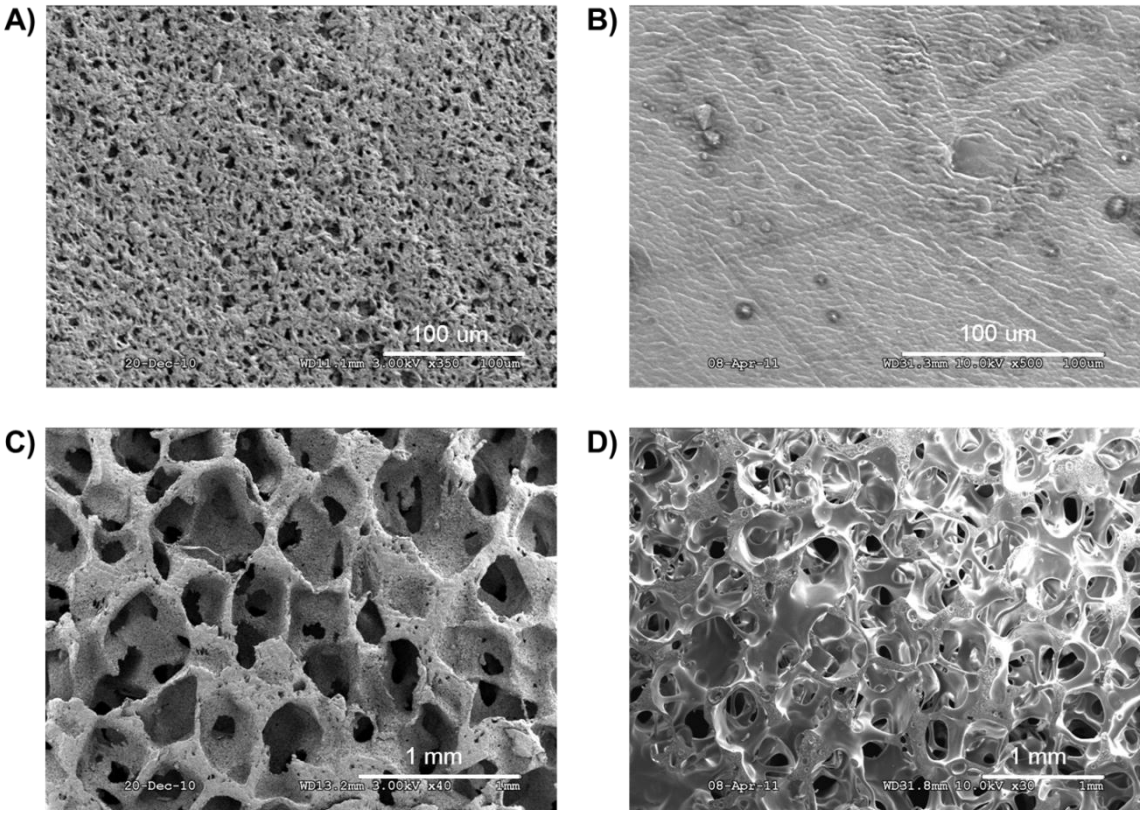

Figure 3.2 Morphology of PCL (A,C) and PLGA (B,D) polymer constructs formed in the absence (A, B) or presence (C,D) of porogen as determined by SEM.

intervening material (Figure 3.2C), whereas the porous PLGA construct contains the large pores formed by the NaCl porogen but the intervening material is nonporous (Figure 3.2D). In subsequent text the term “porous” describes the constructs created with the porogen. For simplicity, “nonporous” will be used to describe the constructs created in the absence of porogen, although PCL constructs formed in the absence of porogen contain micropores.

Bilayer wrap formulations for unidirectional drug delivery were created by laminating a drug-free construct, to serve as a blockade to extravascular drug release, onto another drug-loaded construct to serve as a drug reservoir for sustained release to the blood vessel wall. Images of the constructs are shown in Figure 3.3. With PLGA, the drug-loaded layer was either a porous (middle column) or a nonporous (far right column) construct. The porous layer was infused with sunitinib-loaded hydrogel. As sunitinib is bright yellow, infusion of the drug-laden hydrogel imparted color to the porous PLGA layer. PLGA cast in the absence of a porogen was amber colored even though no drug was present (nonporous layer, first column). With the bilayer PCL construct, the top layer cast with porogen and the bottom layer cast without porogen were both white (first column). When the porous layer was infused with sunitinib-containing hydrogel, both layers became yellow. The nonporous layer absorbed drug from the porous hydrogel-infused layer, likely because even in the absence of porogen, the PCL monolith contains micropores (Figure 3.2). In light of this contamination of the lower nonporous monolith with drug, a PCL construct was not made that consisted of a nonporous drug containing layer and a drug-free nonporous layer.

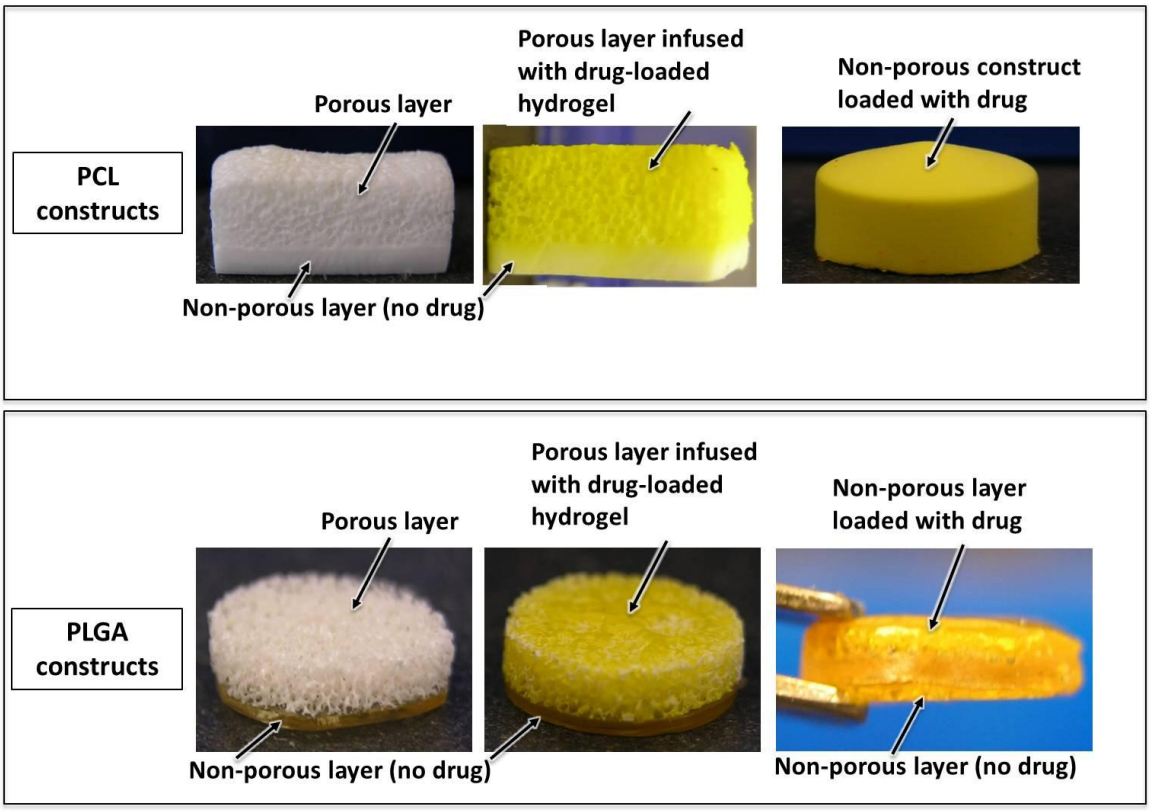

Figure 3.3 PCL and PLGA constructs. PCL constructs are shown in the first row. The first column shows a "porous/nonporous" bilayer construct created without drug. The second column shows the same construct as the first except drug-laden hydrogel was infused into the porous layer. The drug (sunitinib) is bright yellow. Note the nonporous PCL layer is yellow as it has absorbed some of the drug-laden hydrogel likely because of the micropores present in that layer. The third column shows a monolayer nonporous construct containing drug that was added during casting. No drug-free nonporous layer was present in this construct. PLGA constructs are shown in the second row. Bilayer PLGA constructs were formed by laminating a PLGA layer formed in the presence of a porogen during casting, on to a PLGA layer formed without addition of a porogen during casting. The image in the first column shows the "porous/nonporous" bilayer construct formed without drug in either layer. The PLGA polymer appears amber when formed without a porogen even in the absence of drug. The image in the second column shows the same construct as the first except drug-laden hydrogel was infused into the porous layer. The third column shows a nonporous layer cast with drug and laminated to a nonporous layer with no drug.

3.3.2 Testing PCL or PLGA Bilayer Constructs for Unidirectional Solute Release

The foundational PCL or PLGA backing formed in the absence of porogen was expected to curtail release of drug or solute to the extravascular space. To test this, a modified transwell system was created where discs of the PCL or PLGA nonporous constructs were substituted for the cell culture insert. The discs served to separate an upper and a lower media chamber. Sunitinib-laden hydrogel was placed in the upper chamber above the PCL discs. Sunitinib dissolved in media was placed in the upper chamber above the PLGA discs. Oil Red O, a hydrophobic dye with a molecular weight similar to sunitinib, was also used, except the dye was dissolved in media in the upper chambers above either PCL or PLGA discs. As shown in Figure 3.4, a very small amount of drug was detected in media collected at 72 h from the lower chamber below the PCL insert (~0.01% of the amount of drug detected in the upper chamber). However, no drug was detectable in the lower chamber beneath the PLGA insert. Oil Red O levels were below detection in the lower chamber beneath either PLGA or PCL inserts.

3.3.3 In Vitro Drug Release Profile from Hydrogel

Both the salt form of suntinib (sunitinib malate) and the free base (FB) form were used for drug release studies. Either drug form was mixed with hydrogel prior to gel crosslinking. Sunitinib malate readily dissolved into the hydrogel whereas the sunitinib FB remained in particulate form within the matrix. The cumulative release profiles of either form of sunitinib are shown in Figure 3.5. Almost complete release of sunitinib malate was observed from the hydrogel by five days. In contrast, release of sunitinib FB was much slower with only 50%

A) PCL

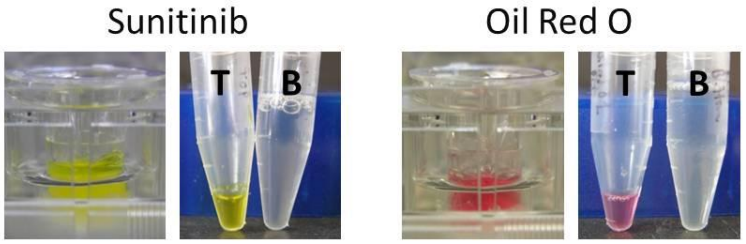

Release media	Sunitinib (μg/mL) LC/MS/MS	Oil Red O Abs (521nm)
Top	20.5±7.5	0.232±0.13
Bottom	0.018±0.003	Below detection

B) PLGA

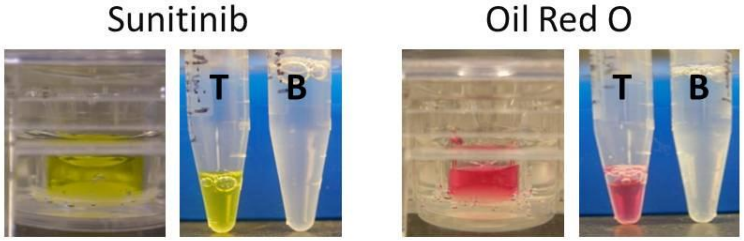

Release media	Sunitinib (μg/mL) LC/MS/MS	Oil Red O Abs (521nm)
Top	129±17.6	0.401±0.028
Bottom	Below detection	Below detection

Figure 3.4. A) Unidirectional release study using monolithic PCL as an insert to separate upper and lower media chambers. Sunitinib free base was added to hydrogel that was then placed in the upper chamber on top of the PCL monolith. After 72 hr, the media was collected from the top (T) and bottom (B) chambers and analyzed by HPLC/MS/MS for presence of drug. Oil Red O was dissolved in media and placed in the upper chamber. After 72 hr, the media was similarly collected and analyzed by UV/Vis for absorbance at 521 nm. B) Unidirectional release study using monolithic PLGA as the separating insert. Sunitinib malate or Oil Red O was dissolved in media that was placed in the upper chamber above the PLGA monoliths. Media was collected from the top (T) and bottom (B) chambers and analyzed similar to the PCL experiments. Media in the lower chamber surrounds the upper chamber.

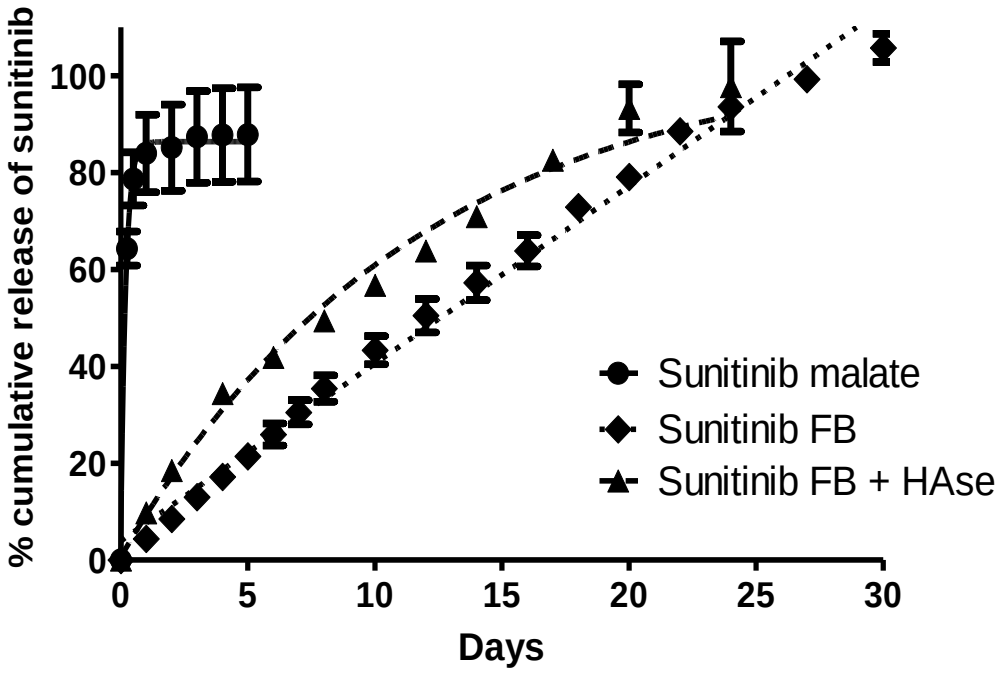

Figure 3.5. In vitro release profile of drug from hydrogel. Sunitinib malate (solid circles), sunitinib free base (FB) (diamonds), and sunitinib FB in the presence of hyaluronidase (HAse) (5mU/mL) (triangles).

release occurring by day 15 and 100% release occurring between 24 and 30 days, at which point the hydrogel had hydrolyzed completely. Table 3.1 shows the half-lives ($t_{1/2}$) and release constant (k) values for release of either form of sunitinib from the hydrogel. With the addition of HAse, an enzyme present in wound tissue that breaks down the major hydrogel component, hyaluronate, the drug release curve had a steeper incline in the first five days indicating enhanced release of drug in that time period. However, complete release of drug in the presence of HAse occurred by 24 days, which is similar to that seen in the absence of HAse, suggesting that the hydrolysis of hydrogel over enzymatic cleavage may be the more important factor in hydrogel breakdown. The free base form of sunitinib underwent a much slower release from hydrogel. Sunitinib FB was also able to inhibit PDGF-induced smooth muscle cell proliferation (IC_{50} ~ 17 nM).

3.3.4 In Vitro Drug Release Profiles from PCL Formulations

Sunitinib FB was mixed with hydrogel then infused under vacuum into the porous layer of a porous/nonporous PCL bilayer construct. Compared to what was observed previously with sunitinib FB release from hydrogel alone (Figure 3.6 diamonds), a slower release of drug was observed from sunitinib FB-loaded hydrogel infused into the PCL constructs (Figure 3.6) solid circle). Eighty percent of drug was released from the PCL construct by 50 days at which time the study was terminated. When sunitinib was loaded into the porous PCL layer, without hydrogel, a large burst of drug release was observed in the first 10 days (~67% release) followed by a slower constant release to 35 days (Figure 3.6). The rapid initial release of drug was likely due to drug that was not bound by the PCL; the later slow release was likely drug that was interacting with the

Table 3.1 Summary of release constants (k) and half-lives ($t_{1/2}$) for each polymer construct

Delivery system	k or k_1	$t_{1/2}$ (days)	k_2	$t_{1/2}$ (days)	goodness of fit (r^2)
Sunitinib from 45 kDa PCL	0.30	2.28	-		0.952
Sunitinib from 14/80 blend PCL	0.29	2.38	-		0.993
Sunitinib FB from hydrogel in porous bilayer PLGA	0.21	3.27	-		0.937
Sunitinib from 80 kDa PCL	0.15	4.61	-		0.878
Sunitinib FB from porous PCL (no hydrogel)	0.12	5.77	-		0.916
Sunitinib FB from hydrogel in presence of HAse	0.086	8.05	-		0.976
Sunitinib from nonporous bilayer PLGA	0.081	8.56	0.65	1.06	0.982
Sunitinib FB from hydrogel in porous PCL	0.031	22.26	-		0.993
*Sunitinib FB from hydrogel	3.68% release/day	13.6	-		0.989

”sunitinib” indicates sunitinib malate

FB = free base

*****indicates a linear fit, with zero-order release, whereas other fits are exponential and first order

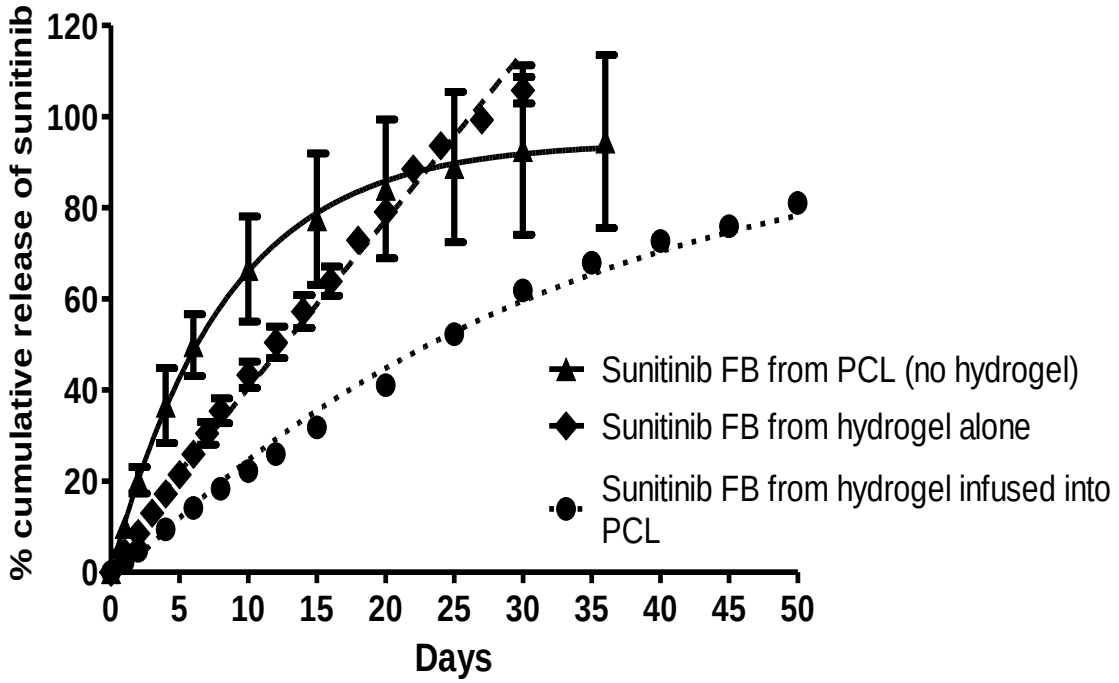

Figure 3.6 In vitro release profiles of sunitinib free base (FB) loaded into porous PCL (no hydrogel) (diamonds), sunitinib FB loaded in hydrogel then infused into porous PCL (solid circles), and sunitinib FB loaded into hydrogel alone (no polymer construct) (triangles).

PCL material. The half-lives and release constants are again shown in Table 3.1. Incorporating drug-laden hydrogel into porous PCL prolonged the release of sunitinib and allowed for more consistent release out of the matrix (compare in Figure 3.6 the broad standard deviations observed in drug release from PCL alone (no hydrogel) with tight standard deviations in drug release from hydrogel-infused PCL).

The previous experiments used 80 kDa PCL for construct formation. The 80 kDa PCL can resist in vivo degradation and remain intact within the body for over eighteen months (40). Our previous report showed that perivascular injections of drug-laden hydrogels to the anastomotic region could provide effective inhibitory concentrations of drug (14, 41). As hemodialysis grafts are subjected to continued pro-hyperplasia insults such as repeated puncturing by dialysis needles and the uremic milieu, later perivascular drug application may be needed after drug depletion occurs from a perivascular wrap. Thus attempts were made to create PCL-based constructs with faster degradation profiles that retained mechanical characteristics useful for wrapping vessels. Such a wrap could be placed at the anastomosis directly after AV graft creation to maintain drug at the region for a specific period but this treatment could be followed by perivascular injection of drug at later time points if needed. Nonporous constructs made from lower molecular weight PCL or blends of PCL were tested. Sunitinib was loaded into PCL constructs formed using either 45 kDa, 80 kDa, or a blend of two-thirds 80 kDa and one third 14 kDa molecular weight PCL. For these experiments, the constructs did not have the monolithic backing. The three molecular weight preparations of PCL demonstrated an initial rapid drug release within the first seven days followed by a slower continuous release (data shown in Figure 3.7). All drug was released from both the

lower molecular weight construct and blend construct around day 10. The initial burst of sunitinib was greater in the first ten days from the 45 kDa and 14/80 kDa blend PCL than from the 80 kDa PCL. The release constants are shown in Table 3.1. Attempts to form constructs from 14 kDa PCL failed as the polymer had little mechanical integrity and readily crumbled after thermal phase inversion.

3.3.5 In Vitro Drug Release Profile from PLGA Formulations

PLGA is degradable and degradation rates can be modified based on the ratio of lactide to glycolide (42) making this polymer an attractive option for vascular wrap development. Release of sunitinib was tested from two PLGA bilayer wrap formulations, a porous/nonporous bilayer construct and a nonporous/nonporous bilayer construct. Drug release from hydrogel loaded with sunitinib FB infused into the porous layer of the porous/nonporous PLGA construct was complete by approximately 15 days (Figure 3.8). When sunitinib was loaded into a nonporous layer of a nonporous/nonporous bilayer PLGA construct, complete drug release did not occur until approximately 35 days. The release occurred in a biphasic fashion with an initial slow release until 30 days whereupon a rapid release occurred. This construct initially provided a steady release of drug, similar to commercially available drug-eluting stents. The rapid release was accompanied by physical degradation of the construct as determined by visual assessment.

Release constants (k) and half lives ($t_{½}$) for drug release from each polymer construct. The release constant (k) and the half life ($t_{1/2}$) for drug release from each polymer construct were calculated and presented in Table 3.1. These data in Table 3.1 illustrate that a wide variation of

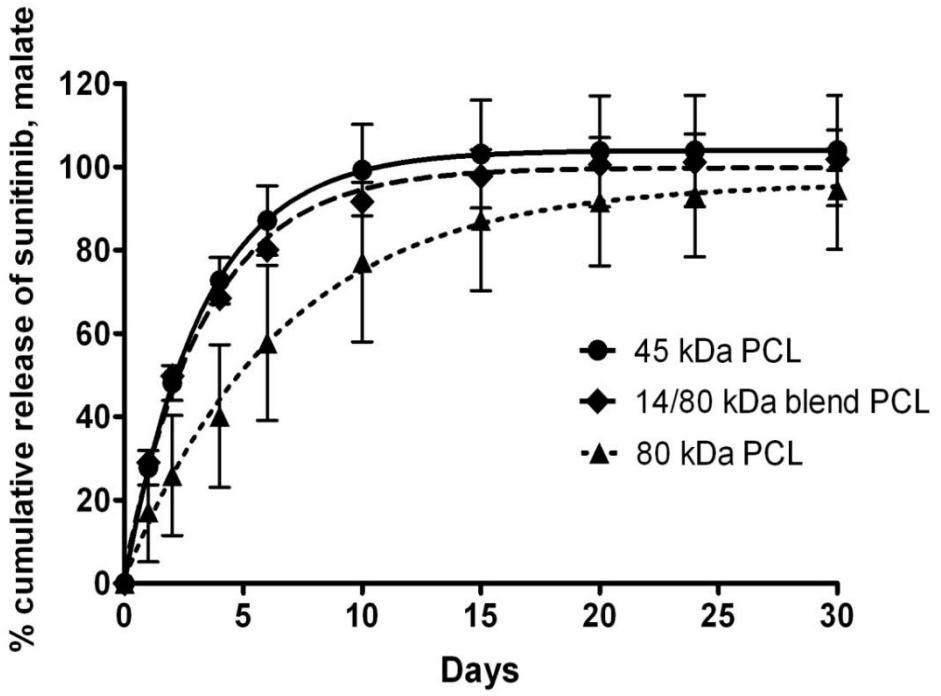

Figure 3.7 In vitro release profile of sunitinib from different molecular weight nonporous unilayer PCL (45 kDa, 14/80 kDa blend, and 80 kDa) constructs.

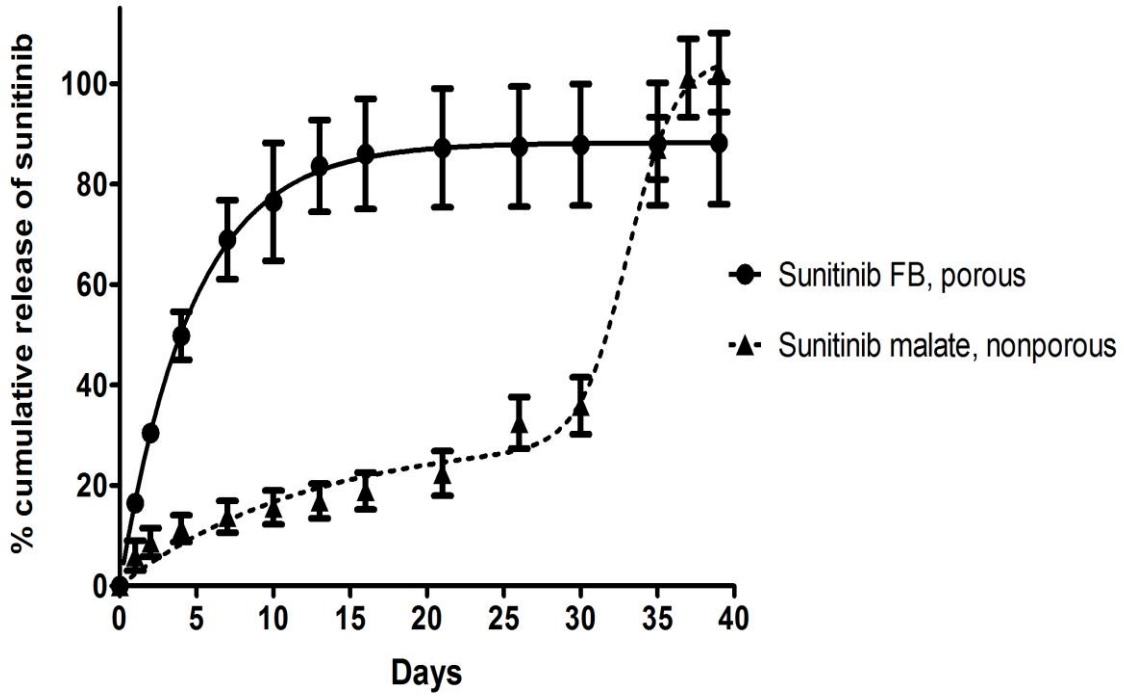

Figure 3.8 In vitro release profile of sunitinib malate from PLGA construct consisting of a drug-loaded nonporous/drug-free nonporous bilayer (triangles), or PLGA construct consisting of a sunitinib FB-loaded hydrogel infused into a porous/nonporous bilayer (circles).

release profiles can be accomplished by not only the use of different polymers for construct formation but also by modifying the porosity, the molecular weight of the polymers and also by combining hydrogels with polymers. In the instance of drug release from the nonporous bilayer PLGA construct, a biphasic release profile was observed and one release constant for each phase is shown. Drug release from the porous 80kDa PCL construct infused with drug-loaded hydrogel had the longest $t_{1/2}$. However, the 80kDa construct is predicted to have a very long life in vivo based on other reports.

3.3.6.In Vivo Drug Distribution in Porcine Tissue

Sterile PLGA bilayer constructs (sunitinib-loaded nonporous layer/drug-free nonporous layer) of 3 cm x 3 cm x 1 mm dimensions were placed around the external jugular vein (EJV) in swine. Drug-free bilayer constructs were placed on the contralateral EJV. After placement, the wounds were sutured and the animals were survived for 1, 2 or 4 weeks (one animal each time point) whereupon they were euthanized and the EJV and surrounding tissues were explanted for histology and drug detection. The wounds were evaluated weekly and no infections or remarkable swellings or delays in wound healing in the neck area were noted in any animals. However, in the first animal that was maintained for 4 weeks, we additionally placed a drug-loaded wrap and a drug-free wrap around the femoral veins in the upper hind limbs. In this location the femoral veins are very close to the surface with little surrounding tissue to compress the region. In addition the femoral veins have numerous branches that required ligation prior to wrap placement. Due to such factors, noteworthy amounts of edema formed in the hind limbs that

required draining. Thus wraps were not placed around the femoral veins in subsequent animals and the drug's pharmacokinetics was not analyzed in the tissue of those regions. Although edema formed in the hind limbs in the one animal that received wraps in that area, the wraps in the neck region were always well tolerated.

At explant, no signs of infection or serous fluid near the wraps in the neck were observed at any time point. After 1 week, the PLGA wrap remained intact as determined by visual assessment after explant (Figure 3.9). At 2 weeks, the wrap appeared to be degrading and becoming incorporated with tissue. At 4 weeks, the wrap was only visually detectable as small flakes of material that had become incorporated with fibrous tissue. It was observed that the wrap material was quite stiff at explant at every time point whereas the wraps were flexible prior to implant.

Distribution of sunitinib into the EJV wall, any surrounding fibrous tissue, the sternocleidomastoid muscle, and tissue adjacent to the vein, was assessed as illustrated in Figure 3.10. At 2 weeks, drug concentration more than doubled in the wrapped vein segment compared to the amount present at one week and remained elevated even at 4 weeks when the wrap had degraded considerably. Sunitinib concentrations detected in the wrapped portion of the EJV at all three time points were much greater than the experimentally determined IC_{50} needed to inhibit proliferation of PDGF-stimulated smooth muscle cells.

Drug was detected in the EJV at 2 cm proximal of where the wrap was placed at one week, but was at least four times less than seen in the wrapped vein area. At 2 weeks and 4 weeks after placement, sunitinib was detected in the sternocleidomastoid muscle, but at concentrations

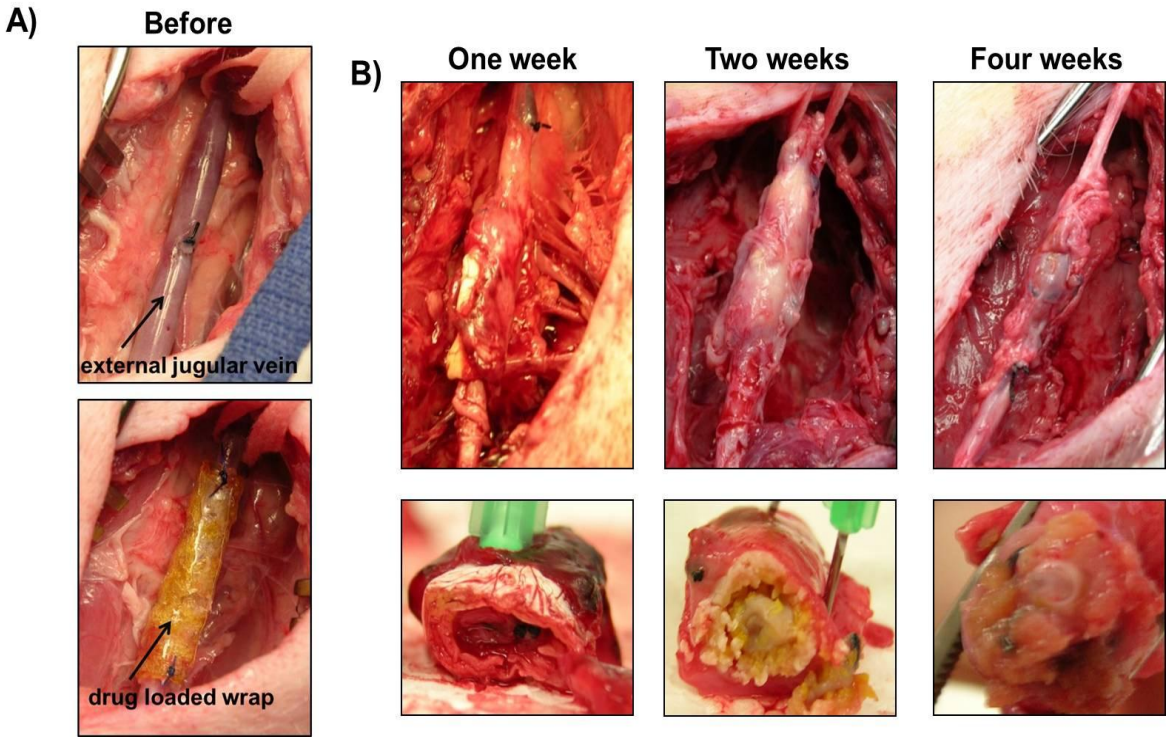

Figure 3.9 Drug-laden PLGA bilayer perivascular wraps in a porcine model. Panel A) Upper picture: The dissected porcine external jugular vein (EJV) just prior to wrap placement. Lower picture: A sunitinib-loaded PLGA bilayer wrap placed around the EJV. Panel B) Drug-loaded wraps imaged in situ after dissection at 1, 2, or 4 weeks after placement in vivo. Cross-sectional images taken after explant of the same drug-loaded wraps shown in the upper row.

much less than in the wrapped vein (Figure 3.10). Sunitinib was undetectable at the three time points in the distal portion of wrapped vein segments, tissue adjacent to the vein, and in all tissue sections on the control side. Blood was drawn weekly from each pig until euthanasia and systemic concentrations were undetectable except at four weeks after wrap placement wherein 3.6 ng/mL was detected. The animal with detectable systemic concentrations of drug was the animal that had received two drug-laden wraps, one in the hind-limb and one in the neck. Thus the contribution of the wrap in the hind-limb to systemic concentrations could not be separated from the contribution of the wrap in the neck. However, as there was significant fluid accumulation in the hind-limb area, this wrap may have contributed more to the systemic circulation.

The remaining wrap and any incorporated fibrous tissue was removed at each time point and analyzed to determine remaining drug concentrations. The amount of drug initially loaded into each bilayer wrap was 143±5.5 μg. At 1 week, 82% of the drug remained in the wrap and another 16% was further released after 2 weeks. By four weeks, the PLGA wrap had degraded significantly and intact wrap was not readily observable, thus the fibrous tissue that had incorporated into the wrap was analyzed. The fibrous tissue, with traces of polymer, contained 2.2% of the total loaded drug.

.

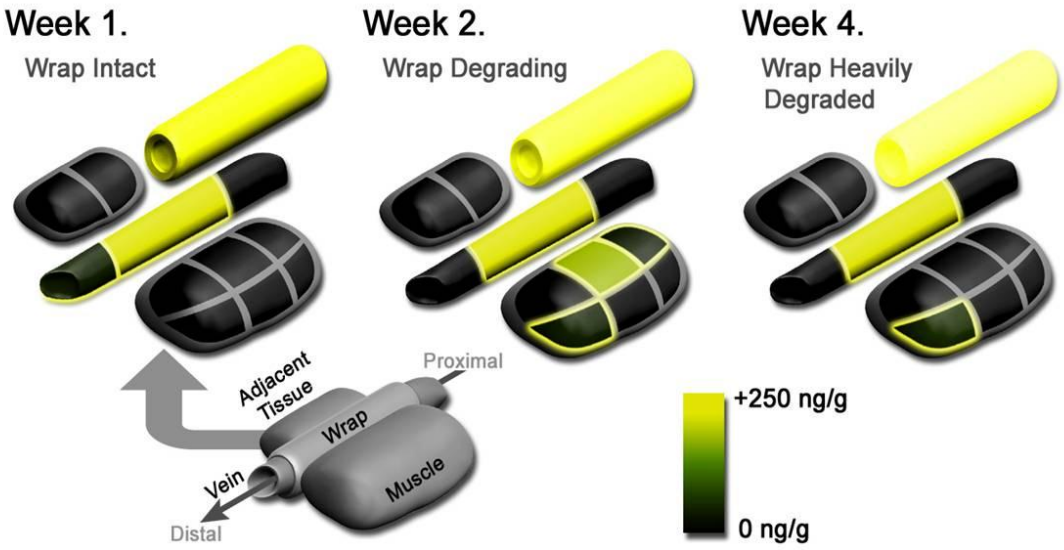

Time point	Adjacent Tissue	EJV (proximal) (2cm)	EJV (distal) (2cm)	EJV (wrapped) (2cm)	PLGA Wrap (% released)	Muscle (~10 g)
7 days	b.d.	41.2 ng/g 103 nM	b.d.	1048.4 ng/g 2631 nM	117,000 ng (18%)	b.d.
14 days	b.d.	b.d.	b.d.	2387.4 ng/g 5991 nM	95,000 ng (34%)	247.6 ng/g 621 nM
28 days	b.d.	b.d.	b.d.	1742 ng/g 4372 nM	3260 ng (97.8%)	52.1 ng/g 131 nM

EJV = external jugular vein
Proximal indicates closer to the heart; distal further from the heart.
b.d. = below detection; detection limit was 3 ng/mL
Drug values given for wrap includes the fibrous tissue incorporating the wrap over time.

Figure 3.10 Sunitinib concentrations in segments of porcine tissue collected at various postoperative time points. Upper panel: Graphic representation of measured sunitinib concentrations in various segments of tissue collected at each time point. Sunitinib concentrations are listed in the table for each segment of tissue that was analyzed.

3.3.7 Mechanical Properties

The Young's modulus of elasticity is a measure of material stiffness. Table 3.2 lists the Young's modulus of elasticity for drug-free or drug-loaded nonporous monolayer PLGA constructs at various time points before and after incubation in 1X PBS. Prior to incubation in PBS, the drug-free PLGA was elastic and flexible; after seven days in PBS the Young's modulus increased indicating the PLGA became brittle with exposure to PBS. Addition of sunitinib into the PLGA matrix further decreased the elasticity of the PLGA compared to the drug-free constructs as demonstrated by the increase in the Young's modulus. Also increased hydration time of the drug-loaded constructs (7 days) resulted in samples becoming so brittle that testing of elasticity failed, since the material fragmented when trying to place in the clamps of the Instron.

3.4 Discussion

The objective of this work was to develop a degradable, drug-loaded perivascular wrap that can direct drug release towards the graft and vascular wall to inhibit AV graft hyperplasia. A bilayer wrap design employing a drug-free nonporous backing with either a porous or nonporous drug-loaded layer, was anticipated to provide unidirectional drug delivery towards the vessel while minimizing drug loss to surrounding extravascular tissue. Limiting drug encroachment into surrounding nontarget tissues serves to mitigate the incidence of unwanted side effects and toxicities.

The solvent casting and thermal phase inversion techniques used to fabricate the wraps in this study are versatile since both porous and nonporous constructs could be made using two

Table 3.2 Effects of hydration on mechanical strength of monolithic PLGA

Samples	Days hydrated	Young's modulus (MPa)
Drug-free PLGA	0 days	1.12±0.14
Drug-free PLGA	1 day	2.53±0.69
Drug-free PLGA	7 days	30.13±2.88
Drug-loaded PLGA	0 days	40.15±0.35
Drug-loaded PLGA	1 day	51.9±11.3
Drug-loaded PLGA	7 days	Too brittle to test

relevant degradable polymers. By altering the polymer concentration and nonsolvent system composition during casting, mechanical and structural properties can be manipulated. For this application, polymer formulations were assigned to provide a strong but flexible construct for both layers that could be easily wrapped around a surgically accessed vessel. An additional benefit of the fabrication methods described is the toxicologically benign solvent systems employed, predominantly acetone.

Typically, harsh chlorinated solvents like chloroform or dichloromethane are used to create various PCL and PLGA matrices (21, 43-45). High levels of residual solvent can still remain in these matrices even after extensive removal efforts (46) leading to potential toxicity risk. There are currently no guidelines from the United States Pharmacopoeia (USP) regulating the maximum allowed residual solvent concentrations for these type of implantable materials (47). Therefore, employing solvent systems that are both i) facile to eliminate from the final polymer construct, and ii) innocuous if left behind in trace quantities, is desirable.

For both bilayer wrap formulations, a nonporous backing was integrated into the design to help prevent drug loss to the surrounding tissue and to direct drug toward the target tissue. As seen in Figure 3.4, both nonporous PCL and PLGA membranes severely restricted diffusion of sunitinib and Oil red O (hydrophobic dye) over 72hrs. In the case of PCL, sunitinib was detected in the lower media chamber but at a concentration one thousand times lower than that which was detected in the upper chamber. The PCL layer created in the absence of porogen still had micropores formed as a result of the phase inversion process used to create the construct (Figure 3.2). The micropores likely permit a faster diffusion of a drug through the bulk than through a

crystalline (nonporous) analog. However, the nonporogen-created backing should still act as a barrier to decrease drug loss to the extravascular surroundings and thus promote a heavily favored net release towards the vessel.

The versatility of the various wrap iterations permits incorporation of drug i) directly into the porous or nonporous polymer during casting or ii) into hydrogels that then can be incorporated into the porous polymer network. Drug loaded into the porous layer would be expected to exhibit a steeper release profile than drug incorporated into the nonporous polymer network, given that the porogen-derived surface area would provide more opportunity for interaction with the solvent environment. The hydrogel matrix used to load and suspend sunitinib in the porous layer was hyaluronic acid (HA)-based. HA is a naturally occurring polysaccharide and a major component of the extracellular matrix (ECM) present in mammalian tissues (48). This nonsulfonated, polyanionic GAG regulates cell motility and adhesion (49, 50), and is also implicated in maintaining water homeostasis within the ECM (51). HA hydrogels have been developed that are biocompatible, degradable, and injectable by making thiolated HA derivatives that can be crosslinked with PEGDA (52). Attempts were made to create a monolayer wrap from the HA directly but its mechanical properties proved unsuitable (not shown) for this application. However, the hydrogels proved easy to infuse into the porous layer of the bilayer wraps and provided another means to influence the drug-release profiles.

Release of sunitinib from the hydrogel was initially tested using both the salt (sunitinib malate) and free base forms. Sunitinib malate diffused swiftly out of the hydrogel with approximately 83% released in the first 24 hr (Figure 3.5). In the case of the free base, a slower 30 day release was

observed, at which point the hydrogel had degraded. The markedly dissimilar release profiles are likely due to the different interactions occurring between the salt and non-salt forms of sunitinib and the hydrogel. HA found in the Glycosil hydrogel is thiol-functionalized via the available carboxylic acid functional groups, but only 42% of these moieties become modified (53). At pH 7, the unreacted carboxylic acid groups are likely deprotonated while free base sunitinib (pKa~ 8.95 (54)) should possess one protonated amine group, leading to an electrostatic interaction between the two. Thus, release of free base sunitinib from this matrix is governed by ionic interactions, simple diffusion, and polymer degradation. In the case of the malate salt form, sunitinib exhibits one ionized amine, but due to the presence of malate anion, the potential for ionic interaction via amines is reduced compared to the free base form, promoting faster diffusion. The rapid burst of the malate salt from the hydrogel could lead to unacceptable drug levels and subsequent tissue toxicity; thus in proceeding studies with hydrogel, only the free base was incorporated.

Breakdown of the HA hydrogel occurs via i) hydrolysis of the PEG acrylate esters that form after crosslinking, and ii) enzymatic cleaving of the glycosidic linkage by hyaluronidase (HAse). As expected, an initial faster drug release was observed when the hydrogel was incubated in the presence of HAse. Since HAse would be endemic to the wound area after graft placement, a early faster release of sunitinib from the hydrogel-infused construct would be expected in vivo than what is observed in vitro in the absence of relevant enzymes and complex biological milieu.

PCL degrades slowly in vivo (55-57), which is beneficial for particular applications (55, 58-61), such as orthopedic devices. However, the current application would benefit from generally simultaneous matrix degradation and drug depletion, allowing for reapplication of drug to the AV

graft site. Polymer constructs were formed using lower molecular weight PCL as such constructs would have a faster degradation rate. However, it was observed that the lower molecular weight constructs released most of the drug within one week, limiting their utility.

Degradation rates of PLGA can be controlled by varying the co-monomer ratios of lactide and glycolide. Increasing the ratio of lactide to glycolide decreases the degradation rate, due to the increasing hydrophobicity and crystallinity of the final polymer (42). A porous/nonporous bilayer wrap and a nonporous/nonporous bilayer wrap were created using 50:50 PLGA, which exhibits the shortest possible degradative timeline. When drug-laden hydrogel was infused into the porous layer of a PLGA porous/nonporous bilayer construct, an initial burst (68%) of sunitinib was observed during the first week, and remaining drug diffused out over the next week with complete release around 15 days (Figure 3.8). Diffusion of drug out of the porous layer occurred before any notable polymer erosion was grossly observable. In contrast, release kinetics of sunitinib from the nonporous/nonporous PLGA bilayer construct formulation were biphasic, exhibiting a continuous controlled release of drug for the first 30 days followed by a rapid release that exhausted after approximately 1 week. Bulk erosion of the polymer network, which was grossly observable over this timeframe, likely permitted the rapid escape and depletion of drug.

In vivo drug distribution studies were performed by placing a bilayer PLGA wrap consisting of a sunitinib-laden nonporous layer laminated to a drug-free nonporous layer around the jugular vein in a porcine model. The adventitial layer of the vein was removed in order to initiate an injury response; the adventitia is also typically removed during hemodialysis arteriovenous graft placement. At 1, 2, and 4 week postsurgical intervals, the highest levels of sunitinib in the tissue

were observed in vein segment that was in direct apposition to the wrap. The drug concentrations obtained in these wrapped vein segments demonstrated levels higher than sunitinib's in vitro effective IC_{50} against PDGF-stimulated smooth muscle cell proliferation at all time points. By 2 weeks, the wrap showed signs of degradation, which likely resulted in increased drug release to the extravascular space. Drug was also detected, albeit in low concentrations, in the sternocleidomastoid muscle at 2 and 4 weeks. These proof-of-concept experiments suggest that the nonporous drug-free backing was able to direct net drug release toward the vein in the early period after placement while diminishing inevitable loss to the surrounding extravascular tissue.

Possible design improvements that could be made to inhibit further the loss of drug to the extravascular space include i) increasing the thickness and/or density of the drug-free nonporous backing, ii) increasing the ratio of lactide to glycolide polymer to decrease the degradation rate of the wrap, and iii) increasing the molecular weight of the utilized PLGA. In addition, lower concentrations of drug could be loaded into the polymer so that drug release to the extravascular space would be below IC_{50} levels. Of note, at 1 week, drug was detected in vein proximal of the wrapped segment. However, the concentration was barely above detection limits for the assay and was not detectable at other time points. It would be difficult to design a wrap that could prevent such release from the ends of the construct.

Our in vitro studies showed that only approximately 10% of sunitinib was released from the wrap within the first week. In vivo, approximately 18% of the drug load was released in week one. Drug release was also quicker in vivo at 2 and 4 weeks compared to in vitro. The discrepancy in

the release rates is likely due to a faster degradation of PLGA in vivo. Sink conditions with daily removal of the release media were performed for the in vitro experiments. However an acidic environment due to buildup of acidic degradation products (lactic and glycolic acids) is postulated to occur around the PLGA wrap in vivo. The lowered pH would result in an autocatalytic effect accelerating polymer degradation (44, 62). A total of 53.5 μg of sunitinib released from the wrap is accounted for throughout the 4 weeks, which is only ~38% of the total 145 μg of drug that was loaded in the wraps. The drug unaccounted for was most likely eliminated from the vascular tissue by metabolism, diffusion through the vein into systemic circulation, or dispersed into surrounding tissue that was not analyzed. Possibly due to the faster degradation rate of the wrap in vivo, the major drug burst that occurs because of polymer breakdown could have happened sooner than 4 weeks. So at the four week time point, the majority of released drug due to degradation was already eliminated from the vascular tissue, which would explain why a greater amount of drug was unaccounted for.

Prior to formation into the polymer wrap constructs, the PLGA polymer is stiff. However, after solvent casting into the monolithic films, the PLGA was ductile and could easily be wrapped around a blood vessel, and while not explicitly tested, even demonstrated properties of elastic recovery. The increased ductility and improved handling characteristics are likely due to a change in the polymer chain conformation after casting, allowing for greater interchain mobility and altered gross material properties. However, it was observed after both in vitro and in vivo testing that the PLGA constructs were much less flexible than what was observed prior to exposure to an aqueous environment. To better understand this phenomenon, tensile testing was performed to

assess changes in stiffness of the PLGA constructs as a function of temporal in vitro hydration. The drug-free, nonporous PLGA was readily deformable and quite ductile when tested prior to hydration as demonstrated by the low Young's modulus (Table 3.2). Hydration of the PLGA over time caused the Young's modulus to rapidly increase; the material became very brittle after 7 days hydration, revealing an anti-plasticizing effect of water that has been reported for PLGA films (63). The incorporation of sunitinib into the PLGA markedly decreased material extensibility, as shown by the increased stiffness compared to drug-free PLGA as was reported before with several drugs (64-66). This increased stiffness was postulated to occur to pronounced drug-polymer interactions, reducing the mobility of the polymer chains in the matrix (21, 65, 67). Hydration of the drug-laden PLGA polymer increased the Young's modulus further.

Possible explanations for the loss in extensibility upon hydration include i) thermodynamically driven polymer chain rearrangement to minimize contact with the infiltrating water molecules (63), and/or ii) the elimination of plasticization phenomena through the replacement of residual solvent molecules that enable high degrees of chain network mobility relative to water. As the material becomes hydrated, any residual solvent is displaced and the individual chains lose translational freedom. Others have reported the phenomena of residual solvents like dichloromethane or chloroform altering mechanical properties in various degradable polymer materials (68, 69). Regardless of the cause of the change in mechanical properties after exposure to water, the increased stiffness may be particularly advantageous in decreasing hyperplasia at the vein-graft anastomosis. It has been postulated that the enhanced circumferential tensile stress that occurs in a vein after introduction of arterial flow may significantly contribute to subsequent hyperplasia

formation (70, 71). Others have shown that restricting the vein distension by application of perivascular supportive stents inhibits intimal hyperplasia in vein interposition grafts exposed to arterial flow (70-72). In kind, the stiffening of the bilayer PLGA wrap after application around the vein-graft anastomosis could be beneficial in decreasing hyperplasia by inhibiting subsequent circumferential expansion.

3.5 Conclusion

A PLGA-based perivascular drug delivery system was created that is degradeable over a period of 30 days, provides early directed drug delivery due to the incorporation of an impermeable backing, is well-tolerated in vivo, and tunable to provide different drug release rates by either direct incorporation of drug, or by infusion of a drug-loaded hydrogel into a porous layer. Further work is needed however to slow the sudden degradation that resulted in a rapid release of drug after 30 days. The PLGA construct was also found to undergo a rapid increase in elastic modulus after in vivo placement that may be useful as a perivascular support against circumferential tensile stress in the vein. This study also revealed a novel interaction of the positively charged free base form of sunitinib with a selectively modified natural hydrogel, indicating for the first time, the hydrogel could be used for prolonged delivery of positively charged small molecule drugs. The PLGA construct presented in this study is a promising perivascular drug delivery system for the local treatment of AV graft NH and possibly other hyperplastic vascular disorders.

3.6 References

1. United States Renal Data System: 2002 Annual Data Report. Bethesda: National Institutes of Health, National Institute of Diabetes and Digestive Diseases; 2002.

2. Foundation NK. KDOQI Clinical Practice Guidelines for Vascular Access; 2000 2001 (suppl 1).

3. Cheung AK, Terry C, Li L. Pathogenesis and local drug delivery for prevention of vascular access stenosis. J Ren Nutr. 2008;18:140-5.

4. Lee T, Roy-Chaudhury P. Advances and new frontiers in the pathophysiology of venous neointimal hyperplasia and dialysis access stenosis. Adv Chronic Kidney Dis. 2009;16:329-38.

5. Moist LM, Churchill DN, House AA, Millward SF, Elliott JE, Kribs SW, et al. Regular monitoring of access flow compared with monitoring of venous pressure fails to improve graft survival. J Am Soc Nephrol. 2003;14:2645-53.

6. Ram SJ, Work J, Caldito GC, Eason JM, Pervez A, Paulson WD. A randomized controlled trial of blood flow and stenosis surveillance of hemodialysis grafts. Kidney Int. 2003;64:272-80.

7. Allon M. Stent graft or balloon angioplasty alone for dialysis-access grafts. The New England journal of medicine. 2010;362:1939; author reply 40.

8. Haskal ZJ, Trerotola S, Dolmatch B, Schuman E, Altman S, Mietling S, et al. Stent graft versus balloon angioplasty for failing dialysis-access grafts. N Engl J Med. 2010;362:494-503.

9. Osborn G, Escofet X, Da Silva A. Medical adjuvant treatment to increase patency of arteriovenous fistulae and grafts. Cochrane database of systematic reviews. 2008:CD002786.

10. Dixon BS, Beck GJ, Vazquez MA, Greenberg A, Delmez JA, Allon M, et al. Effect of dipyridamole plus aspirin on hemodialysis graft patency. N Engl J Med. 2009;360:2191-201.

11. Dixon BS, Beck GJ, Dember LM, Vazquez MA, Greenberg A, Delmez JA, et al. Use of aspirin associates with longer primary patency of hemodialysis grafts. Journal of the American Society of Nephrology : JASN. 2011;22:773-81.

12. Li L, Terry CM, Blumenthal DK, Kuji T, Masaki T, Kwan BC, et al. Cellular and morphological changes during neointimal hyperplasia development in a porcine arteriovenous graft model. Nephrology, dialysis, transplantation : official publication of the European Dialysis and Transplant Association - European Renal Association. 2007;22:3139-46.

13. Misra S, Doherty MG, Woodrum D, Homburger J, Mandrekar JN, Elkouri S, et al. Adventitial remodeling with increased matrix metalloproteinase-2 activity in a porcine arteriovenous polytetrafluoroethylene grafts. Kidney international. 2005;68:2890-900.

14. Masaki T, Rathi R, Zentner G, Leypoldt JK, Mohammad SF, Burns GL, et al. Inhibition of neointimal hyperplasia in vascular grafts by sustained perivascular delivery of paclitaxel. Kidney Int. 2004;66:2061-9.

15. Edelman ER, Adams DH, Karnovsky MJ. Effect of controlled adventitial heparin delivery on smooth muscle cell proliferation following endothelial injury. Proc Natl Acad Sci U S A. 1990;87:3773-7.

16. Melhem M, Kelly B, Zhang J, Kasting G, Li J, Davis H, et al. Development of a local perivascular paclitaxel delivery system for hemodialysis vascular access dysfunction: polymer preparation and in vitro activity. Blood Purif. 2006;24:289-98.

17. Signore PE, Machan LS, Jackson JK, Burt H, Bromley P, Wilson JE, et al. Complete inhibition of intimal hyperplasia by perivascular delivery of paclitaxel in balloon-injured rat carotid arteries. J Vasc Interv Radiol. 2001;12:79-88.

18. Lopez JJ, Edelman ER, Stamler A, Morgan JP, Sellke FW, Simons M. Local perivascular administration of basic fibroblast growth factor: drug delivery and toxicological evaluation. Drug Metab Dispos. 1996;24:922-4.

19. Brauner R, Laks H, Drinkwater DC, Jr., Chaudhuri G, Shvarts O, Drake T, et al. Controlled periadventitial administration of verapamil inhibits neointimal smooth muscle cell proliferation and ameliorates vasomotor abnormalities in experimental vein bypass grafts. J Thorac Cardiovasc Surg. 1997;114:53-63.

20. Kelly B, Melhem M, Zhang J, Kasting G, Li J, Krishnamoorthy M, et al. Perivascular paclitaxel wraps block arteriovenous graft stenosis in a pig model. Nephrology, dialysis, transplantation : official publication of the European Dialysis and Transplant Association - European Renal Association. 2006;21:2425-31.

21. Jackson JK, Smith J, Letchford K, Babiuk KA, Machan L, Signore P, et al. Characterization of perivascular poly(lactic-co-glycolic acid) films containing paclitaxel. Int J Pharm. 2004;283:97-109.

22. Kohler TR, Toleikis PM, Gravett DM, Avelar RL. Inhibition of neointimal hyperplasia in a sheep model of dialysis access failure with the bioabsorbable Vascular Wrap paclitaxel-eluting mesh. J Vasc Surg. 2007;45:1029-37; discussion 37-8.

23. Robinson MJ, Ronchese F, Miller JH, La Flamme AC. Paclitaxel inhibits killing by murine cytotoxic T lymphocytes in vivo but not in vitro. Immunol Cell Biol. 2010;88:291-6.

24. Jang JJ, Krishnaswami A, Fang J, Go M, Ben VC. Images in cardiovascular medicine. Pseudoaneurysm and intracardiac fistula caused by an infected paclitaxel-eluting coronary stent. Circulation. 2007;116:e364-5.

25. Swedberg SH, Brown BG, Sigley R, Wight TN, Gordon D, Nicholls SC. Intimal fibromuscular hyperplasia at the venous anastomosis of PTFE grafts in hemodialysis patients. Clinical, immunocytochemical, light and electron microscopic assessment. Circulation. 1989;80:1726-36.

26. Jawien A, Bowen-Pope DF, Lindner V, Schwartz SM, Clowes AW. Platelet-derived growth factor promotes smooth muscle migration and intimal thickening in a rat model of balloon angioplasty. J Clin Invest. 1992;89:507-11.

27. Majesky MW, Reidy MA, Bowen-Pope DF, Hart CE, Wilcox JN, Schwartz SM. PDGF ligand and receptor gene expression during repair of arterial injury. J Cell Biol. 1990;111:2149-58.

28. Weiss MF, Scivittaro V, Anderson JM. Oxidative stress and increased expression of growth factors in lesions of failed hemodialysis access. Am J Kidney Dis. 2001;37:970-80.

29. Roy-Chaudhury P, Kelly BS, Miller MA, Reaves A, Armstrong J, Nanayakkara N, et al. Venous neointimal hyperplasia in polytetrafluoroethylene dialysis grafts. Kidney Int. 2001;59:2325-34.

30. Ferns GA, Raines EW, Sprugel KH, Motani AS, Reidy MA, Ross R. Inhibition of neointimal smooth muscle accumulation after angioplasty by an antibody to PDGF. Science. 1991;253:1129-32.

31. Myllarniemi M, Frosen J, Calderon Ramirez LG, Buchdunger E, Lemstrom K, Hayry P. Selective tyrosine kinase inhibitor for the platelet-derived growth factor receptor in vitro inhibits smooth muscle cell proliferation after reinjury of arterial intima in vivo. Cardiovasc Drugs Ther. 1999;13:159-68.

32. Faivre S, Demetri G, Sargent W, Raymond E. Molecular basis for sunitinib efficacy and future clinical development. Nat Rev Drug Discov. 2007;6:734-45.

33. Bhardwaj S, Roy H, Heikura T, Yla-Herttuala S. VEGF-A, VEGF-D and VEGF-D(DeltaNDeltaC) induced intimal hyperplasia in carotid arteries. Eur J Clin Invest. 2005;35:669-76.

34. Dalton JE, Maroof A, Owens BM, Narang P, Johnson K, Brown N, et al. Inhibition of receptor tyrosine kinases restores immunocompetence and improves immune-dependent chemotherapy against experimental leishmaniasis in mice. The Journal of clinical investigation. 2010;120:1204-16.

35. Dechert TA, Ducale AE, Ward SI, Yager DR. Hyaluronan in human acute and chronic dermal wounds. Wound Repair Regen. 2006;14:252-8.

36. Baratte S, Sarati S, Frigerio E, James CA, Ye C, Zhang Q. Quantitation of SU1 1248, an oral multi-target tyrosine kinase inhibitor, and its metabolite in monkey tissues by liquid chromatograph with tandem mass spectrometry following semi-automated liquid-liquid extraction. J Chromatogr A. 2004;1024:87-94.

37. Minkin P, Zhao M, Chen Z, Ouwerkerk J, Gelderblom H, Baker SD. Quantification of sunitinib in human plasma by high-performance liquid chromatography-tandem mass spectrometry. J

Chromatogr B Analyt Technol Biomed Life Sci. 2008;874:84-8.

38. Zhou Q, Gallo JM. Quantification of sunitinib in mouse plasma, brain tumor and normal brain using liquid chromatography-electrospray ionization-tandem mass spectrometry and pharmacokinetic application. J Pharm Biomed Anal. 2010;51:958-64.

39. Duvvuri S, Gaurav Janoria K, Mitra AK. Effect of polymer blending on the release of ganciclovir from PLGA microspheres. Pharm Res. 2006;23:215-23.

40. de Valence S, Tille JC, Mugnai D, Mrowczynski W, Gurny R, Moller M, et al. Long term performance of polycaprolactone vascular grafts in a rat abdominal aorta replacement model. Biomaterials. 2012;33:38-47.

41. Owen SC, Li H, Sanders WG, Cheung AK, Terry CM. Correlation of tissue drug concentrations with in vivo magnetic resonance images of polymer drug depot around arteriovenous graft. J Control Release. 2010;146:23-30.

42. Miller RA, Brady JM, Cutright DE. Degradation rates of oral resorbable implants (polylactates and polyglycolates): rate modification with changes in PLA/PGA copolymer ratios. J Biomed Mater Res. 1977;11:711-9.

43. Nottelet B, Pektok E, Mandracchia D, Tille JC, Walpoth B, Gurny R, et al. Factorial design optimization and in vivo feasibility of poly(epsilon-caprolactone)-micro- and nanofiber-based small diameter vascular grafts. J Biomed Mater Res A. 2009;89:865-75.

44. Lu L, Peter SJ, Lyman MD, Lai HL, Leite SM, Tamada JA, et al. In vitro and in vivo degradation of porous poly(DL-lactic-co-glycolic acid) foams. Biomaterials. 2000;21:1837-45.

45. Dorta MJ, Santovena A, Llabres M, Farina JB. Potential applications of PLGA film-implants in modulating in vitro drugs release. Int J Pharm. 2002;248:149-56.

46. Hile DD, Amirpour ML, Akgerman A, Pishko MV. Active growth factor delivery from poly(D,L-lactide-co-glycolide) foams prepared in supercritical CO(2). J Control Release. 2000;66:177-85.

47. Koegler WS, Patrick C, Cima MJ, Griffith LG. Carbon dioxide extraction of residual chloroform from biodegradable polymers. J Biomed Mater Res. 2002;63:567-76.

48. Luo Y, Kirker KR, Prestwich GD. Cross-linked hyaluronic acid hydrogel films: new biomaterials for drug delivery. J Control Release. 2000;69:169-84.

49. Dowthwaite GP, Edwards JC, Pitsillides AA. An essential role for the interaction between hyaluronan and hyaluronan binding proteins during joint development. J Histochem Cytochem. 1998;46:641-51.

50. Cheung WF, Cruz TF, Turley EA. Receptor for hyaluronan-mediated motility (RHAMM), a hyaladherin that regulates cell responses to growth factors. Biochem Soc Trans. 1999;27:135-42.

51. Tufveson G, Gerdin B, Larsson E, Laurent T, Wallander J, Wells A, et al. Hyaluronic acid accumulation; the mechanism behind graft rejection edema. Transpl Int. 1992;5 Suppl 1:S688-9.

52. Zheng Shu X, Liu Y, Palumbo FS, Luo Y, Prestwich GD. In situ crosslinkable hyaluronan hydrogels for tissue engineering. Biomaterials. 2004;25:1339-48.

53. Liu Y, Zheng Shu X, Prestwich GD. Biocompatibility and stability of disulfide-crosslinked hyaluronan films. Biomaterials. 2005;26:4737-46.

54. Rodamer M, Elsinghorst PW, Kinzig M, Gutschow M, Sorgel F. Development and validation of a liquid chromatography/tandem mass spectrometry procedure for the quantification of sunitinib (SU11248) and its active metabolite, N-desethyl sunitinib (SU12662), in human plasma: application to an explorative study. J Chromatogr B Analyt Technol Biomed Life Sci. 2011;879:695-706.

55. Pektok E, Nottelet B, Tille JC, Gurny R, Kalangos A, Moeller M, et al. Degradation and healing characteristics of small-diameter poly(epsilon-caprolactone) vascular grafts in the rat systemic arterial circulation. Circulation. 2008;118:2563-70.

56. Pitt CG, Gratzl MM, Kimmel GL, Surles J, Schindler A. Aliphatic polyesters II. The degradation of poly (DL-lactide), poly (epsilon-caprolactone), and their copolymers in vivo. Biomaterials. 1981;2:215-20.

57. Vandamme TF, Legras R. Physico-mechanical properties of poly (epsilon-caprolactone) for the construction of rumino-reticulum devices for grazing animals. Biomaterials. 1995;16:1395-400.

58. Wong DY, Hollister SJ, Krebsbach PH, Nosrat C. Poly(epsilon-caprolactone) and poly (L-lactic-co-glycolic acid) degradable polymer sponges attenuate astrocyte response and lesion growth in acute traumatic brain injury. Tissue Eng. 2007;13:2515-23.

59. Silva-Cunha A, Fialho SL, Naud MC, Behar-Cohen F. Poly-epsilon-caprolactone intravitreous devices: an in vivo study. Invest Ophthalmol Vis Sci. 2009;50:2312-8.

60. Innocente F, Mandracchia D, Pektok E, Nottelet B, Tille JC, de Valence S, et al. Paclitaxel-eluting biodegradable synthetic vascular prostheses: a step towards reduction of neointima formation? Circulation. 2009;120:S37-45.

61. Cheng L, Guo S, Wu W. Characterization and in vitro release of praziquantel from poly(epsilon-caprolactone) implants. Int J Pharm. 2009;377:112-9.

62. Grayson AC, Voskerician G, Lynn A, Anderson JM, Cima MJ, Langer R. Differential

degradation rates in vivo and in vitro of biocompatible poly(lactic acid) and poly(glycolic acid) homo- and co-polymers for a polymeric drug-delivery microchip. J Biomater Sci Polym Ed. 2004;15:1281-304.

63. Santovena A, Alvarez-Lorenzo C, Concheiro A, Llabres M, Farina JB. Structural properties of biodegradable polyesters and rheological behaviour of their dispersions and films. J Biomater Sci Polym Ed. 2005;16:629-41.

64. Ubrich N, Bouillot P, Pellerin C, Hoffman M, Maincent P. Preparation and characterization of propranolol hydrochloride nanoparticles: a comparative study. J Control Release. 2004;97:291-300.

65. Liggins RT, Burt HM. Paclitaxel-loaded poly(L-lactic acid) microspheres 3: blending low and high molecular weight polymers to control morphology and drug release. Int J Pharm. 2004;282:61-71.

66. Takada S, Kurokawa T, Miyazaki K, Iwasa S, Ogawa Y. Utilization of an amorphous form of a water-soluble GPIIb/IIIa antagonist for controlled release from biodegradable microspheres. Pharm Res. 1997;14:1146-50.

67. Miyajima M, Koshika A, Okada J, Ikeda M. Mechanism of drug release from poly(L-lactic acid) matrix containing acidic or neutral drugs. J Control Release. 1999;60:199-209.

68. Giordano RA, Wu BM, Borland SW, Cima LG, Sachs EM, Cima MJ. Mechanical properties of dense polylactic acid structures fabricated by three dimensional printing. J Biomater Sci Polym Ed. 1996;8:63-75.

69. Manson J, Dixon D. The Influence of Solvent Processing on Polyester Bioabsorbable Polymers. J Biomater Appl. 2010.

70. El-Kurdi MS, Hong Y, Stankus JJ, Soletti L, Wagner WR, Vorp DA. Transient elastic support for vein grafts using a constricting microfibrillar polymer wrap. Biomaterials. 2008;29:3213-20.

71. Liu SQ, Ruan YY, Tang D, Li YC, Goldman J, Zhong L. A possible role of initial cell death due to mechanical stretch in the regulation of subsequent cell proliferation in experimental vein grafts. Biomech Model Mechanobiol. 2002;1:17-27.

72. Mehta D, George SJ, Jeremy JY, Izzat MB, Southgate KM, Bryan AJ, et al. External stenting reduces long-term medial and neointimal thickening and platelet derived growth factor expression in a pig model of arteriovenous bypass grafting. Nat Med. 1998;4:235-9.

CHAPTER 4

SUMMARY AND FUTURE WORK

4.1 Summary

In the US, more than 20% of all hemodialysis patient hospitalizations are due to vascular access dysfunction costing approximately 1 billion dollars annually (1). The complex nature of the pathogenesis leading to AV graft stenosis makes treating the problem challenging. A better understanding of the pathogenesis causing NH formation is emerging (2), but the molecular mechanisms of each pathogenic factor have not been delineated. Inflammation is one common reoccurring factor and therefore likely plays an important role in NH (3-5).

Based on the above observation, we investigated the involvement of inflammation in arteriovenous hemodialysis graft stenosis. In our porcine AV graft model, macrophage and T-cell accumulation increased over the 7 week time course corresponding with an increase in the NH formation at the venous anastomosis. Elevated expression of prominent cytokine/chemokines TNF-α and MCP-1, was seen in vein-graft anastomotic tissue. Both of these factors are known to influence NH development (6-8). Our results have led us to conclude that recruitment and activation of inflammatory cells around the graft anastomoses likely plays an influential role in causing NH in AV ePTFE grafts used in hemodialysis.

An experimental anti-inflammatory drug (sEHI) targeting soluble epoxide hydrolase (sEH) to inhibit proinflammatory cytokine and chemokine release from primary macrophages was evaluated. sEH converts anti-inflammatory EETs to less active DHETs. Inhibiting this conversion could prolong the anti-inflammatory activity of EETs. sEH expression was observed in both vein-graft anastomotic tissue and primary macrophages, making it a potential target in treating NH. sEHI significantly inhibited LPS induced MCP-1 release and TNF-α from primary macrophages, but did not significantly affect the release of MIP-1α or IL-6 (other proinflammatory cytokine/chemokines). sEHI also inhibited MCP-1 release from bone-marrow macrophages (BMMΦs) in wild-type mice, but not inhibit release in sEH knockout mice suggesting sEHI attenuates MCP-1 release through a direct effect on sEH. The nuclear translocation of NF-κB was not decreased with sEHI, but the phosphorylation of jun-N-terminal kinase (JNK) was completely abrogated. These findings indicate that sEHI could be useful in inhibiting inflammation seen around the anastomotic regions in AV grafts by inhibiting MCP-1 and TNF-α not through the typical NF-κB pathway, but instead via the JNK pathway.

We next developed a perivascular delivery system for controlled and directed release of sunitinib as a model drug, this system can be expanded to use other therapeutics for the treatment of AV graft stenosis. A bilayer wrap design was employed containing a monolithic backing to provide unidirectional release and to prevent loss of drug to the extravascular space, and either a drug loaded non-porous layer, or a porous layer that could be infused with drug loaded hydrogel. The wrap was created using either polylactide-co-glycolide (PLGA) or polycaprolactone (PCL). A wide range of release profiles was established by the use of the different polymers for construct

formation and by modifying the porosity and the molecular weight of the polymers. The control over release profile was further tuned by combining hydrogels with the porous polymers. In vivo tissue pharmacokinetics was analyzed from the nonporous bilayer PLGA construct. The backing directed drug release for at least the first week, but upon degradation allowed for some drug loss into the extravascular space after 2 weeks. Sustained release of sunitinib at efficacious levels around the wrapped external jugular vein was accomplished for at least four weeks. These promising results encourage further investigation into using this bilayer perivascular wrap loaded with sunitinib for the treatment of hemodialysis AV graft stenosis.

4.2 Future Work

4.2.1 sEHI Studies

We have examined sEH expression in primary human macrophages by confocal microscopy and western immunoblotting indicating the presence of the enzyme; however, this only indicates the presence of the enzyme and does not provide any information about sEH activity. The sEH enzyme is a homodimer and each monomer is comprised of two distinct structural domains, each of which has catalytic activity. The two catalytic domains, one on the N-terminus is a functional phosphatase and the second on the C-terminus has the epoxide hydrolase activity that catalyzes the addition of a water molecule to the epoxide resulting in the formation of a diol (9). Borhan et al developed [^{3}H]-trans-diphenyl-propene oxide (t-DPPO) in order to measure sEH activity by radiometric assay (10). Epoxide hydrolase activity then can be measured in primary human

macrophage by using racemic [^{3}H]-t-DPPO as a substrate and measuring the quantity of radioactive diol formed in the aqueous phase using a scintillation counter (11).

sEH catabolizes EETs into DHETs, which lack the anti-inflammatory effects of the parent compounds. The sEH inhibitor should increase the production and accumulation of EETs by preventing EET turnover. We have demonstrated that sEHI is working through sEH to lower MCP-1 secretion. We postulate that the decrease in MCP-1 and TNF-α secretion is a result of the accumulation of EETS. Obtaining the ratio of EETs to DHETs in primary macrophages after sEHI treatment would provide evidence that EETs are being accumulated and are the effective agents in decreasing MCP-1 and TNF-α expression. Macrophages would be pretreated with or without sEHI for 1 hr than stimulated with LPS for 24 hr. Media would be collected and cell extracts would be produced to assay for 5,6 EETs, 8,9 EETs, 11,12 EETs, 14,15 EETs, 5,6 DHETs, 8,9 DHETS, 11,12 DHETS, and 14,15 DHETS by using HPLC/negative mode electrospray ionization with a tandem mass spectral detection (12, 13). EETs to DHETs ratios would be calculated. These experiments would determine if 1) the sEH present in macrophages is active and 2) that EETs accumulation is occurring due to sEH inhibition.

4.2.2 Perivascular Wrap Studies

Early pathogenic factors such as vessel injury due to graft placement likely causes the maximal cellular activation within the first couple of days after placement requiring an initial burst of drug to combat these issues. Repeated puncturing of the graft for dialysis and constant hemodynamic stresses makes NH formation in AV grafts a chronic problem that might require an

extended continuous release of drug to inhibit NH or repeated dosing for treatment. Here, we suggest a number of studies that will facilitate the translation of the bilayer perivascular wrap to clinical research.

We demonstrated the ability of our bilayer wrap design to deliver sunitinib around the wrapped vein at efficacious levels for at least 4 weeks, at which time the wrap had significantly degraded. The ideal release kinetics for treatment of AV graft stenosis needs to be tested. Combination approaches incorporating drug directly into the porous PLGA during fabrication and infusing drug loaded hydrogel into the porous layer could be an initial starting point. A larger initial burst could be attained from release of drug out of the hydrogel, followed by a slower extended release of drug diffusing out of the PLGA material until the material bulk degrades and releases the remainder of the drug.

By varying the copolymer composition of PLGA and molecular weight, the degradation time of PLGA, and subsequently, the release profile can be altered accordingly for the bilayer wrap. Increasing the ratio of lactide to glycolide and molecular weight has been demonstrated to slow down drug release and degradation due to increasing the hydrophobicity of the polymer matrix (14, 15). Both of these concepts could be applied to the monolithic backing and drug loaded layer. Increasing the lactide ratio in the PLGA used for the backing would prolong the ability of the backing to direct release and prevent extravascular drug loss. Extended release of drug from the drug loaded layer could also be accomplished. However, this also lowers the initial burst of drug from the matrix, which now may not reach effective levels to inhibit the early cellular responses that contribute to NH. Incorporating polyethylene glycol (PEG), a water soluble

polymer, with PLGA can greatly enhance the initial burst (16, 17). This permits increased water uptake into the matrix causing the creation of water-filled channels that triggers faster drug release rates. Blending PEG and increasing the copolymer ratio of lactide to glycolide used in the PLGA in the drug loaded layer would likely allow for the initial drug burst and prolong release needed to treat NH formation in AV hemodialysis grafts. The information gathered in these studies would aid in determining ways to improve the bilayer wrap design, which then could be tailored for perivascular delivery of other potential therapeutics for treatment of AV graft stenosis.

After determining the best wrap design to attain the desired release kinetics of sunitinib for NH prevention, efficacy studies of the bilayer wrap in our porcine AV graft model (18, 19) would be tested. Yorkshire cross domestic swine, weighing 30 kg would be used for these studies. Expanded PTFE grafts (spiral re-enforced, 7-cm length, 6-mm internal diameter) would be placed between the common carotid artery and the ipsilateral external jugular vein bilaterally. Sunitinib loaded and control bilayer wraps would be placed around the venous anastomoses. One side would receive a drug loaded wrap and the other side would receive an unloaded wrap that serves as a control. Doppler ultrasound would be used to monitor graft patency weekly. Six weeks after graft placement, the animals would be euthanized and the grafts would be explanted en bloc along with 1-2 cm of the adjacent native blood vessels. Explanted tissue would be subjected to (i) tissue pharmacokinetics and (ii) histological analysis for NH quantification using H&E and Van Gieson stain, as previously done in our lab (18). Different animals would be utilized in order to do both. These studies will determine if sunitinib delivered perivascularly is an effective treatment option to inhibit NH formation in AV grafts.

Tissue pharmacokinetics would be performed similar to what was previously done in our lab (20). Following explantation, the tissue block with any remaining wrap would be immediately placed in sodium phosphate buffer (100 mM, pH 7.4) and flash-frozen. Both the venous and arterial anastomosis would be cut cross-sectionally into five segments of 1-cm in length each and weighed. Any remaining wrap would be removed from the vein-graft anastomosis and weighed. Interstitial tissues around the anastomoses would be sampled with their distances from the anastomosis measured. Sunitinib would be extracted from each tissue sample and any remaining wrap, and assayed using LC-MS/MS. The extraction and LC-MS/MS protocol have been described in Chapter 3. Pharmacokinetic studies will clarify the concentrations of drug needed to be loaded to maintain adequate efficacious tissue levels and indicate if or when repeated dosing options are needed to sustain these levels for treatment. This will lead towards the optimal design of a drug delivery system for prevention of NH.

Future work to be considered is delivery of therapeutics that can target the chemokine MCP-1 or its receptor CCR2; the work presented in this thesis suggests such treatments could be beneficial in inhibiting arteriovenous graft stenosis. We demonstrated the upregulation of this proinflammatory mediator at the vein-graft anastomosis in our porcine AV graft model. A variety of potential therapeutics has been developed that target MCP-1/CCR2. Zhang et al. created a plasmid coding for N-terminal deletion mutant of MCP-1 called 7-ND (21). This mutant MCP-1 binds to the CCR2 receptor and has been shown to inhibit MCP-1 mediated monocyte chemotaxis (21). 7-ND has been effective in inhibiting hyperplasia development in different arterial injury animal models (22-24). Short interfering RNA (siRNA) targeting CCR2 has been developed and

shown to be successful in decreasing CCR2 mRNA levels in monocytes, which led to a decrease in the accumulation of these monocytes into sites of inflammation (25). A small molecule indazole derivative, bindarit, has been shown to be efficacious in preventing restenosis in porcine coronary arteries after stenting (26). Bindarit selectively inhibits the production of MCP chemokines and IL-12β, likely through the inhibition of a subpopulation of NF-κB proteins (27). These therapeutic agents could be incorporated into the perivascular wrap for local delivery to prevent hyperplasia formation in AV grafts used for hemodialysis.

4.3 References

1. Roy-Chaudhury P, Sukhatme VP, Cheung AK. Hemodialysis vascular access dysfunction: a cellular and molecular viewpoint. J Am Soc Nephrol. 2006;17:1112-27.

2. Lee T, Roy-Chaudhury P. Advances and new frontiers in the pathophysiology of venous neointimal hyperplasia and dialysis access stenosis. Adv Chronic Kidney Dis. 2009;16:329-38.

3. Kornowski R, Hong MK, Tio FO, Bramwell O, Wu H, Leon MB. In-stent restenosis: contributions of inflammatory responses and arterial injury to neointimal hyperplasia. J Am Coll Cardiol. 1998;31:224-30.

4. Simon DI, Dhen Z, Seifert P, Edelman ER, Ballantyne CM, Rogers C. Decreased neointimal formation in Mac-1(-/-) mice reveals a role for inflammation in vascular repair after angioplasty. J Clin Invest. 2000;105:293-300.

5. Li L, Terry CM, Shiu YT, Cheung AK. Neointimal hyperplasia associated with synthetic hemodialysis grafts. Kidney international. 2008;74:1247-61.

6. Egashira K. Molecular mechanisms mediating inflammation in vascular disease: special reference to monocyte chemoattractant protein-1. Hypertension. 2003;41:834-41.

7. Rectenwald JE, Moldawer LL, Huber TS, Seeger JM, Ozaki CK. Direct evidence for cytokine involvement in neointimal hyperplasia. Circulation. 2000;102:1697-702.

8. Juncos JP, Grande JP, Kang L, Ackerman AW, Croatt AJ, Katusic ZS, et al. MCP-1 contributes to arteriovenous fistula failure. Journal of the American Society of Nephrology : JASN. 2011;22:43-8.

9. Newman JW, Morisseau C, Harris TR, Hammock BD. The soluble epoxide hydrolase encoded by EPXH2 is a bifunctional enzyme with novel lipid phosphate phosphatase activity. Proc Natl Acad Sci U S A. 2003;100:1558-63.

10. Borhan B, Mebrahtu T, Nazarian S, Kurth MJ, Hammock BD. Improved radiolabeled substrates for soluble epoxide hydrolase. Anal Biochem. 1995;231:188-200.

11. Harris TR, Morisseau C, Walzem RL, Ma SJ, Hammock BD. The cloning and characterization of a soluble epoxide hydrolase in chicken. Poult Sci. 2006;85:278-87.

12. Newman JW, Watanabe T, Hammock BD. The simultaneous quantification of cytochrome P450 dependent linoleate and arachidonate metabolites in urine by HPLC-MS/MS. J Lipid Res. 2002;43:1563-78.

13. Luria A, Weldon SM, Kabcenell AK, Ingraham RH, Matera D, Jiang H, et al. Compensatory mechanism for homeostatic blood pressure regulation in Ephx2 gene-disrupted mice. J Biol Chem. 2007;282:2891-8.

14. Mittal G, Sahana DK, Bhardwaj V, Ravi Kumar MN. Estradiol loaded PLGA nanoparticles for oral administration: effect of polymer molecular weight and copolymer composition on release behavior in vitro and in vivo. J Control Release. 2007;119:77-85.

15. Gumusderelioglu M, Deniz G. Sustained release of mitomycin-C from poly(DL-lactide) /poly(DL-lactide-co-glycolide) films. J Biomater Sci Polym Ed. 2000;11:1039-50.

16. Wang F, Lee T, Wang CH. PEG modulated release of etanidazole from implantable PLGA/PDLA discs. Biomaterials. 2002;23:3555-66.

17. Jackson JK, Smith J, Letchford K, Babiuk KA, Machan L, Signore P, et al. Characterization of perivascular poly(lactic-co-glycolic acid) films containing paclitaxel. Int J Pharm. 2004;283:97-109.

18. Li L, Terry CM, Blumenthal DK, Kuji T, Masaki T, Kwan BC, et al. Cellular and morphological changes during neointimal hyperplasia development in a porcine arteriovenous graft model. Nephrol Dial Transplant. 2007;22:3139-46.

19. Kuji T, Masaki T, Goteti K, Li L, Zhuplatov S, Terry CM, et al. Efficacy of local dipyridamole therapy in a porcine model of arteriovenous graft stenosis. Kidney Int. 2006;69:2179-85.

20. Zhu W, Masaki T, Bae YH, Rathi R, Cheung AK, Kern SE. Development of a sustained-release system for perivascular delivery of dipyridamole. J Biomed Mater Res B Appl Biomater. 2006;77:135-43.

21. Zhang YJ, Rutledge BJ, Rollins BJ. Structure/activity analysis of human monocyte chemoattractant protein-1 (MCP-1) by mutagenesis. Identification of a mutated protein that inhibits

MCP-1-mediated monocyte chemotaxis. The Journal of biological chemistry. 1994;269:15918-24.

22. Ohtani K, Usui M, Nakano K, Kohjimoto Y, Kitajima S, Hirouchi Y, et al. Antimonocyte chemoattractant protein-1 gene therapy reduces experimental in-stent restenosis in hypercholesterolemic rabbits and monkeys. Gene Ther. 2004;11:1273-82.

23. Usui M, Egashira K, Ohtani K, Kataoka C, Ishibashi M, Hiasa K, et al. Anti-monocyte chemoattractant protein-1 gene therapy inhibits restenotic changes (neointimal hyperplasia) after balloon injury in rats and monkeys. Faseb J. 2002;16:1838-40.

24. Egashira K, Zhao Q, Kataoka C, Ohtani K, Usui M, Charo IF, et al. Importance of monocyte chemoattractant protein-1 pathway in neointimal hyperplasia after periarterial injury in mice and monkeys. Circ Res. 2002;90:1167-72.

25. Leuschner F, Dutta P, Gorbatov R, Novobrantseva TI, Donahoe JS, Courties G, et al. Therapeutic siRNA silencing in inflammatory monocytes in mice. Nat Biotechnol. 2011;29:1005-10.

26. Ialenti A, Grassia G, Gordon P, Maddaluno M, Di Lauro MV, Baker AH, et al. Inhibition of in-stent stenosis by oral administration of bindarit in porcine coronary arteries. Arterioscler Thromb Vasc Biol. 2011;31:2448-54.

27. Mora E, Guglielmotti A, Biondi G, Sassone-Corsi P. Bindarit: An anti-inflammatory small molecule that modulates the NFkB pathway. Cell cycle. 2012;11:159-69.

APPENDIX A

AUTOLOGUS ADIPOSE TISSUE DEPOTS TO INHIBIT ARTERIOVENOUS GRAFT STENOSIS

A.1 Introduction

Adipose tissue (AT) is now considered a complex and highly metabolically active endocrine organ. AT is primarily composed of adipocytes, but also consists of macrophages, fibroblasts, and mesenchymal stem cells (1). White and brown AT are the two types of AT found in humans. There are two categories of white AT: i) subcutaneous, and ii) visceral which is also known as organ fat. Visceral AT typically contains increased numbers of resident inflammatory cells compared to subcutaneous AT, giving it a more inflammatory phenotype but the exact reason is for this is not known (2, 3). To illustrate this point, monocyte chemotactic protein-1 (MCP-1) release was greater in human visceral AT than subcutaneous AT (2) and coronary artery AT had greater expression of pro-inflammatory mediators, such as MCP-1, TNF-α, and IL-6 than subcutaneous AT (4). Ohman et al. verified this concept in vivo, visceral AT transplanted from ApoE-/- mice into recipient ApoE-/- mice developed significantly more atherosclerosis compared to those mice transplanted with subcutaneous AT even though plasma levels of adiponectin were similar between the two (5).

AT generates many proteins, including leptin, MCP-1, TNF-α, IL-6, IL-10, resistin, and

adiponectin (1). Adiponectin, a 29 kDa protein secreted primarily by AT has potent anti-inflammatory properties. The adiponectin monomer oligomerizes to form low, medium, or high molecular weight (LMW, MMW, or HMW) multimeric complexes in blood.(6). The HMW isoform of adiponectin has been associated with good cardiovascular outcomes and vascular protection (7-10). For example, low serum levels of HMW adiponectin correlated with cardiovascular events in patients with coronary artery disease (11). Adiponectin possesses many functions that may be valuable in preventing hyperplasia including the inhibition of i) TNF-α-stimulated expression of adhesion molecules, such as intracellular adhesion molecule-1, vascular cellular adhesion molecule-1, and E-selectin (12), ii) activation of NF-κB in TNF-α-stimulated endothelial cells (13), and iii) IL-6 and TNF-α release from LPS-stimulated macrophages (14). Adiponectin also iv) promotes the conversion of macrophages from the classically activated (pro-inflammatory) state to the alternatively activated (anti-inflammatory) state (15), v) induces expression of the anti-inflammatory IL-10 from human macrophages (16), vi) inhibits SMC proliferation (17), and vii) inhibits platelet activation (18). Recombinant adiponectin delivered perivascularly using a gelatin hydrogel inhibited neointimal hyperplasia in an artery wire injury model in adiponectin knockout mice. Similarly, transplantation of subcutaneous AT around the injured artery also inhibited hyperplasia (19). Such findings suggest that adiponectin is a vasculoprotective molecule and adiponectin supplementation could be beneficial for treatment of vascular hyperplasia.

Glitazone (thiazolidinediones) drugs are anti-diabetic insulin-sensitizer drugs that promote insulin-dependent glucose uptake into target tissues. Pioglitazone and rosiglitazone are currently

FDA-approved for treatment of diabetes. The glitazone drugs preferentially bind to the γ isoforms of the nuclear peroxisome-proliferator activator receptors (PPAR) but pioglitazone can also activate PPARα. The PPAR proteins are transcription factors that control the expression of genes that regulate lipid and glucose metabolism and cellular proliferation, apoptosis, and anti-inflammatory responses. The PPARs are expressed in many cell types including AT, macrophages, and cells of the vasculature. PPARγ is most highly expressed in AT whereas PPARα is more highly expressed in cells of the vasculature including smooth muscle and endothelial cells. These drugs can also bind to the outer mitochondrial membrane protein mitoNEET, which effects mitochondrial function by inhibiting the oxidative capacity of the mitochondria (20, 21). Therefore, the biological effects of glitazones may not be mediated just through PPAR activation.

Glitazones have potent anti-inflammatory effects such as i) the inhibition of SMC proliferation (22, 23), ii) inhibition of pro-inflammatory cytokine release, such as MCP-1 and TNF-α (24, 25), iii) inhibition of platelet aggregation (26, 27), and iv) attenuation of matrix metalloproteinase expression (28, 29). Another important aspect of these drugs is that they are potent inducers of adiponectin protein expression from AT. Tsuchida et al. demonstrated that rosiglitazone administered orally in obese diabetic KKAy mice could increase both serum adiponectin concentration and the ratio of HMW multimers of adiponectin to total adiponectin (30). Of particular relevance to the current work, subcutaneous AT explants from obese patients exposed to pioglitazone in vitro had increased adiponectin secretion compared to non-drug treated AT (31). With this knowledge, we propose that treating autologous AT explants with glitazone drug and

then transplanting the AT around the venous anastomosis of AV grafts would trigger adiponectin secretion from the AT. The adiponectin would then interact with adiponectin receptors on the medial smooth muscle cells and adventitial fibroblasts to inhibit proliferation and migration, and also on the endothelium to induce nitric oxide release and inhibit procoagulant expression. Glitazone drugs are lipophilic (hydrophobic) molecules, as indicated by Log P values greater than 2.5 (32),that should incorporate readily into the hydrophobic AT explants. Thus, we also propose that subcutaneous AT explants could act as a controlled delivery depot, providing sustained release of the vasculoprotective glitazones, which then could also inhibit graft hyperplasia by decreasing inflammation and inhibiting fibroblast and smooth muscle cell proliferation.

We report in vitro experiments testing the feasibility of using autologous subcutaneous AT explants treated with rosiglitazone to i) stimulate the production of adiponectin, and ii) to provide controlled delivery of rosiglitazone. Additionally, in vitro anti-inflammatory effects of the AT explants on SMC proliferation and MCP-1 release from AT are reported.

A.2 Materials and Methods

A.2.1. Materials

Rosiglitazone and the deuterated internal standard rosiglitazone-D3 were purchased from Toronto Research Chemicals (North York, ON, Canada). HEPES, insulin, and transferrin were all purchased from Invitrogen. Dexamethasone, acetonitrile (ACN), methyl-tert-butyl ether (MTBE), and 1-chlorobutane were of HPLC grade was acquired from Sigma-Aldrich (St. Louis, MO).

A.2.2. AT Collection and Culture

Abdominal subcutaneous AT left over after lipoaspiration or slab excision during breast reconstruction surgeries was obtained from human patients. The AT was de-identified and obtained under a blanket IRB approval for use of tissue samples collected during surgery that would normally be discarded. Lipoaspirated AT was present in small pieces (approximately 2-4 mm globules). The slab AT was excised from the skin and minced into small pieces before culturing. Powdered rosiglitazone was thoroughly but gently mixed directly into the AT explants using a sterile spatula to yield a concentration of 1000 μM (calculated using the conversion of 1g AT = 1 mL). Untreated AT explants were physically mixed in the same fashion but in the absence of powdered drug (control). AT explants were cultured in low glucose Dulbecco's modified Eagle's medium (DMEM, Invitrogen) containing HEPES (25 mM), insulin (1 nM), transferrin (10 μg/mL), dexamethasone (30 nM), and antibiotics. For thirteen days media was removed and replaced with fresh media approximately every 2 days. The conditioned media was frozen immediately at -80 ^{o}C then assayed by ELISA for adiponectin (R&D Systems, Minneapolis, MN) and MCP-1 (PeproTech, Rocky Hill, NJ) in accordance with the manufacturer's instructions.

The conditioned media samples for HPLC MS/MS analysis of rosiglitazone were spiked with rosiglitazone-D3 (internal standard (IS)) at known concentrations to monitor recovery efficiency. Rosiglitazone and IS were extracted from the conditioned media by vortexing with 1:1 MTBE:1-chlorobutane for 2 min and centrifugation at 25 ^{o}C at 2000xg for 15 min. The organic layer was collected and solvent evaporated at 42 ^{o}C overnight then reconstituted in acetonitrile-deionized H_2O (65:35, v/v) running buffer containing 0.1% formic acid.

A.2.3. Drug Sample Analysis by HPLC Tandem Mass Spectrometry

The sample analysis protocol was modified from a previously published protocol (33). The analytical separation of rosiglitazone and rosiglitazone-D3 were performed using an Atlantis dC_{18} column (2.1 x 30 mm, 3.0 μm) (Waters Corp., Milford, MA), protected by a 4mm x 2mm C_{18} packed guard column (Phenomenex) at 25 ^{o}C on an Acquity 2695 HPLC system (Waters Corp.) equipped with a refrigerated autosampler. The mobile phase consisted of acetonitrile–deionized H_2O (65:35, v/v) containing 0.1% formic acid and was ran isocratically at a flow rate of 0.3 mL/min. Sample run times were 6 min followed by a 2-min needle wash process to prevent possible carryover. The IS and rosiglitazone eluted at 0.69 min.

A triple quadropole tandem mass spectrometer (Micromass® Quattro II, Waters Corp.) equipped with an electrospray ionization (ESI) interface was used for analytical detection. Quantification was performed in positive-ion mode using multiple reaction monitoring (MRM) of the transition masses of rosiglitazone (m/z 358.3 → 135) and the internal standard rosiglitazone-D3 (m/z 361.1 → 138). Instrument parameters were optimized for simultaneous detection of both rosiglitazone and the IS. The capillary energy was set at 3.50 kV, cone voltage at 35 V, extractor at 3 V, source block temp at 125 ^{o}C, desolvation temperature at 325 ^{o}C, and the optimal collision energy was determined to be 27 V. Calibration curves for both rosiglitazone and rosiglitazone-D3 were established using standard samples at seven concentrations ranging from 1000 ng/mL to 5 ng/mL. The coefficient of determination (r^2) from a least squares linear regression was found to be 0.999 for both rosiglitazone and rosiglitazone-D3. Validation for accuracy and precision of the

HPLC MS/MS method was performed using spiked samples of media. Sample recovery of >80% was attained, as determined by percent recovery of the IS.

A.2.4. Smooth Muscle Cell Proliferation

Human venous vascular SMCs were seeded in 96-well tissue culture plates at 5000 cells/well in SMC media (Cascade Biologicals) without serum for 48 hr to quiesce the cells. Media was replaced with conditioned media (1:10 dilution) from either rosiglitazone-treated or untreated AT collected at various time points. Platelet-derived growth factor-BB (PDGF-BB, 50 ng/mL) was added to stimulate cell proliferation and cells were incubated for 48 hr whereupon cell proliferation was measured by a fluorescence-based DNA-binding assay (CyQuant, Invitrogen).

A.3 Results

A.3.1. Increased Adiponectin Secretion from Rosiglitazone-treated AT

Increased adiponectin secretion was observed from human AT mixed with rosiglitazone compared to control untreated AT: adiponectin levels were doubled by four days and elevated 3-fold above levels from untreated AT at eight days (Figure A.1).

A.3.2. In Vitro Drug Release of Rosiglitazone from AT

The cumulative release of rosiglitazone from AT is shown in Figure A.2. Approximately 20% of drug is released within the first 2 days followed by a slower controlled release over the next eleven days. Approximately 45% of the drug is released by day thirteen.

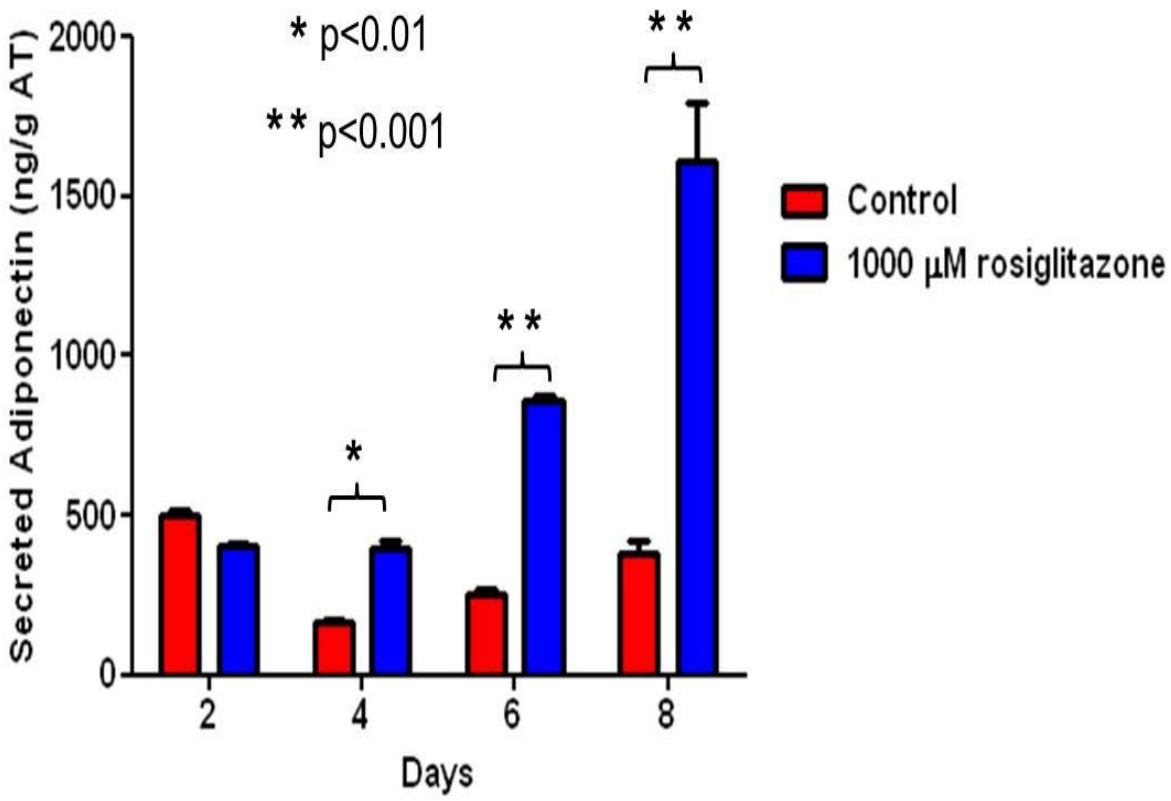

Figure A.1 Release of adiponectin from human AT treated with (red) or without (blue) rosiglitazone at various time points. Media was removed every 2 days analyzed for total adiponectin by ELISA. Asterisks denote statistically significant difference (*<0.01 or **<0.001) between untreated- and rosiglitazone-treated AT at each time point. AT was from one patient.

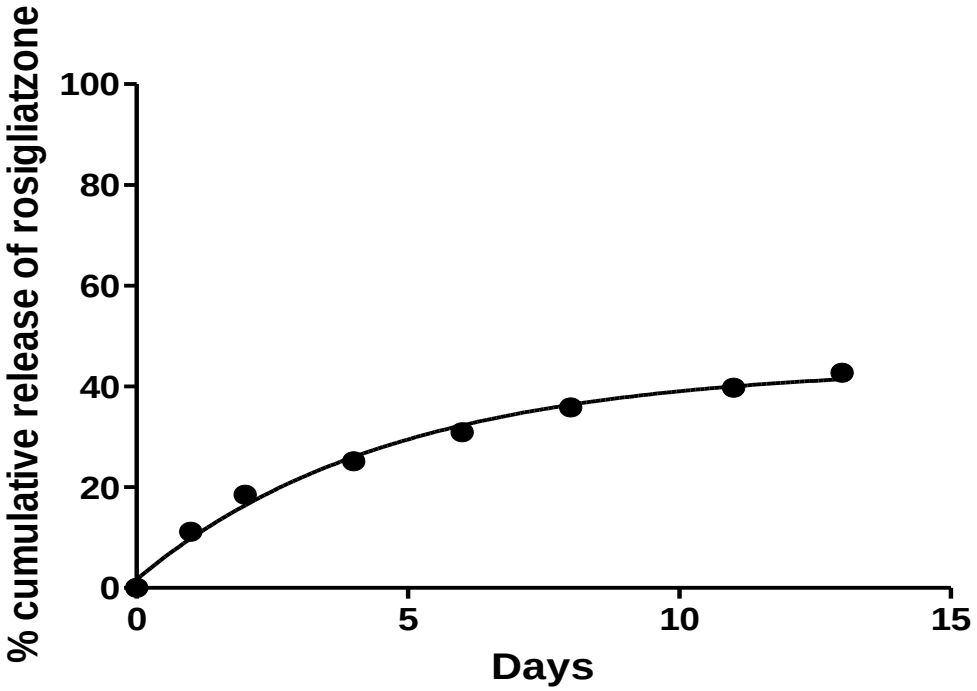

Figure A.2 In vitro drug release profile of rosiglitazone from human AT explant.

A.3.3. Attenuation of MCP-1 Release from Rosiglitazone-treated AT

Using media from the same experiment that was assessed for adiponectin release, it was observed that MCP-1 release from the rosiglitazone-treated AT was significantly decreased compared to untreated AT at day two and four (Figure A.3). By day four, secretion of MCP-1 was diminished in both treated and untreated AT yet MCP-1 release was still significantly lower from rosiglitazone-treated AT compared to control.

A.3.4. Conditioned Media from AT Inhibits SMC Proliferation

The conditioned media collected at days 2 and 8 from both untreated- and rosiglitazone-treated AT significantly inhibited PDGF-stimulated SMC proliferation ($p<0.05$) (Figure A.4).

A trend towards greater inhibition of SMC prolieration with conditioned media from rosiglitazone-treated AT was observed but this did not reach significance. In addition, proliferation of SMC exposed to conditioned media from AT incubated for 8 days with rosiglitazone was the same as that seen in SMC incubated in the absence of PDGF. The concentrations of adiponectin and rosiglitazone determined in the conditioned media at days 2 and 8 are listed in the table in Figure A.3. Conditioned media from rosiglitazone-stimulated AT at these time points had similar concentrations of drug, but at day eight adiponectin levels were approximately 16 times greater than at day two.

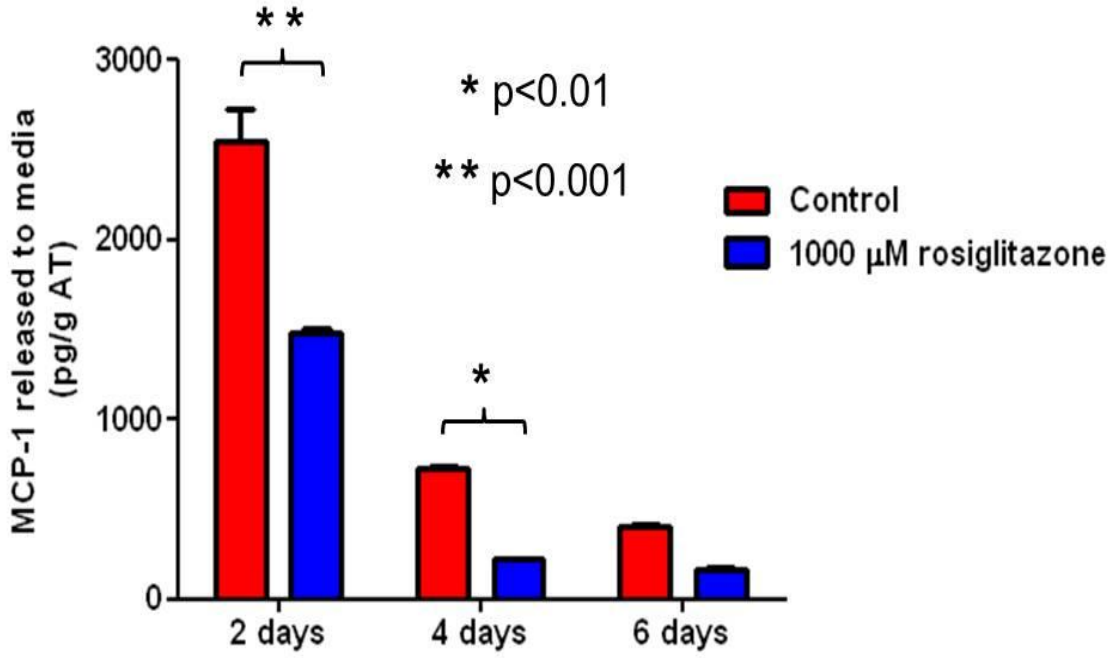

Figure A.3 Release of MCP-1 from human AT treated with (red) or without (blue) rosiglitazone at various time points. Media was removed every 2 days and analyzed for MCP-1 by ELISA. Asterisks denote statistically significant difference (*<0.01 or **<0.001) between control and rosiglitazone treated AT at each time point. AT was from one patient.

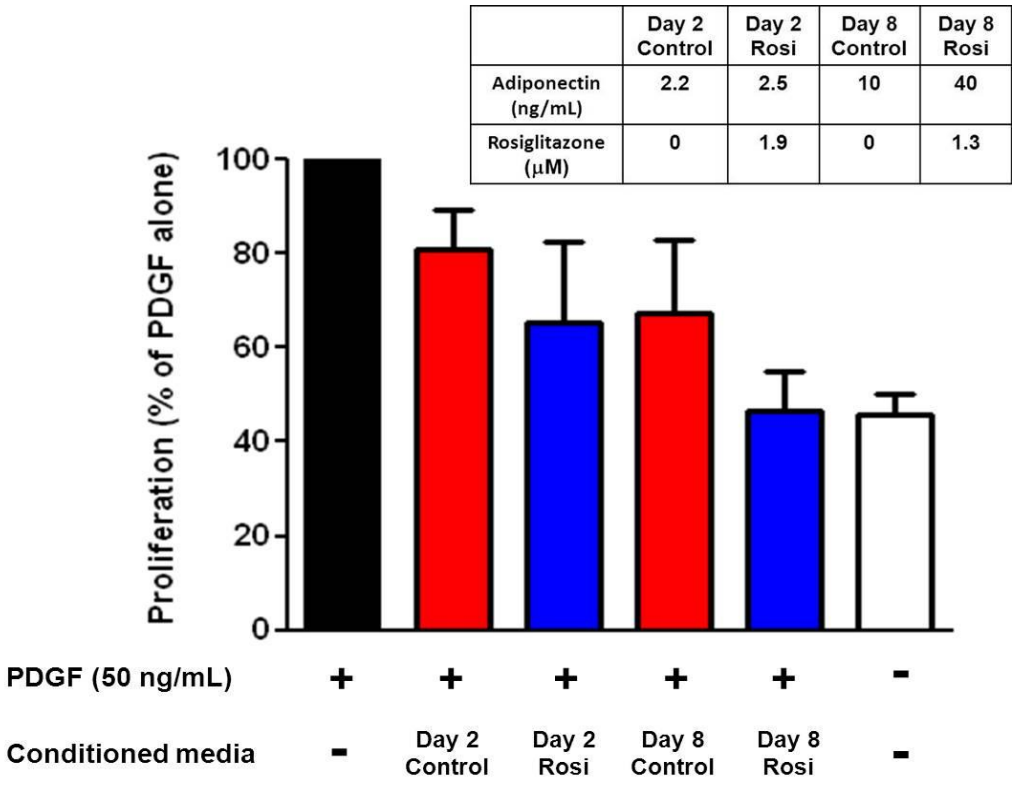

Figure A.4 PDGF stimulated SMC proliferation was inhibited by conditioned media at days 2 and 8 from untreated- (control) or rosiglitazone treated-AT. AT was from one patient. Adiponectin and rosiglitazone concentrations in conditioned media are listed in the table. Cell proliferation in samples treated with conditioned media from untreated- and rosiglitazone-treated AT was statistically less than proliferation in samples treated with PDGF alone (black) ($p<0.05$).

A.4 Discussion

We have hypothesized that AT could serve as an autologous drug delivery depot for glitazone drugs and as a biofactory for endogenously produced adiponectin. Glitazone drugs are themselves vasculoprotective and induce adiponectin which also has vasculoprotective properties. The primary objective of these initial studies was to characterize whether dry rosiglitazone (in the absence of added solvent) mixed in AT would induce adiponectin and inhibit inflammation. The long-term goal of our studies is to determine if autologous AT mixed with glitazone then transplanted back to the venous anastomosis of arteriovenous hemodialysis grafts in a porcine model would inhibit graft stenosis.

Several studies have reported the ability of rosiglitazone to stimulate adiponectin secretion from AT in vitro and in vivo (34-38). In the previous in vitro studies, the rosiglitazone was dissolved in solvent and added to media surrounding the AT explants. In the present study, we examined if powdered rosiglitazone, not dissolved in solvent, could induce adiponectin after mixing into human AT. Solvents were omitted since the final goal is to reapply the drug-treated AT as autologous transplants and solvents may negatively impact AT viability. Rosiglitazone stimulated the release of adiponectin by 4 days and adiponectin expression remained elevated at eight days (Figure A.1). Cabanelas et al. reported a significant decrease in adiponectin release at 48 hours after incubating rosiglitazone with subcutaneous rat AT compared to untreated AT (39). However, no time points later than 48 hr were investigated. We did not examine adiponectin release at time points earlier than 48 hr thus adiponectin expression may have been decreased at

that time point. Our work did not investigate why rosiglitazone required up to four days to induce adiponectin secretion.

MCP-1 (CCL2), a CC chemokine, is a potent chemoattractant that recruits peripheral monocytes and memory T-cells into sites of inflammation (40). Besides monocytes/macrophages, many other cell types secrete MCP-1 including T-cells, endothelial cells, SMC, and fibroblasts (41); all cell types that likely play a role in hyperplasia formation. Increased MCP-1 expression occurs in many experimental models of neointimal hyperplasia. For instance, up-regulation of MCP-1 appeared early in arteries after balloon injury in hypercholesterolemic rabbits (42) and femoral artery interpositional venous bypass grafting in rats (43). Inhibiting MCP-1 using either a neutralizing antibody for MCP-1 or a plasmid coding for N-terminal deletion mutant MCP-1 has been effective in diminishing neointimal hyperplasia in different animal models of arterial injury (44-46). MCP-1 is also expressed in AT and expression levels have been found to correlate positively with the degree of obesity (47, 48). Incubating AT with rosiglitazone significantly inhibited MCP-1 release at days 2 and 4 compared to control untreated AT (Figure A.2.). However, MCP-1 release was noticeably decreased whether rosiglitazone was present or not by day four. It is likely that dexamethasone, a typical ingredient of standard adipose culture media, inhibited release at these later time points. Further studies are needed to test the effect of rosiglitazone on MCP-1 release from AT in the absence of dexamethasone.

Proliferating and migrating SMCs and myofibroblasts compose the majority of cells that populate hyperplasia in AV grafts. Several studies have reported that either rosiglitazone or adiponectin can attenuate SMC proliferation (17, 23, 49-52). Rosiglitazone binds to PPAR γ and

induces apoptosis of SMC and inhibit SMC proliferation and migration (23, 53) which likely mediates the inhibition of transcription factor function critical for SMC proliferation. Adiponectin hinders SMC proliferation by binding to several mitogenic growth factors, such as platelet derived growth factor-BB (PDGF-BB) and basic fibroblast growth factor (FGF), preventing them from interacting with their respective receptors. In this study, we examined the effect of conditioned media from untreated control AT and rosiglitazone-treated AT on human SMC proliferation stimulated by PDGF. Conditioned media removed from both control and rosiglitazone-treated AT at days two and eight significantly inhibited SMC proliferation (Figure A.4). These data indicate that rosiglitazone-treated AT depots could be effective in preventing SMC proliferation, which would be valuable in preventing AV graft hyperplasia. Further studies are needed to define exactly which AT-derived mediators are participating in the SMC inhibition.

In addition to AT serving as a bioreactor for the production of adiponectin, our approach has AT also serving as a drug delivery depot for controlled release of rosiglitazone. Thus the release of rosiglitazone from AT was examined. After adding powdered rosiglitazone to the AT, the AT was placed in culture media and the media was examined longitudinally for presence of rosiglitazone by LC/MS/MS. Rosiglitazone was detected in the media early and also slowly released over time suggesting that the AT can serve as a drug release depot. The effects of rosiglitazone alone on SMC proliferation was not tested in these studies but previously rosiglitazone was reported to completely inhibit PDGF-induced SMC proliferation at a concentration of 1 μM (54). However, in our studies, conditioned media that contained 1.9 μM rosiglitazone (Day 2 Rosi in Fig. A.3) resulted in approximately a 50% reduction in PDGF-induced

SMC proliferation. A similar concentration of rosiglitazone was detected in conditioned media collected at eight days but with four times the concentration of adiponectin. This eight day media completely inhibited SMC proliferation suggesting that adiponectin was playing an important role in the observed inhibitory effects of the AT conditioned media. Recently, a release profile for rosiglitazone from an injectable hydrogel made from a mixture of naturally derived materials (chitosan, teleostean and oxidized dextran) was described (55). Rosiglitazone was dissolved in DMSO before loading into the hydrogel and about 80% of the drug was released by day 14. In contrast, our results showed much slower release from AT, which is likely due to the greater hydrophobicity of the AT delivery depot and the lack of DMSO solvent. Hydrophobic molecules like rosiglitazone (experimental Log P 2.78 (32) incorporate more readily into the hydrophobic AT depot, which allows for slower release. Hence, our data indicates AT can act as an autologous controlled sustained delivery depot for rosiglitazone or other hydrophobic drugs that may be considered for future use.

The initial data presented in this study is from a limited number of patient samples (n=1) and AT explants from additional patients are needed to confirm these findings. Also, total adiponectin levels were measured, which does not provide information on the type of MW isoforms of adiponectin being produced. In future studies, the MW of adiponectin being secreted will be characterized by ELISAs specific for the various MW adiponectin complexes or by native polyacrylamide gel electrophoresis. Another caveat with this study is that the remaining amount of drug in the AT depots was not quantified. For future in vitro drug release experiments, any remaining drug will be extracted and quantified by HPLC MS/MS to determine how much remains

within the AT.

This study is the first to report the study of autologous AT explants as means to deliver drug and adiponectin. These preliminary in vitro studies indicate that i) powdered rosiglitazone can induce sustained production of adiponectin when mixed with AT explants, ii) AT can act as a drug delivery depot, and iii) rosiglitazone and/or adiponectin released from AT have potent anti-inflammatory and anti-proliferative properties that could be beneficial in deterring vascular hyperplasia development.

A.5 References

1. Trayhurn P, Beattie JH. Physiological role of adipose tissue: white adipose tissue as an endocrine and secretory organ. Proc Nutr Soc. 2001;60:329-39.

2. Bruun JM, Lihn AS, Pedersen SB, Richelsen B. Monocyte chemoattractant protein-1 release is higher in visceral than subcutaneous human adipose tissue (AT): implication of macrophages resident in the AT. J Clin Endocrinol Metab. 2005;90:2282-9.

3. Curat CA, Wegner V, Sengenes C, Miranville A, Tonus C, Busse R, et al. Macrophages in human visceral adipose tissue: increased accumulation in obesity and a source of resistin and visfatin. Diabetologia. 2006;49:744-7.

4. Mazurek T, Zhang L, Zalewski A, Mannion JD, Diehl JT, Arafat H, et al. Human epicardial adipose tissue is a source of inflammatory mediators. Circulation. 2003;108:2460-6.

5. Ohman MK, Shen Y, Obimba CI, Wright AP, Warnock M, Lawrence DA, et al. Visceral adipose tissue inflammation accelerates atherosclerosis in apolipoprotein E-deficient mice. Circulation. 2008;117:798-805.

6. Kadowaki T, Yamauchi T. Adiponectin and adiponectin receptors. Endocr Rev. 2005;26:439-51.

7. Kobayashi H, Ouchi N, Kihara S, Walsh K, Kumada M, Abe Y, et al. Selective suppression of endothelial cell apoptosis by the high molecular weight form of adiponectin. Circ Res. 2004;94:e27-31.

8. Halperin F, Beckman JA, Patti ME, Trujillo ME, Garvin M, Creager MA, et al. The role of total

and high-molecular-weight complex of adiponectin in vascular function in offspring whose parents both had type 2 diabetes. Diabetologia. 2005;48:2147-54.

9. Pajvani UB, Hawkins M, Combs TP, Rajala MW, Doebber T, Berger JP, et al. Complex distribution, not absolute amount of adiponectin, correlates with thiazolidinedione-mediated improvement in insulin sensitivity. J Biol Chem. 2004;279:12152-62.

10. Aso Y, Yamamoto R, Wakabayashi S, Uchida T, Takayanagi K, Takebayashi K, et al. Comparison of serum high-molecular weight (HMW) adiponectin with total adiponectin concentrations in type 2 diabetic patients with coronary artery disease using a novel enzyme-linked immunosorbent assay to detect HMW adiponectin. Diabetes. 2006;55:1954-60.

11. Inoue T, Kotooka N, Morooka T, Komoda H, Uchida T, Aso Y, et al. High molecular weight adiponectin as a predictor of long-term clinical outcome in patients with coronary artery disease. The American journal of cardiology. 2007;100:569-74.

12. Ouchi N, Kihara S, Arita Y, Maeda K, Kuriyama H, Okamoto Y, et al. Novel modulator for endothelial adhesion molecules: adipocyte-derived plasma protein adiponectin. Circulation. 1999;100:2473-6.

13. Ouchi N, Kihara S, Arita Y, Okamoto Y, Maeda K, Kuriyama H, et al. Adiponectin, an adipocyte-derived plasma protein, inhibits endothelial NF-kappaB signaling through a cAMP-dependent pathway. Circulation. 2000;102:1296-301.

14. Wulster-Radcliffe MC, Ajuwon KM, Wang J, Christian JA, Spurlock ME. Adiponectin differentially regulates cytokines in porcine macrophages. Biochem Biophys Res Commun. 2004;316:924-9.

15. Ohashi K, Parker JL, Ouchi N, Higuchi A, Vita JA, Gokce N, et al. Adiponectin promotes macrophage polarization toward an anti-inflammatory phenotype. J Biol Chem. 2010;285:6153-60.

16. Wolf AM, Wolf D, Rumpold H, Enrich B, Tilg H. Adiponectin induces the anti-inflammatory cytokines IL-10 and IL-1RA in human leukocytes. Biochem Biophys Res Commun. 2004;323:630-5.

17. Wang Y, Lam KS, Xu JY, Lu G, Xu LY, Cooper GJ, et al. Adiponectin inhibits cell proliferation by interacting with several growth factors in an oligomerization-dependent manner. J Biol Chem. 2005;280:18341-7.

18. Kato H, Kashiwagi H, Shiraga M, Tadokoro S, Kamae T, Ujiie H, et al. Adiponectin acts as an endogenous antithrombotic factor. Arterioscler Thromb Vasc Biol. 2006;26:224-30.

19. Takaoka M, Nagata D, Kihara S, Shimomura I, Kimura Y, Tabata Y, et al. Periadventitial adipose tissue plays a critical role in vascular remodeling. Circ Res. 2009;105:906-11.

20. Colca JR, McDonald WG, Waldon DJ, Leone JW, Lull JM, Bannow CA, et al. Identification of a novel mitochondrial protein ("mitoNEET") cross-linked specifically by a thiazolidinedione photoprobe. Am J Physiol Endocrinol Metab. 2004;286:E252-60.

21. Paddock ML, Wiley SE, Axelrod HL, Cohen AE, Roy M, Abresch EC, et al. MitoNEET is a uniquely folded 2Fe 2S outer mitochondrial membrane protein stabilized by pioglitazone. Proc Natl Acad Sci U S A. 2007;104:14342-7.

22. Shinohara E, Kihara S, Ouchi N, Funahashi T, Nakamura T, Yamashita S, et al. Troglitazone suppresses intimal formation following balloon injury in insulin-resistant Zucker fatty rats. Atherosclerosis. 1998;136:275-9.

23. Law RE, Goetze S, Xi XP, Jackson S, Kawano Y, Demer L, et al. Expression and function of PPARgamma in rat and human vascular smooth muscle cells. Circulation. 2000;101:1311-8.

24. Sanchez-Hidalgo M, Martin AR, Villegas I, Alarcon De La Lastra C. Rosiglitazone, an agonist of peroxisome proliferator-activated receptor gamma, reduces chronic colonic inflammation in rats. Biochem Pharmacol. 2005;69:1733-44.

25. Mohanty P, Aljada A, Ghanim H, Hofmeyer D, Tripathy D, Syed T, et al. Evidence for a potent antiinflammatory effect of rosiglitazone. J Clin Endocrinol Metab. 2004;89:2728-35.

26. Ishizuka T, Itaya S, Wada H, Ishizawa M, Kimura M, Kajita K, et al. Differential effect of the antidiabetic thiazolidinediones troglitazone and pioglitazone on human platelet aggregation mechanism. Diabetes. 1998;47:1494-500.

27. Khanolkar MP, Morris RH, Thomas AW, Bolusani H, Roberts AW, Geen J, et al. Rosiglitazone produces a greater reduction in circulating platelet activity compared with gliclazide in patients with type 2 diabetes mellitus--an effect probably mediated by direct platelet PPARgamma activation. Atherosclerosis. 2008;197:718-24.

28. Marx N, Froehlich J, Siam L, Ittner J, Wierse G, Schmidt A, et al. Antidiabetic PPAR gamma-activator rosiglitazone reduces MMP-9 serum levels in type 2 diabetic patients with coronary artery disease. Arterioscler Thromb Vasc Biol. 2003;23:283-8.

29. Game BA, Maldonado A, He L, Huang Y. Pioglitazone inhibits MMP-1 expression in vascular smooth muscle cells through a mitogen-activated protein kinase-independent mechanism. Atherosclerosis. 2005;178:249-56.

30. Tsuchida A, Yamauchi T, Takekawa S, Hada Y, Ito Y, Maki T, et al. Peroxisome proliferator-activated receptor (PPAR)alpha activation increases adiponectin receptors and reduces obesity-related inflammation in adipose tissue: comparison of activation of PPARalpha, PPARgamma, and their combination. Diabetes. 2005;54:3358-70.

31. Phillips SA, Ciaraldi TP, Oh DK, Savu MK, Henry RR. Adiponectin secretion and response to pioglitazone is depot dependent in cultured human adipose tissue. Am J Physiol Endocrinol Metab. 2008;295:E842-50.

32. Giaginis C, Theocharis S, Tsantili-Kakoulidou A. Investigation of the lipophilic behaviour of some thiazolidinediones. Relationships with PPAR-gamma activity. J Chromatogr B Analyt Technol Biomed Life Sci. 2007;857:181-7.

33. Lin ZJ, Desai-Krieger D, Shum L. Simultaneous determination of glipizide and rosiglitazone unbound drug concentrations in plasma by equilibrium dialysis and liquid chromatography-tandem mass spectrometry. J Chromatogr B Analyt Technol Biomed Life Sci. 2004;801:265-72.

34. Muhlhausler BS, Morrison JL, McMillen IC. Rosiglitazone increases the expression of peroxisome proliferator-activated receptor-gamma target genes in adipose tissue, liver, and skeletal muscle in the sheep fetus in late gestation. Endocrinology. 2009;150:4287-94.

35. Pita J, Panadero A, Soriano-Guillen L, Rodriguez E, Rovira A. The insulin sensitizing effects of PPAR-gamma agonist are associated to changes in adiponectin index and adiponectin receptors in Zucker fatty rats. Regul Pept. 2011.

36. Ryan VH, German AJ, Wood IS, Hunter L, Morris P, Trayhurn P. Adipokine expression and secretion by canine adipocytes: stimulation of inflammatory adipokine production by LPS and TNFalpha. Pflugers Arch. 2010;460:603-16.

37. Nam JS, Nam JY, Yoo JS, Cho M, Park JS, Ahn CW, et al. The effect of rosiglitazone on insulin sensitivity and mid-thigh low-density muscle in patients with Type 2 diabetes. Diabet Med. 2010;27:30-6.

38. Sutinen J, Kannisto K, Korsheninnikova E, Fisher RM, Ehrenborg E, Nyman T, et al. Effects of rosiglitazone on gene expression in subcutaneous adipose tissue in highly active antiretroviral therapy-associated lipodystrophy. Am J Physiol Endocrinol Metab. 2004;286:E941-9.

39. Cabanelas A, Cordeiro A, Santos Almeida NA, Monteiro de Paula GS, Coelho VM, Ortiga-Carvalho TM, et al. Effect of triiodothyronine on adiponectin expression and leptin release by white adipose tissue of normal rats. Horm Metab Res. 2010;42:254-60.

40. Niu J, Kolattukudy PE. Role of MCP-1 in cardiovascular disease: molecular mechanisms and clinical implications. Clin Sci (Lond). 2009;117:95-109.

41. Melgarejo E, Medina MA, Sanchez-Jimenez F, Urdiales JL. Monocyte chemoattractant protein-1: a key mediator in inflammatory processes. Int J Biochem Cell Biol. 2009;41:998-1001.

42. Mori E, Komori K, Yamaoka T, Tanii M, Kataoka C, Takeshita A, et al. Essential role of monocyte chemoattractant protein-1 in development of restenotic changes (neointimal hyperplasia

and constrictive remodeling) after balloon angioplasty in hypercholesterolemic rabbits. Circulation. 2002;105:2905-10.

43. Stark VK, Hoch JR, Warner TF, Hullett DA. Monocyte chemotactic protein-1 expression is associated with the development of vein graft intimal hyperplasia. Arterioscler Thromb Vasc Biol. 1997;17:1614-21.

44. Horvath C, Welt FG, Nedelman M, Rao P, Rogers C. Targeting CCR2 or CD18 inhibits experimental in-stent restenosis in primates: inhibitory potential depends on type of injury and leukocytes targeted. Circ Res. 2002;90:488-94.

45. Ohtani K, Usui M, Nakano K, Kohjimoto Y, Kitajima S, Hirouchi Y, et al. Antimonocyte chemoattractant protein-1 gene therapy reduces experimental in-stent restenosis in hypercholesterolemic rabbits and monkeys. Gene Ther. 2004;11:1273-82.

46. Nakano K, Egashira K, Ohtani K, Zhao G, Funakoshi K, Ihara Y, et al. Catheter-based adenovirus-mediated anti-monocyte chemoattractant gene therapy attenuates in-stent neointima formation in cynomolgus monkeys. Atherosclerosis. 2007;194:309-16.

47. Sartipy P, Loskutoff DJ. Monocyte chemoattractant protein 1 in obesity and insulin resistance. Proc Natl Acad Sci U S A. 2003;100:7265-70.

48. Kanda H, Tateya S, Tamori Y, Kotani K, Hiasa K, Kitazawa R, et al. MCP-1 contributes to macrophage infiltration into adipose tissue, insulin resistance, and hepatic steatosis in obesity. J Clin Invest. 2006;116:1494-505.

49. de Dios ST, Bruemmer D, Dilley RJ, Ivey ME, Jennings GL, Law RE, et al. Inhibitory activity of clinical thiazolidinedione peroxisome proliferator activating receptor-gamma ligands toward internal mammary artery, radial artery, and saphenous vein smooth muscle cell proliferation. Circulation. 2003;107:2548-50.

50. Murthy SN, Obregon DF, Chattergoon NN, Fonseca NA, Mondal D, Dunne JB, et al. Rosiglitazone reduces serum homocysteine levels, smooth muscle proliferation, and intimal hyperplasia in Sprague-Dawley rats fed a high methionine diet. Metabolism. 2005;54:645-52.

51. Matsuda M, Shimomura I, Sata M, Arita Y, Nishida M, Maeda N, et al. Role of adiponectin in preventing vascular stenosis. The missing link of adipo-vascular axis. J Biol Chem. 2002;277:37487-91.

52. Arita Y, Kihara S, Ouchi N, Maeda K, Kuriyama H, Okamoto Y, et al. Adipocyte-derived plasma protein adiponectin acts as a platelet-derived growth factor-BB-binding protein and regulates growth factor-induced common postreceptor signal in vascular smooth muscle cell. Circulation. 2002;105:2893-8.

53. Lim S, Jin CJ, Kim M, Chung SS, Park HS, Lee IK, et al. PPARgamma gene transfer sustains apoptosis, inhibits vascular smooth muscle cell proliferation, and reduces neointima formation after balloon injury in rats. Arterioscler Thromb Vasc Biol. 2006;26:808-13.

54. Hansmann G, de Jesus Perez VA, Alastalo TP, Alvira CM, Guignabert C, Bekker JM, et al. An antiproliferative BMP-2/PPARgamma/apoE axis in human and murine SMCs and its role in pulmonary hypertension. J Clin Invest. 2008;118:1846-57.

55. Zhang H, Qadeer A, Mynarcik D, Chen W. Delivery of rosiglitazone from an injectable triple interpenetrating network hydrogel composed of naturally derived materials. Biomaterials. 2011;32:890-8.